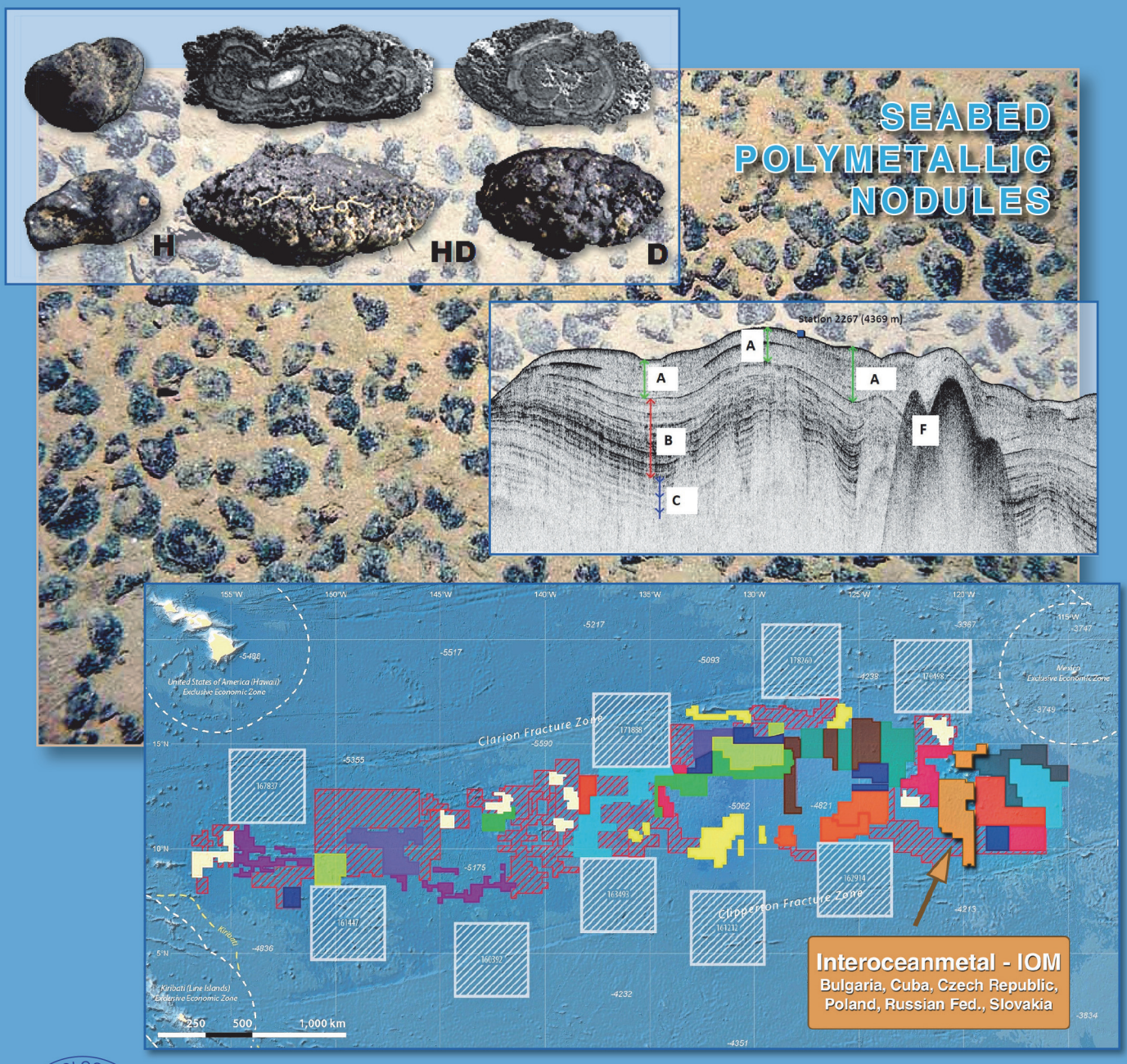
53/1/2021
ISSN 1338-3523
ISSN 0369-2086

Mineralia Slovaca



Štátny geologický ústav Dionýza Štúra Bratislava

Mineralia Slovaca

Časopis pre regionálnu a environmentálnu geológiu
a aktivity Slovenskej geologickej spoločnosti a geologických asociácií

PREDSEDA VYDAVATEĽSKEJ RADY – CHAIRMAN OF EDITORIAL BOARD

IGOR SLANINKA
Štátny geologický ústav Dionýza Štúra Bratislava

VEDECKÝ / VEDÚCI REDAKTOR – SCIENTIFIC AND MANAGING EDITOR

ZOLTÁN NÉMETH
Štátny geologický ústav Dionýza Štúra
Regionálne centrum Košice
Jesenského 8, 040 01 Košice
zoltan.nemeth@geology.sk

REDAKČNÁ RADA – EDITORIAL BOARD

Klement Fordinál, Štátny geologický ústav D. Štúra Bratislava
Ľubomír Hraško, Štátny geologický ústav D. Štúra Bratislava
Jozef Kordík, Štátny geologický ústav D. Štúra Bratislava
Peter Malík, Štátny geologický ústav D. Štúra Bratislava
Jozef Michalík, Ústav vied o Zemi SAV Bratislava
Ľubomír Petro, Štátny geologický ústav D. Štúra Košice
Dušan Plašienka, Prírodovedecká fakulta UK Bratislava
Marián Putiš, Prírodovedecká fakulta UK Bratislava
Ján Soták, Ústav vied o Zemi Banská Bystrica
Ladislav Šimon, Štátny geologický ústav D. Štúra Bratislava
Pavel Uher, Prírodovedecká fakulta UK Bratislava

REDAKCIA – EDITORIAL STAFF

Vedúci oddelenia vydavateľstva ŠGÚDŠ a propagácie – Head of the Department of ŠGÚDŠ Publishers and Promotion

LADISLAV MARTINSKÝ
ladislav.martinsky@geology.sk

Jazykoví redaktori – Lingual editors

Janka Hrtusová – Zoltán Németh
janka.hrtusova@geology.sk

Grafická úprava a technické spracovanie – DTP processing

Slávka Žideková
slavka.zidekova@geology.sk

Mineralia Slovaca (Web ISSN 1338-3523, ISSN 0369-2086), EV 3534/09, vychádza dvakrát ročne. Vydavateľ a tlač: Štátny geologický ústav Dionýza Štúra, Mlynská dolina 1, 817 04 Bratislava, IČO 31 753 604. Dátum vydania čísla 53/1/2021: júl 2021. Predplatné v roku 2021 vrátane DPH, poštovného a balného pre jednotlivcov 22,00 €, pre členov SGS a geologických asociácií 20,90 €, pre organizácie v SR 31,90 €, pre organizácie v ČR 55,00 €. Cena jednotlivého čísla pri osobnom nákupe v predajniach ŠGÚDŠ v Bratislave a v Košiciach je 6,05 € vrátane DPH. Časopis možno objednať v redakcii a v knižnici regionálneho centra v Košiciach. Adresa redakcie: Štátny geologický ústav D. Štúra – RC Košice (Mineralia Slovaca), Jesenského 8, 040 01 Košice. Telefón: 055/625 00 43; fax: 055/625 00 44, e-mail: mineralia.slovaca@geology.sk, e-mail knižnica: secretary.ke@geology.sk

Mineralia Slovaca (Web ISSN 1338-3523, ISSN 0369-2086) is published twice a year by the State Geological Institute of Dionýz Štúr Bratislava, Slovak Republic. The date of issuing of the number 53/1/2021: July 2021.
Subscription for the whole 2021 calendar year (two numbers of the journal): 66.00 € (Europe), 77.00 € (besides Europe), including VAT, postage and packing cost. Claims for nonreceipt of any issue will be filled gratis.
Order of the Editorial Office: Štátny geologický ústav D. Štúra – RC Košice (Library), Jesenského 8, SK-040 01 Košice, Slovak Republic. Phone: +421/55/625 00 43; fax: +421/55/625 00 44, e-mail: mineralia.slovaca@geology.sk, library: secretary.ke@geology.sk

© Štátny geologický ústav Dionýza Štúra Bratislava

www.geology.sk/mineralia

PÔVODNÉ ČLÁNKY – ORIGINAL PAPERS

Baláž, P.

Results of the first phase of the deep-sea polymetallic nodules geological survey in the Interoceanmetal Joint Organization licence area (2001–2016)

Výsledky prvej fázy geologického prieskumu hlbokomorských polymetalických konkrécií v prieskumnom území Spoločnej organizácie Interoceanmetal (2001 – 2016) 3

Pelech, O., Boorová, D., Hók, J. & Rakús, M.†

Upper Cretaceous limestones olistoliths in the Rázová Formation (Horné Belice Group), Považský Inovec Mts. (Western Carpathians)

Olistolity vápencov vrchnej kriedy v rázovskom súvrství hornobelickej skupiny Považského Inovca (Západné Karpaty) 37

Teťák, F.

Lithology and position of the Biele Karpaty Unit SE of Lednica (Biele Karpaty Mts., Western Carpathians)

Litológia a pozícia bielokarpatskej jednotky juhovýchodne od Lednice (Biele Karpaty, Západné Karpaty) 47

Cheikhaoui, Y., Bensehamdi, C., Cheniti, H., Kanli, A. I. & Benselhoub, A.

New formula for evaluation of strength pillar in the underground mine of Chaabet El-Hamra (Setif, Algeria)

Nový matematický postup hodnotenia pevnosti pilierov na príklade banskej prevádzky Chaabet El-Hamra (Setif, Alžírsko) 57

Danková, Z., Štyriaková, I., Čechovská, K., Šuba, J., Nováková, J., Kollárová, V., Bekényiová, A., Lenhardtová, E., Fedorová, E. & Briančin, J.

Influence of bacteria on toxic elements leaching from the contaminated soil

Vplyv baktérií na lúhovanie toxických prvkov z kontaminovanej pôdy 69

OBÁLKA:

Hlbokomorské polymetalické konkrécie v oblasti zlomového pásma Clarion-Clipperton vo východnom Pacifiku. Centrálna fotografia (v pozadí): Morské dno s vysokou hustotou polymetalických konkrécií: ich veľkosť je 2 – 8 cm, vzdialenosť kamery odo dna je asi 4,5 m. Kompozícia vľavo hore: Hlavné genetické typy konkrécií: H – hydrogenetický, HD – kombinovaný, D – diagenetický. Spodná fotografia: Polygóny prieskumných území v pásme Clarion-Clipperton na konci prvého obdobia kontraktu (2016) Spoločnej organizácie Interoceanmetal s Medzinárodnou organizáciou pre morské dno. Stredná fotografia vpravo: Interpretácia geoakustického profilu č. 707, fragment 2,7 – 6,0 km, situovaného na prieskumnom území organizácie Interoceanmetal. Problematika je prezentovaná v článku Baláža v tomto čísle časopisu (na stranách 1 – 36).

COVER:

Seabed polymetallic nodules in the area of Clarion-Clipperton Fracture Zone in eastern central Pacific. Central background photograph: The high nodule abundance: Their size is 2–8 cm, camera is positioned approx. 4.5 m above the seabed. Upper left picture: Main genetic types of nodules: H – hydrogenetic, HD – combined, D – diagenetic. Lower picture: The outlines of exploration areas in the Clarion--Clipperton Zone at the end of the first contract period (2016) of the Interoceanmetal Joint Organization with the International Seabed Authority. Central right picture: Interpretation of geoacoustic profile No. 707, fragment 2.7–6.0 km, located in this exploration area. The topic is treated in the article by Baláž in this issue (on pages 1–36).

Mineralia Slovaca, Web ISSN 1338-3523, ISSN 0369-2086
53 (2021), 03 – 36, © Author 2021. CC BY 4.0

Results of the first phase of the deep-sea polymetallic nodules geological survey in the Interoceanmetal Joint Organization licence area (2001–2016)

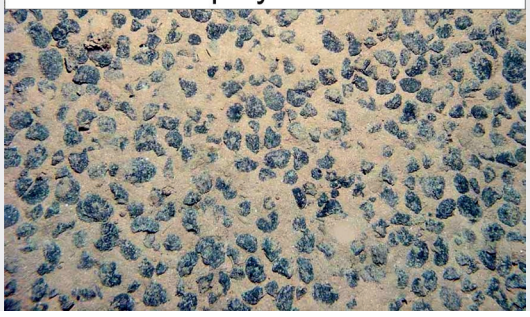
PETER BALÁŽ

Interoceanmetal Joint Organization, Szczecin, Poland

Abstract: The Interoceanmetal Joint Organization's exploration licence relate to the area located within the Clarion-Clipperton Fracture Zone (CCZ) of eastern central Pacific. Exploration area covers 75,000 km^2 and consists of two sectors (B1 and B2). The B2 sector comprises two exploration blocks (H11 and H22), delineated as the most prospective areas. The article presents information based on the data collected during the IOM's exploration expeditions. Data were obtained using the distance methods (bathymetry, side-scan sonar, profiler) and contact methods (box-corer, gravity corer and trawl sampling) of exploration. Exploration area's lithology, stratigraphy, geotechnical properties and general characteristics of seabed sediments and polymetallic nodules are provided. Estimation of mineral resources was caried out using the geostatistical method of ordinary block kriging, supported by Yamamoto correction. Regarding the level of geological knowledge and confidence, the polymetallic nodule resources have been classified within the Inferred, and Indicated Resources categories of the CRIRSCO classification system.

Key words: deep sea exploration, seabed minerals, polymetallic nodules, Clarion-Clipperton Zone

Graphical abstract



Highlights

- The Interoceanmetal Joint Organization's exploration area, located within the Clarion-Clipperton Fracture Zone (CCZ) of eastern central Pacific, covers 75,000 km^2.
- Paper provides the exploration area's lithology, stratigraphy, geotechnical properties and general characteristics of seabed sediments and polymetallic nodules.
- Inferred and Indicated mineral resources were determined of the CRIRSCO classification system.

Introduction

The exploration rights of the Interoceanmetal Joint Organization are granted to an area located within the Clarion-Clipperton Zone (CCZ) in the eastern central Pacific Ocean. All activities related to exploration of minerals in the CCZ (the Area – the seabed and ocean floor beyond the limits of national jurisdiction) come under the Law of the Sea – United Nations Convention on the Law of the Sea (1982), the Agreement relating to the implementation of Part XI of the Convention (1994) as well as Regulations on Prospecting and Exploration for Polymetallic Nodules in the Area – regulations established by the International Seabed Authority (ISA). The organization currently has 168 member states, including Slovakia and the European Union as a whole.

The ISA issues legal documents regulating the conduct of research and the future use of the seabed. The IOM´s contract for exploration of polymetallic nodules was granted for 15 years and provided the contractor security of tenure and exclusive right to explore for polymetallic nodules in the exploration area, as well as to move to a contract for exploitation (regulations for exploitation of mineral resources in the Area are under the development process by the ISA). In 2016, the contract was extended for the following 5 years. The exploration area is common for all 6 IOM member states: Bulgaria, Cuba, the Czech Republic, Poland, the Russian Federation and Slovakia, without exactly positiones parts of the area. Only the potential profit will be shared or the country will be able to sell its stake in the joint venture. For this reason, it is planned to transform IOM from a research organization into a joint stock company.

In addition to geological survey and related research, IOM is working on research into the technology of mining and processing of deep-sea polymetallic nodules (PMN), as well as on environmental research.

Locality

The IOM exploration area covers 75,000 km^2 of the eastern part of the CCZ and consists of two sectors: B1 and B2 with two exploration blocks H11 and H22 (Tab. 1, Fig. 2).

Tab. 1

IOM´s Exploration area (sectors and exploration blocks).

Exploration area	Area [km^2]
B1 sector	11 952
B2 sector	63 075
H11 exploration block	5 390
H22 exploration block	4 150
Total	**75 000**

Survey methodology

In recent decades, several methods have been developed to survey and sample seabed and polymetallic nodules. Following distance methods were used during IOM expeditions:

Multibeam bathymetry

Bathymetry is used to measure depth and map the bottom morphology using multibeam sonar, while providing information on the character of the seabed based on the intensity of the reflected signal (backscatter). The device is installed on a research vessel.

Geoacoustic survey

Geoacoustic profiling with side-scan sonar is used for detailed mapping of the seabed in a width of about 2 km and obtaining the acoustic bottom profile to a depth of about 100 m (Fig. 3). It helps to identify areas covered by nodules, types of sediments as well as bottom relief and potential obstacles, that may limit future mining. The device is towed behind a reconnaissance vessel 80 to 120 m above the seabed.

Photo and video profiling

Photo and video profiling (Fig. 4, Fig. 5) provides information for the analysis of bottom coverage by nodules

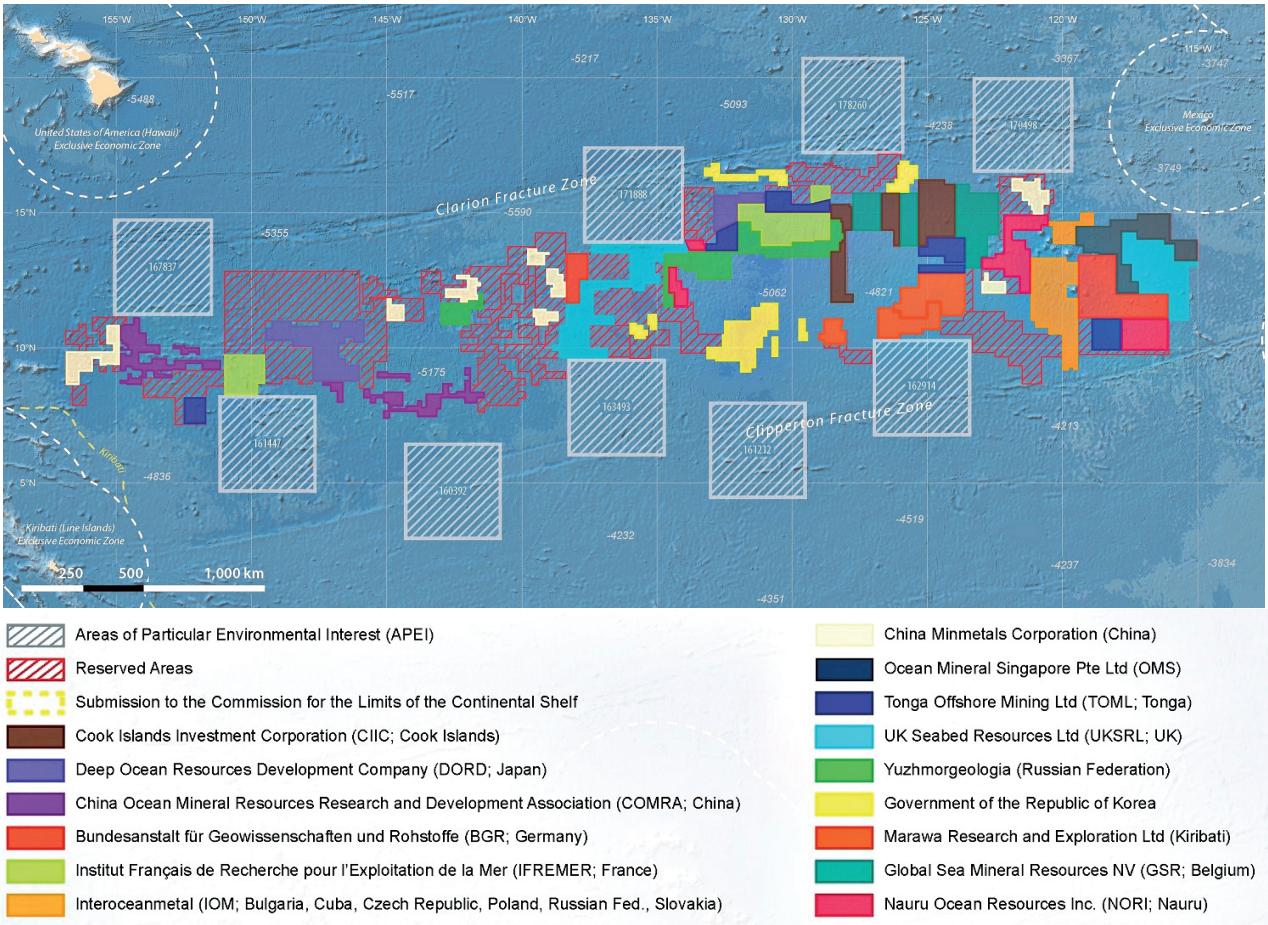


Fig. 1. The outlines of exploration areas in the Clarion-Clipperton Zone at the end of the first contract period between the ISA and IOM (https://www.isa.org.jm/map/clarion-clipperton-fracture-zone, 2016).

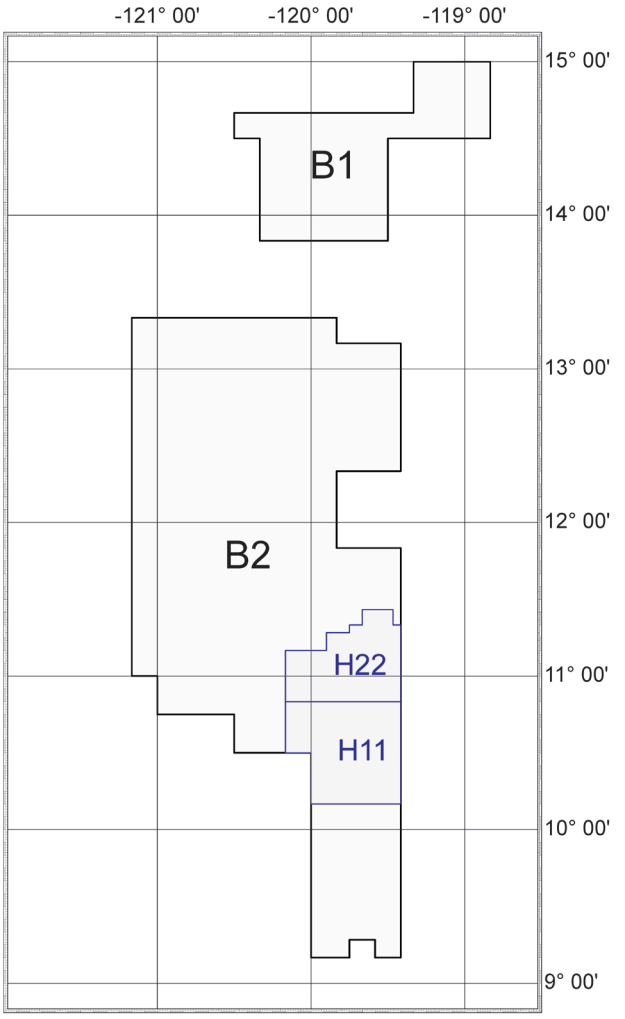


Fig. 2. IOM exploration area (B1 and B2 – sectors, H11 and H22 – exploration blocks).

(individual images of the bottom) and the identification of zones with the occurrence of PMN, as well as the identification of obstacles to potential mining (continuous video recordings). The device is towed behind a research vessel about 4 m above the seabed, individual images cover about 5 m^2 of the seabed.

Following seabed sampling systems were applied during the exploration expeditions (contact methods):

- sampling of PMK and sediments using a *box-corer device* to obtain a sample measuring 0.5 x 0.5 x 0.5 m,
- sediment sampling using a *gravity-corer device* to obtain a core sediment sample to a depth of 4 m,
- sampling of large-capacity PMN samples by *trawl* obtaining up to 1 000 kg of raw material per sample.

Laboratory chemical analyses and geotechnical measurements were performed by standard methods. Basic analyses and measurements requiring immediate sample processing were performed on board of the research vessel during the shipment.

Geotechnical measurements

Geotechnical measurements of the physical and mechanical properties of the sediments (eg water content, bulk density, rip-off force resistance, vane shear strength, penetration resistance, residual strength) and polymetallic nodules (water content, bulk density, apparent density, compression strength) were performed in the on-board laboratories of the research vessel. Sediment measurements were performed on intact samples directly in the sampling device (box-corer), by cutting with cutting rings in the geochemically active layer (core sample diameter 50 mm,

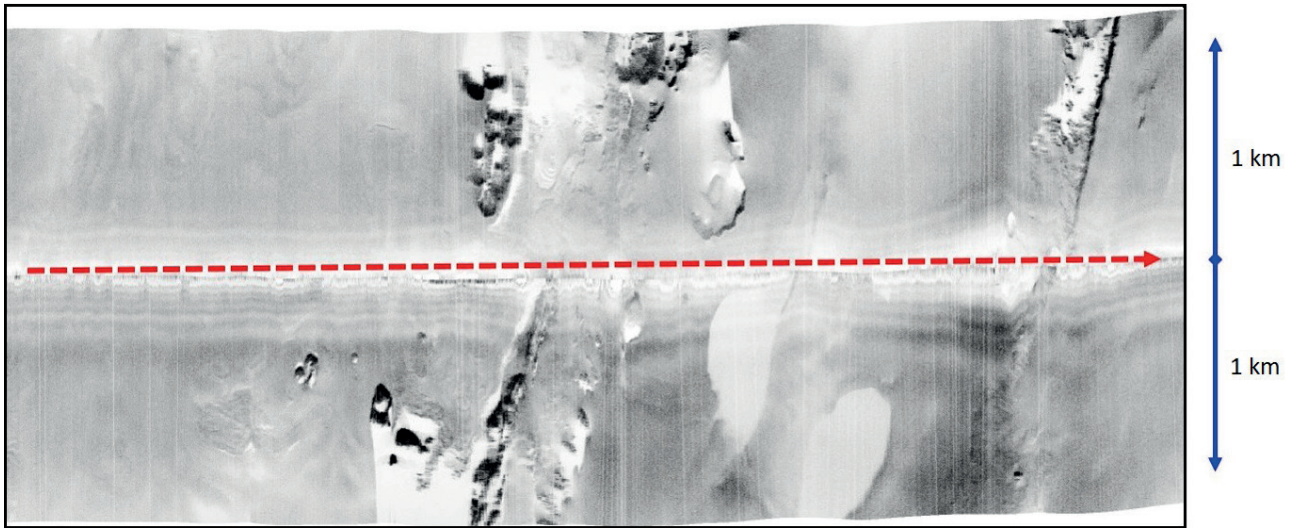


Fig. 3. Example of detailed mapping of the seabed using the side-scan sonar (red arrow – direction of sonar towing, approx. 100 m above the seabed).

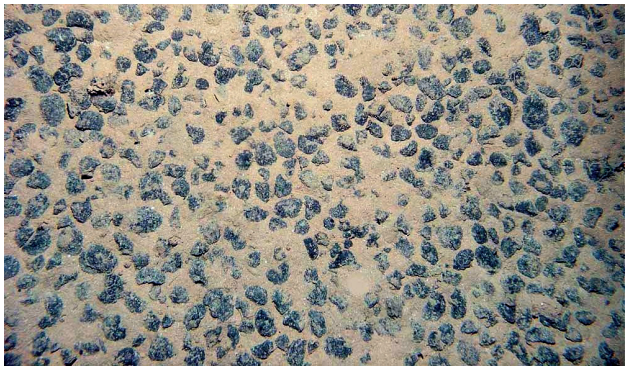


Fig. 4. Section of seabed photo showing high nodule abundance, low blanketing (nodule size 2–8 cm, camera positioned approx. 4,5 m above seabed.

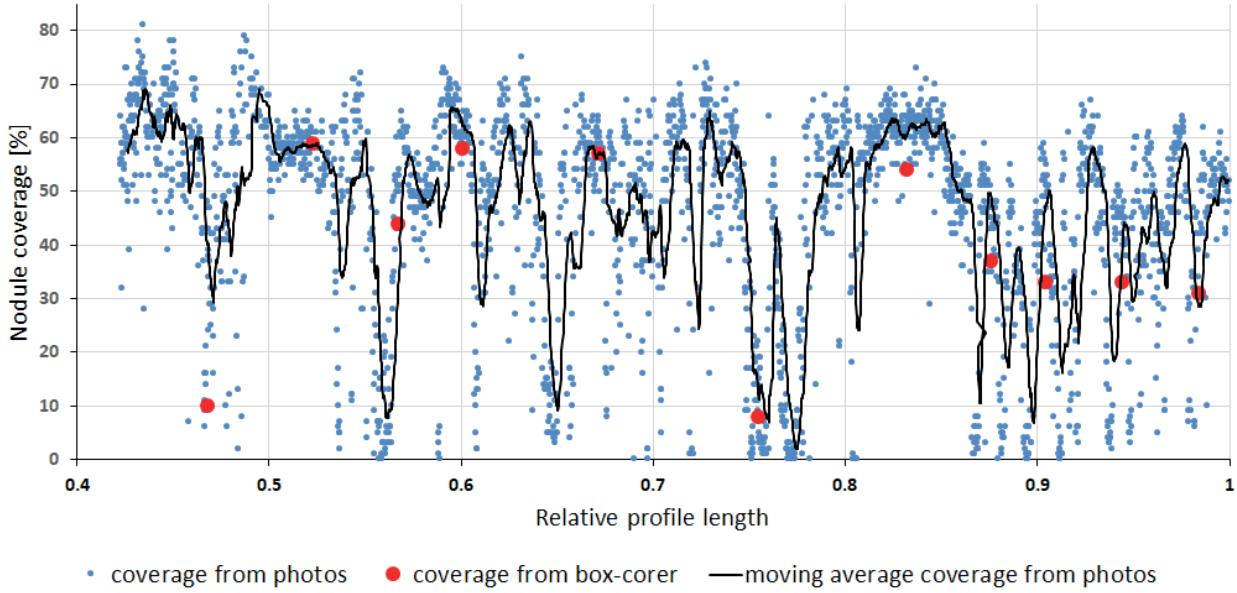


Fig. 5. Demonstration analysis of bottom nodule coverage within the photoprofile No.710.

height 25 mm) and in the underlying sediments (diameter 70 mm and height 50 mm). Depending on the amount of sediment in the sample box, depth intervals 2–5, 10–15, resp. 25–30 cm were tested. PMN samples for analysis were selected from the predominant morphological types and fractions. The determination of the parameters of the physical properties of the nodules was performed in accordance with the methodological recommendations (Andreev, 1994).

Laboratory analyses

Analyses were performed in on-board and land laboratories. The metal content of the samples taken was determined by various methods, including atomic absorption spectroscopy and X-ray fluorescence. Standard methods and equipment were used to determine the pore water content of the sediment (centrifuge, polycarbonate filter device with vacuum pump), pH and Eh values (electrodes, calibrated pH-meter/ionometer), opal SiO_{2am} content (spectrophotometry), metal content in the sediment (atomic absorption spectroscopy), As content (inverse voltamperometry), calcite and dolomite content, organic carbon, concentrations of nitrites, nitrates, phosphates and silicates in porous water (special laboratory measurements and spectrophotometry) and metal contents in pore waters (inverse oltamperometry). All measurements were performed using certified methodologies and standard.

Geotechnical measurements of sediments and nodules included the determination of bulk density, water content, dry unit weight, porosity, void ratio and specific density (using the pycnometric method).

Results

The presented results include data relevant for the estimation of resources in the examined area. At the same time, they represent a basic set of data for other purposes, such as the planning of potential exploitation and processing of raw materials, as well as environmental impact assessment.

Overview of expeditions made in the period 2001–2016

Prior to the signing of the exploration contractt between the ISA and IOM in 2001, 21 research expeditions to the CCZ area were made. In the first phase of the contract (2001–2016), 4 expeditions were organised. The work

was carried out in accordance with the five-year action programs approved by the ISA. The work included a geological survey focused on determination of PMN abundance, nodule coverage, determination of metal content and chemical composition of PMNs and seabed sediments, study of their geotechnical properties as well as collection of basic oceanographic, meteorological and environmental data.

Data sets and samples obtained within expeditions during the contract period (2001–2016):

IOM-2001
- 262 km of photo and video profiles (12,540 seabed photos)
- 103 samples of sediment and nodules taken using a box-corer
- 8 samples taken using a gravity-corer
- 700 kg of nodules taken by the trawl
- 44 samples of sediment for pore water and other research
- 110 biological samples

IOM-2004
- 158 samples of sediment and nodules taken using a box-corer
- 250 kg of nodules taken by the trawl
- 2 samples of bedrock (basalt) taken by dredging

IOM-2009
- 295.8 km of seabed profile mapped by side-scan sonar
- 344.3 km of photo and video profiles (13,945 photos)
- 51 samples of sediments and nodules taken using a box-corer
- 740 kg of nodules taken by the trawl

IOM-2014
- 57.2 km of seabed profile mapped by side-scan sonar
- 584.5 km of photo and video profiles (12 profiles, 32,209 photos)
- 52 samples of sediments and nodules taken using a box-corer
- 2 309 kg of nodules taken by trawl
- 94 biological samples

The results of the survey were summarized after particular expeditions in reports on geological and environmental research, in semi-annual reports for IOM Council meetings as well as in annual reports for the ISA. An overview and results of previous survey work have been summarized in a technical report (Szamałek et al., 2016).

Seabed topography

In 1999, before the start of the 15-year contract period, the IOM carried out a bathymetric mapping of the entire exploration area (sectors B1 and B2). The result of the measurements is a bathymetric map of the seabed, compiled at a scale of 1 : 200,000. The map was compiled with isobat intervals of 25 m.

Lithology and stratigraphy

The studied area is formed by volcanic bedrock (basalts) and mainly clayey-siliceous-calcareous sediments. The sedimentary cover in the CCZ is a mixture of carbonates (e.g. carbonate oozes), red brown clays, and siliceous sediments (siliceous oozes, and siliceous-argillaceous oozes). At the scale of the whole CCZ, the sediment lithofacies exhibit unidirectional gradient trending from predominant carbonate sediments in the SE extreme to predominant red brown clays, and siliceous-argillaceous oozes in the WNW (Kotliński et al., 2009). The sediment cover is characterized by a gradual decrease in the age of sediments, from the Late Cretaceous to the Quaternary, and a gradual decrease in their thickness towards the east, from about 300 m to about 100 m (Kotliński, 2011). Sediment accumulation in the area does not exceed the rate of 10 mm/1,000 years. Participation of the silica-clay ingredients of sediments has been increasing since the Miocene. Changes in the lithodynamic conditions has led to periodic activation of erosional processes on the seabed (ISA, 2010b).

Based on the origin and composition, the bottom sediments within the IOM exploration area can be divided into the following four litho-stratigraphic units (Kotliński, 2010):
- F_{MI} (Oligocene–Miocene) – the lowest lithofacies consisting of biogenic calcareous ooze (foraminifera silty clay and coccolith-foraminifera silty clay – products of primarily biogenic accumulation); the lithofacies thickness is 70 cm and the amorphous silica content amounts to 1.36–7.75 %;
- F_{MII} (Miocene) – represented by X-ray amorphous radiolarian silty clay; the sediments are biogenic, pelagic and detrital, and are partly produced by halmyrolysis and partly by erosion of basalt; the lithofacies is max. 255 cm thick, its amorphous silica content amounts to 0.9–16.3 %;
- F_{CIIII} (Miocene–Pliocene) – includes zeolitic clay (phillipsite) or reddish brown clay and denser zeolitic crusts; the zeolitic clay layer is max. 273 cm thick, and its amorphous silica content ranges between 0.48 and 8.8 %;

– F_{CIIV} (Pleistocene–Holocene) – consists of siliceous silty clay, ethmodiscus clay and calcareous silty clay; its upper max. 41 cm thick layer gradually transits with depth into lighter-coloured sediment with a mottled appearance; this section is of biogenic and detrital origin, the total thickness is more than 5 m.

Sediments of lithofacies F_{MI} and F_{MII} are associated with the Marquise Formation (Oligocene and Miocene age), the sediments of lithofacies F_{CIII} and F_{CIIV} represent the Clipperton Formation (mostly Pliocene–Holocene age).

The maximum thicknesses of the respective lithostratigraphic units, obtained by the sampling device, and selected chemical-physical properties of bottom sediments in the IOM exploration area are given in Tab. 2. The sedimentary cover within the IOM exploration area is about 100 m thick (Dreiseitl & Kondratenko, 2012). The sediment profile is topped by slightly siliceous silty clay and siliceous silty clay. The top 1–15 cm layer comprises the geochemically active layer (GAL), which is the medium for nodule formation. Sediments of this layer contain 3.04–28.6 % of amorphous silica and are characterised by reduced bulk density and increased moisture content.

Seismic acoustic profiles of the seabed (to a depth of about 100 m) provide data for the identification of geoacoustic complexes. Interpretation led to distinguishment of four geoacoustic facies (units) within the eastern part of the CCZ (Kotliński & Tkatchenko, 1997):

A – the upper acoustically transparent layer (sedimentary unit of Quaternary to late Miocene age),
B – the upper stratified (acoustically semi-transparent) layer (sedimentary unit of late Miocene to early Miocene age),

Tab. 2

Chemical-physical properties of bottom sediments in the IOM exploration area (Kotliński, 2010).

Litho-stratigraphic units, age	Litofacies	Origin	Thickness [cm]	pH	Eh [mV]	SiO_{2am} [%]	$CaCO_3$ [%]	C_{org} [%]	Fraction < 4 µm [%]	Water content w [%]	Bulk density ρ [g/cm³]
F_{CIIV} Pleistocene–Holocene	**Geochemically active layer** (siliceous silty clay, slighlty siliceous clayey silt)	eluvial-deluvial	1–15	6,47–8,17	343–622	3,04–28,64	< 14,1	0,13–0,78	5,1–88,6	248–470	1,15–1,23
	(siliceous silty clay/clayey silt)		41	6,87–8,14	390–666	2,10–25,67	< 9,60	0,09–0,75	6,1–86,0	210–437	1,16–1,28
			480	7,27–7,81	422–600	1,73–32,15	< 0,976	0,02–0,31	30,6–84,7	205–309	1,20–1,28
	Biogenic ooze/ silty clay (Ethmodiscus silty clay)	deluvial-solifluction	39	7,19–8,05	396–592	13,78–32,54	< 0,083	0,21–0,40	71,9–84,3	224–434	1,16–1,24
	(slightly calcareous silty clay)	eluvial-deluvial	24	7,42–8,31	443–584	7,95–12,1	5,09–9,67	0,40–0,68	64,9–81,3	265–424	1,17–1,23
	(calcareous silty clay)		29	7,10–7,88	427–561	6,51–10,74	10,0–47,0	0,19–0,84	49,9–72,0	247–335	1,20–1,25
F_{CIII} Miocene–Pliocene	**Pelagic clay** (reddish brown clay, zeolithic clay and zeolithic crust)	eluvial	408	7,01–7,96	389–615	0,48–8,80	< 3,178	0,02–0,75	47,6–88,4	85–303	1,16–1,60
F_{MII} Miocene	**Biogenic** (siliceous silty clay, radiolarian clayey silt)	eluvial	255	7,19–8,02	476–625	0,90–16,29	< 4,767	0,05–0,15	38,9–80,2	255–599	1,12–1,25
F_{MI} Igocene–Miocene	**Biogenic** (calcareous ooze, calcareous silty clay)	biogenic	70	7,47–8,09	505–625	0,50–7,75	18,40–71,14	0,01–0,23	45,1–78,9	150–165	1,33–1,37

C – the lower acoustically transparent layer (sedimentary unit of early Miocene age),

D – the basement composed of tholeiitic basalt.

The A, B, C and F geoacoustic complexes, identified on the basis of side-scan sonar profiling (Fig. 6), correspond to the seismic A, B, C and F acoustic units described above. Thickness of unit A is on average 10 m and does not exceed 20 m, which is related to topographic variations of the ocean floor, as well as to the deep-sea currents affecting the erosion processes.

Interpretation of eight gravity corer stations (expedition IOM-2001) is shown in the form of profile (Fig. 7). The seventh sampling tube encountered basalt exposure (without sampling).

Sediment properties

Physical and chemical properties of sediments play major role in evaluating protection and preservation of the marine environment. Physical properties of sediments

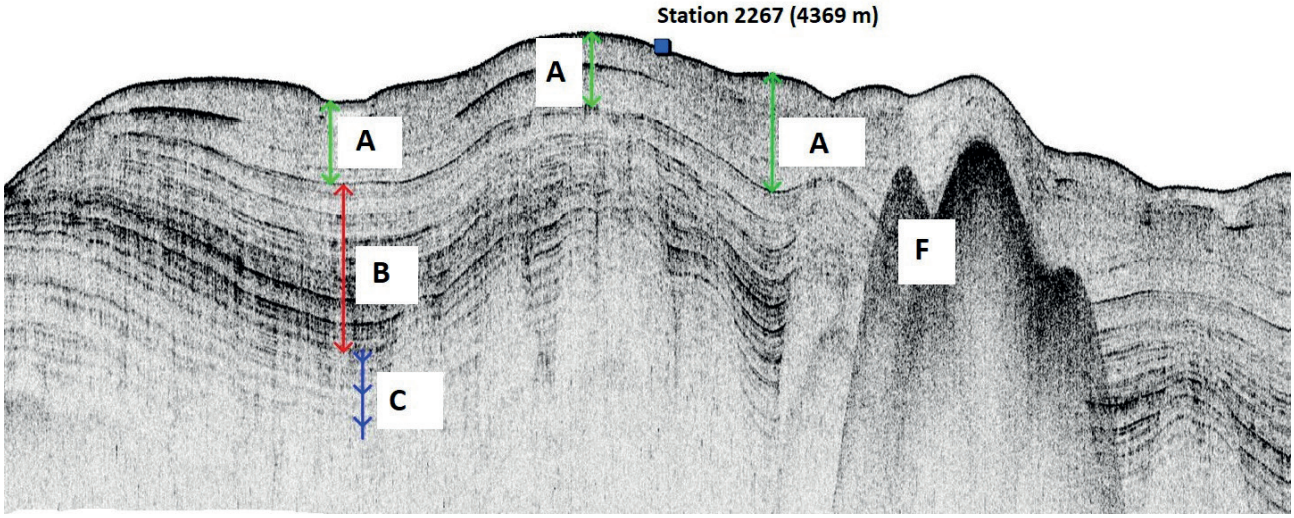


Fig. 6. Interpretation of geoacoustic profile No. 707, fragment 2.7–6.0 km (Dreiseitl & Kondratenko, 2013).

Tab. 3

Physical properties for sediments in the IOM exploration area (Dreiseitl & Bednarek, 2011). Explanations: m – measured value, v – calculated value; data in the reader: min. – max. value, denominator value: number of analyses, ρ – bulk density, w′ – true water content (corrected for pore water mineralization), ρ_d – dry unit weight, n – porosity, e – void ratio, ρ_s – specific density.

Sediment type	**ρ [g/cm³]**	**w' [%]**	**ρ_d [g/cm³]**	**n [%]**	**e**	**ρ_s [g/cm³]**
m/v	*m*	*m*	*v*	*v*	*v*	*v*
Siliceous silty clay	1.17–1.24 208	254–414 218	0.23–0.36 208	86–92 208	6.05–11.23 208	2.48–3.02 208
Slightly siliceous silty clay	1.18–1.28 389	210–404 406	0.27–0.40 389	84–91 389	5.09–10.02 389	2.40–3.07 389
Red pelagic clays with zeolites	1.20–1.33 79	170–302 82	0.31–0.49 79	82–89 79	4.44–7.95 79	2.42–2.86 79
Radiolarian ooze	1.12–1.25 22	255–591 28	0.16–0.35 22	87–95 22	5.95–17.3 22	2.05–3.00 22
Diatom ooze	1.16–1.20 35	319–437 39	0.22–0.29 35	88–92 35	7.66–11.86 35	2.35–2.95 35
Zeolitic crusts	1.32–1.56 14	85–185 12	0.46–0.84 12	70–84 12	2.35–5.11 12	2.46–2.96 12
∑ sum of samples	747	785	745	745	745	745

encountered in the IOM exploration area, with respect to the sediment types, are reported in Tab. 3. Tab. 4 shows Atterberg limit data (the critical water contents of a fine-grained soil) for various sediment types in the IOM exploration area, except for crusts which are impossible to be penetrated by the cone. The results confirm highly plastic and liquid consistencies of the deep-sea sediments.

Mechanical (strength) properties of sediments, useful for future mining operations, are shown in Tabs. 5 and 6. As reported by Dreiseitl (2011), it is estimated that the difference between the values of sediment strength parameters, determined in shipboard lab and in situ is about 28–32 %. Reason thereof is that the deep seabed sediments lose their characteristics after they come onboard in any kind of sampler. The samples taken from the upper layers appear to be well bioturbated, which decreases the sediment's shear strength values.

The variability of physical and mechanical parameters of siliceous sediments in the near-surface layer is mostly dependent on the opal (SiO_{2am}) content in the sediment. The sediment volume density, as well as shear strength, were found to be inversely correlated with the sediment SiO_{2am}.

The redox potential (Eh) of sediments in exploration blocks was determined in on-*board laboratory using combined platinum electrodes with densified electrolyte. The data analyses show that low Eh values (< 450 mV) of the geochemically active layer seem to result in nodule absence due to reduction of Mn^{4+}, which passes to the pore water and remains dissolved within a layer of sediment. On the other hand, high nodule abundances were delineated where Eh was high (> + 500 mV).

The pH values within the examined clays of the H22 exploration block ranged from weakly alkaline (7.50–7.80) to neutral (7.10–7.50). The above values correspond closely with pH values in all of the sediment layers in the H11 block described in 2009 (Kotliński, 2010). They ranged from weakly alkaline (7.60) to neutral (7.14). In general, the upper sediment layers represent relatively elevated pH values.

Tab. 4

Atterberg limits for sediments in the IOM exploration area (Dreiseitl & Bednarek, 2011). Explanations: m – measured value, v – calculated value, data: min. – max. value, LL – liquid limit, PL – plasticity limit, PI – plasticity index.

Sediment type	LL [%]	PL [%]	PI [%]	Number of analysis
m/v	m	m	v	
Siliceous silty clay	116–241	58–121	58–120	7
Slightly siliceous silty clay	110–186	56–96	55–90	18
Red pelagic clays with zeolites	80–277	38–140	42–137	17
Radiolarian ooze	103–357	51–190	52–167	10
Diatom ooze	142	70	72	1

Polymetallic nodules

General model of nodule formation

The polymetallic nodules in the studied area appear on the ocean floor, usually lying in a semi-liquid surface layer. Quite often they are covered with a thin layer of unconsolidated sediments. Polymetallic nodules are composed of both nuclei and concentric layers of iron and manganese hydroxides and oxides. Beside Mn and Fe, also Cu, Ni, Co are the main metal elements present in nodules.

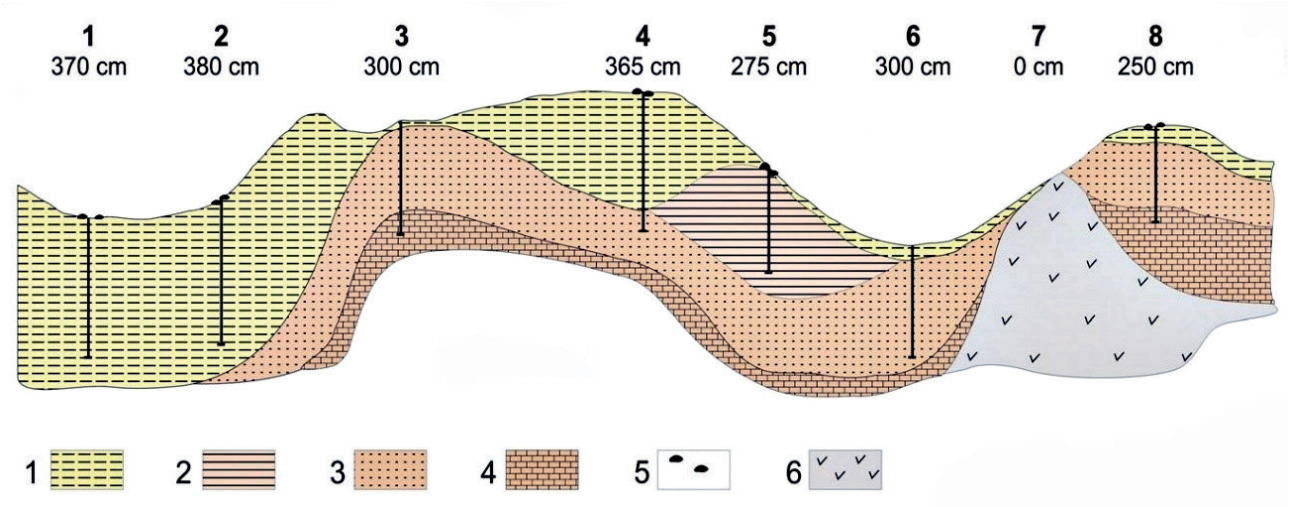


Fig. 7. Geological cross-section of upper layers (up to 4 meters of sea bottom sediments) based on gravity corer sampling (IOM data). 1 – polygenic sediments, 2 – zeolitic clay, 3 – radiolarian oozes, 4 – calcareous oozes, 5 – polymetallic nodules, 6 – basalt.

Tab. 5

Strength characteristics of different types of sediments in the IOM survey area in the depth interval of 10–40 cm, min. – max. values (Dreiseitl, 2011).

Sediment type	Penetration resistance, P [kPa]	Vane shear strength, τ_{max}, [kPa]	Residual strength, τ_{min}, [kPa]	τ_{max}/τ_{min}
Siliceous silty clay	0.7–35.7	1.3–8.3	0.9–4.2	1.2–3.6
Slightly siliceous silty clay	1.5–74.5	1.8–14.3	1.0–5.2	1.2–4.6
Red pelagic clays with zeolites	3.4–41.8	6.9–19.0	1.4–12.0	1.6–3.9
Radiolarian ooze	4.2–37. 1	3.9–16.8	2.1–4.2	1.7–4.0
Diatom ooze	0.9–4.4	0.9–3.1	0.8–1.7	1.1–2.4
Zeolitic crusts	1 400	–	–	–

Tab. 6

Selected physical and mechanical properties of bottom sediments with respect to the exploration blocks H11 and H22 (samples from expeditions IOM-2009 and IOM-2014).

Sediment type	Expl. block	Sampling interval [cm]	ρ [g/cm³]	w [%]	Vane shear strength	Numb. of analysis
Slightly siliceous and siliceous-clayey oozes of geochemically active layer ($SiO_{2am.}$ > 10 %)	H11	2–8	1.16–1.20	327–467	–	20
	H22	2–7	1.17–1.21	323–404	–	31
Siliceous-clayey oozes ($SiO_{2am.}$ > 10 %)	H11	10–30	1.17–1.22	319–397	2.0–4.3	29
	H22	10–30	1.16–1.24	254–387	1.4–7.1	77
Slightly siliceous and siliceous-clayey oozes ($SiO_{2am.}$ 5–10 %)	H11	10–35	1.18–1.23	266–404	1.8–9.4	53
	H22	10–30	1.20–1.25	255–321	2.6–9.1	15
Clayey sediments ($SiO_{2am.}$ < 5 %)	H11	–	–	–	–	–
	H22	25–40	1.23–1.24	270–271	10.54	2/1
Red dep-sea clays	H11	10–30	1.22–1.24	270–298	4.8–9.5	13
	H22	8–44	1.27–1.33	203–231	11.4–14.1	4
Clayey crusts	H11	2–4	1.32–1.42	137–184	–	5
	H22	–	–	–	–	–
Radiolarian oozes	H11	6–20	1.21–1.29	202–321	13.2–13.4	3
	H22	–	–	–	–	–

Occurrences of nodules with such high abundance as in the CCZ result from complex processes present on the regional and on local scales.

According to the way the nodules are structured, the nodules forming metals can be divided into three groups:

- iron exists in the ocean water as colloidal iron oxy-hydroxide particles and mainly supplies the nodule growth, due to dissolution of calcareous skeletons below the CCD zone (ISA, 2010a),
- cobalt accumulates through the hydrogenetic processes that are unrelated to the biogeochemical dependences (Halbach, 1986),
- manganese, nickel and copper are fully dependent on the biogeochemical cycle. The widely accepted model, proposed by Morgan (ISA, 2010a) divides the process of manganese, nickel, and copper delivery into 4 stages: (1) the first stage involves delivery of metals to the ocean from the land (weathering), the ocean ridge of EPR (volcanogenic) and from atmospheric sources. Metals are adsorbed by the surface of fine particles transported, in the form of suspension, by the ocean currents, (2) the second stage involves consumption of the suspended sediment containing metals by zooplankton.

Metals concentrated in fecal pellets (especially Mn) or in plankton shells (after death) fall on the sea bottom, (3) stage three refers to biological reworking of pellets by benthic fauna and its degradation through bacterial metabolic processes. As a consequence, reduced and soluble metals cations are released. During the early diagenesis in the upper layer of semi-liquid sediment, pore water becomes suboxic even to reducing, which intensifies the process and leach metals. Therefore, the pore waters in bottom sediments are strongly enriched in metal ions, (4) the last fourth stage involves only nodule formation during which Mn is oxidized in the uppermost surface layer and forms such manganese minerals (todorokite, birnessite), interstitial layers of which are able to scavenge metals like copper, nickel and others (Morgan, 2012).

According to the growth model for polymetallic nodules in the CCZ presented by ISA (2010b), the following six main factors control the process of nodule growth:

a) metals supply – which is in generally not limited by availability of metals in the sea water and the bottom sediments;
b) nucleus presence (necessary) – nodule nuclei consist of fragments of old nodules, cemented or consolidated sediment, volcanoclastic rocks, fish teeth etc. In fact, all materials which are slightly harder than sediment can serve on the seafloor as nuclei for nodule formation;
c) Antarctic bottom water (AABW) – this current is considered to be a supplier of oxygen and materials becoming nuclei, especially during the Middle to Late Miocene;
d) semi-liquid surface layer (geochemically active layer – GAL) – this is a crucial layer for nodule formation, providing components and chemical environment for their growth;
e) bioturbation – is the mechanism which prevents nodules from fast burial below sediment surface;
f) internal nodule stratigraphy – is a result of the changing geological history of deep-sea sedimentary basins.

What is crucial for supply of metal ions, is the position of growing nodule in relation to the semi-liquid surface layer. There are three widely accepted models of the nodules growth (ISA, 2010b):

– in semi-liquid surface layer – diagenetic (D-type), called R (rough) type because of their complicated morphology;
– on the boundary of sea water and semi-liquid surface layer as a mixed type of hydrogenetic and diagenetic processes (HD-type), called R + S (rough-smooth) type because of their mixed morphology;
– above the sea bottom, on the surface sediments – hydrogenetic (H-type), called S (smooth) type because of their shape.

The nature of the dominant process that controls the nodule growth depends on the distance from the volcanogenic sources of metals (Hein et al., 2013). At close distance to EPR, hydrogenetic growth is possible. However, with increasing distance its role decreases and is gradually replaced by diagenetic processes.

Polymetallic nodules in the CCZ generally grow very slowly, at rates of 1–10 mm/1,000,000 years (Beiersdorf et al., 2003). The average growth rate for H-type nodules is reported to be about 1 mm/1,000,000 years while D-type nodules grow at a rate of about 5–15 mm/1,000,000 years (Amann, 1992; Kotliński, 1998). Some authors indicate that D nodules can grow even 100 mm/1,000,000 years (Seafloor mining, 2014). Such a slow rate of growth indicates that for the nodules to reach the size of centimeters, stable lasting environmental conditions are required. Although also regarded as low, the accumulation rate of sediments within the area is three orders of magnitude higher and stays at a level of several millimeters per thousand years.

Mineral composition

Mineral composition of polymetallic nodules consists of crystalline (mainly manganese oxides) and amorphous (mainly hydrated iron oxides) mineral phases in different proportions, depending on processes responsible for nodule formation (hydrogenetic or diagenetic).

The key manganese mineral components include the following (Burns & Burns, 1977; Usui et al., 1987; Halbach et al., 1988; Kotliński, 1998; 2003):

– todorokite (10Å manganite, buserite), forming probably from dissolved manganese in pore waters during early diagenesis,
– birnessite (7 Å manganite),
– vernadite (δ-MnO_2, birnessite of non-regular structure), poorly crystallized hydrogenetic Fe-Mn oxide.

The major iron component is X-ray amorphous iron oxyhydroxide (δ-FeO(OH)), reported to include goethite, ferroxyhyte, lepidocrocite, akageneite, hematite or ferrihydrite (Kotliński, 1999; Hein & Koschinsky, 2014). Nodules also contain microscopic detrital silicates, feldspar, plagioclases, quartz and phillipsite (Kotliński, 1998). Components, such as aragonite, apathite, amorphous silica (opal), pyroxenes, amphiboles, barite, spinels, rutile, anatase, clay minerals (chlorites, illite and montmorillonite) occur as accessory minerals (Cronan, 1977; Halbach et al., 1982; Piper & Blueford, 1982; Andreev, 1994; Kotliński, 1998). The cement components are represented by clay minerals and zeolites, which mostly occur in the nodules'

nuclei, sometimes as dispersed clusters. Frequently, the content of SiO_2 and Al_2O_3 in nodules reaches the level of 25–30 %. Occasionally, calcite bioclasts can be found (e.g. *Foraminifera*), typically filled with apatite (Kotliński, 1998).

Chemical composition

Polymetallic nodules of the CCZ are characterized by high abundance and high metals content (especially Mn, Ni, Cu, Co, Mo, Zn and REE) as compared to other ocean nodule-bearing fields of potential economic significance (Kotliński, 1998; Kotliński, 2011). The content of elements in PMN depends on the role of hydrogenetic or diagenetic processes. Nodules, in which todorokite predominates, are usually rich in Mn, Ni, Cu and Zn, while nodules, in which vernadite predominates, are rich in Fe, Co and Pb. The average values of the content of the main metals within the IOM exploration area are in the range: Mn 27.64–31.55 %, Ni 1.22–1.30 %, Cu 0.93–1.30 % and Co 0.16–0.20 %.

With the depth increasing from the north to the south, contents of Mn and Cu increase, while the Ni and Co contents decrease. The higher content of Co is characteristic for H and D genetic types of nodules in the northern part. Higher grade of Mn, Cu and Ni is recorded in the D-type nodules collected from the central part, while southwards an increase in the amount of Mn (D-type nodule) is apparent (Abramowski & Kotliński, 2011). Iron together with manganese forms the major component of PMN. The average Fe concentration in the CCZ is close to 6 %.

The results of chemical analysis of the joint sample (10 kg) taken by the trawl in the H22 exploration block are given in Tab. 7. X-ray spectrometry was used to determine Ni, Cu and oxides, AES-ICP was used to determine Co and rare earth elements (Tab. 8), gravimetry was used to determine total sulfur and loss on ignition. The contents of the precious metals Pt, Pd, Au and Ag were below the detection limit of the analytical methods used (AAS-F, ETA-AAS, ICP-MS).

In the CCZ, the nodule ores contain also other metals of economic importance, such as Mo, V, Zn, Li, Zr and REE, that are potential by-products of the major metal mining (Hein, 2012; Hein & Koschinsky, 2014; Halbach & Jahn, 2016). Mo contents are in the range 0,048–0,058 %, Zn 0,124–0,168 %, V 0,045 %, Zr 0,036–0,077 %, Li

Tab. 7

Chemical analysis of a joint sample – H22 exploration block (Mackových et al., 2015).

Parameter	Unit	Mean	Min.	Max.	Standard deviation	Relative standard deviation [%]
SiO_2	[%]	14.40	11.50	15.20	0.70	4.89
Al_2O_3	[%]	4.64	4.19	5.15	0.23	4.96
Fe_2O_3	[%]	8.10	7.74	8.52	0.19	2.31
CaO	[%]	2.37	2.22	2.55	0.07	3.10
MgO	[%]	3.34	3.16	3.47	0.08	2.34
TiO_2	[%]	0.43	0.41	0.44	0.01	2.49
MnO	[%]	41.49	40.50	44.10	0.70	1.69
Na_2O	[%]	3.15	2.90	3.50	0.17	5.29
K_2O	[%]	1.34	1.27	1.46	0.04	3.14
P_2O_5	[%]	0.33	0.30	0.37	0.02	5.31
LOI	[%]	15.67	15.40	16.1	0.19	1.20
S total	[%]	0.14	0.11	0.47	0.06	42.7
Au	[mg/kg]	< 0.01	–	–	–	–
Ag	[mg/kg]	< 1	–	–	–	–
Cu	[mg/kg]	13 059	12 550	13 450	224	1.71
Ni	[mg/kg]	12 903	12 490	13 280	218	1.69
Co	[mg/kg]	1 659	1 603	1 763	38.8	2.34
Pt	[mg/kg]	< 0.1	–	–	–	–
Pd	[mg/kg]	< 0.1	–	–	–	–

Tab. 8

Rare earth content in polymetallic nodules of the IOM exploration area (Franzen & Baláž, 2012; IOM data). Samples analysed in Trondheim and ŠGÚDŠ-GAL. Slovakia (Chemical analysis of a joint sample – H22 exploration block) (n = number of samples) (Franzen & Baláž, 2012; IOM data).

REE	2010				2011		2015 (H22 block)			
	Min. [mg/kg]	Max. [mg/kg]	Mean [mg/kg]	n	PMK 1 [mg/kg]	PMK 2 [mg/kg]	Min. [mg/kg]	Max. [mg/kg]	Mean [mg/kg]	n
Ce	139.6	177.4	163.3	8	332.0	156.0	149.0	170.0	158.0	30
Dy	11.8	15.9	13.9	8	63.1	18.0	16.5	20.1	18.5	30
Er	10.0	13.6	11.8	8	9.6	6.3	8.6	10.4	9.7	30
Eu	–	–	–	–	6.4	3.6	5.2	6.3	5.8	30
Gd	–	–	–	–	24.2	14.9	20.0	24.8	22.3	30
Ho	3.6	4.7	4.2	8	3.8	2.3	2.7	3.4	3.1	30
La	77.9	100.3	89.9	8	89.0	50.0	83.0	93.0	87.5	30
Lu	1.3	1.6	1.4	8	1.4	1.0	1.2	1.6	1.4	30
Nd	96.4	125.7	113.3	8	104.0	62.8	83.6	103.0	92.9	30
Pr	19.9	26.0	23.4	8	25.1	14.7	19.2	24.0	21.4	30
Sm	22.4	28.4	26.0	8	23.9	14.0	22.5	27.8	25.0	30
Tb	3.7	4.8	4.3	8	4.4	2.3	3.4	4.2	3.7	30
Tm	1.3	1.8	1.5	8	1.8	1.2	1.3	1.6	1.5	30
Yb	9.0	11.2	10.2	8	9.6	6.2	7.9	9.4	8.8	30

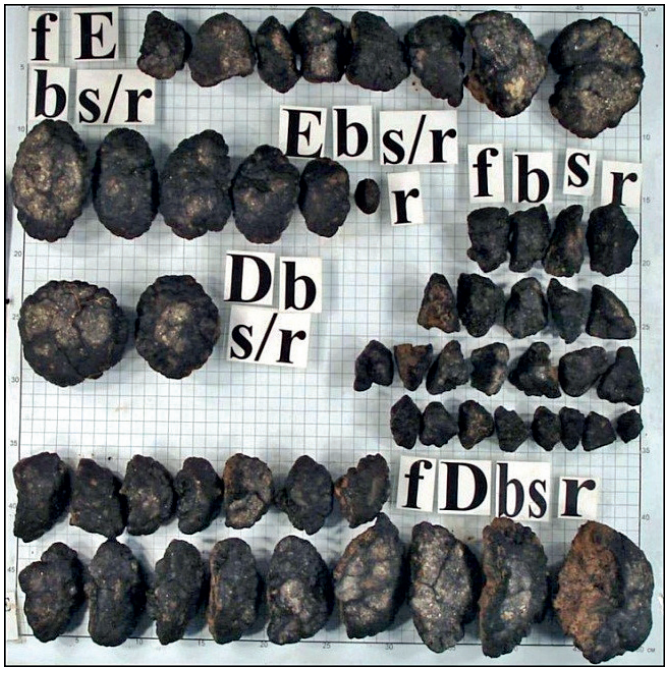


Fig. 8. Morphology of polymetallic nodules. Example of classification according to morphological type. D – discoidal, E – ellipsoidal, b – botryoidal, s – smooth, r – rough, f – fragments.

131 ppm (Hein et al., 2013). Grades of REE in the marine deposits are generally lower than those for the land-based deposits, but in terms of the tonnages they are much greater. Additionally, relative amount of heavy REE (HREEs), which are of higher economic importance than light RRE (LREEs), is quite high when compared to the land ones: HREEs in large terrestrial REE deposits is < 1 %. In PMN it stays for about 26 % of the total REEs (Hein, 2012; Hein et al., 2013; Halbach & Jahn, 2016). The REE grades are related to nodule genetic types: hydrogenetic – the highest, diagenetic – the lowest (Kotliński et al., 1997). Moreover, marine deposits are not contaminated by radioactive elements like Th or U. Results on REE concentrations in the H22 exploration block of IOM exploration area are presented in Tab. 8.

Polymetallic nodules classification

The seafloor polymetallic nodules mostly consist of nuclei and typically concentric layers of iron and manganese hydroxides and oxides. Nucleus can be composed of volcanoclastic debris, lithified sediment, bioclasts or fragments of older nodules.

The following constitute the main morphological nodule types present in the CCZ: discoidal (D), ellipsoidal (E), spheroidal (S), tabular (T), poly-nucleic aggregate (P), botryoidal (B), fusiform (R), irregular (I), fragment of a nodule indicating the morphotype (e.g. fD, fE, fS etc.) and fragments of undetermined morphotype (f). The nodule morphology is conditioned by their mineral composition, nature, size and age of core as well as mechanisms and sources of elements (sea water or pore water) and diagenetic processes (Kotliński, 1998, obr. 8).

The most common nodule textures are: concentric-banding, dendritic, massive and columnar. Layers are frequently cut by other which evidences hiatuses in nodule accretion. Nodules are usually cracked, mostly in radial or tangential pattern. Cracks are effects of internal tension occurring in the processes of dehydration and recrystallization during nodule accretion, or appear as an effect of diagenetic processes. They are usually filled with clay minerals or recrystallized Mn minerals (Kotliński, 1998). The CCZ nodules vary in size from tiny particles visible only under a microscope to large pellets more than 20 centimetres across.

A variety of classifications have been used for polymetallic nodules so far. Those refer to their size and shape, composition and number of cores, thickness of ore crust or mineral and chemical composition of ore material (e.g. Meylan, 1974; Moritani et al., 1977; Halbach et al., 1981; Anikeeva et al., 1984; Haynes et al., 1985; Stackelberg & Beiersdorf 1991; Kotliński, 1998). The one adopted by ISA for the CCZ (ISA, 2010b) defines three main nodule types taking into account their surface features:

- S-type (smooth surface),
- R-type (rough surface),
- S-R type (smooth-rough mixed).

Those refer to the three main genetic nodule types, namely: hydrogenetic (H), diagenetic (D) and mixed hydro-diagenetic (HD). Nodules genetic types are characterized by different mineralogical and chemical composition and different rate of Mn accretion (Tab. 9, Fig. 9).

Nodules of H type have relatively lower average contents of Mn, Ni and Cu and are rich in Fe and Co. In comparison with HD and D types, they are also characterised by higher content of the Rare Earth Elements (Kotliński et al., 1997, 1999). Microcrystalls of vernadite and goethite constitute the main mineral components. The Mn/Fe ratio (modulus), one of the most important parameters in determining nodule genotype, is usually below 4. The nodules have smooth surfaces (S-type), generally spheroidal or irregularly spheroidal of rather small modal sizes, usually below 4 cm in diameter. The nuclei of nodules are mostly represented by volcanic glass, often later transformed into clay minerals (usually zeolites) by halmyrolisis, although fragments of bioclasts are also present. Around the core, laminae of Mn and Fe minerals alternate with clay minerals laminae. The nodules are frequently cracked and characterized by the presence of secondary veins filled with clay or manganese minerals. The growth rate is about 1 mm/1,000,000 years. The H type nodules occur usually on calcareous oozes, above the CCD (Carbonate Compensation Depth).

The D type nodules show higher content of Mn, Ni, Cu and Zn, and lower content of REE. The main manganese minerals are todorokite and birnessite. The Mn/Fe ratio generally exceeds 5. Nodules are usually discoidal or ellipsoidal, with modal size ranging from 6 to 12 or more cm, and are characterized by strongly differentiated or asymmetrical structure with rough surfaces (R-type). Nodules' nuclei are usually represented by fragments of older nodules or bioclasts. The nodules show massive, radial, dendritic or collomorphic texture and are characterized by the presence of radial cracks. Nodules are also characterized by clearly



Fig. 9. Main genetic types of nodules: H – hydrogenetic (smooth surface), HD – combined (smooth surface on top, rough from below) and D – diagenetic (rough surface) (Kotliński, 2011).

Tab. 9

Complex characteristics of polymetallic nodules in the CCZ area with respect to genesis, mineralogy, morphology, size and textures (Kotliński, 2010, modified).

Lithofacies	pelagic red clay, siliceous – argillaceous ooze	siliceous-argillaceous ooze, argillaceous-siliceous ooze	argillaceous-siliceous ooze, siliceous ooze
Genetic (growth) type	H – hydrogenetic	HD – mixed hydrogenetic-diatgenetic	D – diagenetic
Occurence	exposed on sediment surface (extremly low sedimentation rates)	exposed and partly sunken in semi-liquid layer (very low sedimentation rates, biogenic activity)	partly sunken in surface sediment (low sedimentation rates, biogenic activity)
Size [cm]	< 4	4–8	6–12
Surface shape	S (smooth)	S + R (smooth + rough)	R (rough)
Dominant morphotype	spheroidal, polynucleus	elipsoidal, tabular, discoidal, irregular	discoidal, elipsoidal, irregular, fragments
Major Mn-minerals	vernadite (prevalence of amorphous phase, enriched in Fe and Co)	birnessite, todorokite (amorphous and crystalline phases)	todorokite, birnessite (prevalence of crystalline phase, enriched in Mn, Cu and Ni)
Mn/Fe ratio	< 4	4–5	> 5
Nodule abundance	relatively low on avereage	average	relatively higher on average
Nucleus type	multinucleate, volkanoclastic debris and bioclasts	lithified sediments (clayey-zeolitic bioclasts)	fragments of older nodules, micronodules
Lamination – prevalent lamina thickness [mm]	0,1–1,0	0,1–2,0	> 1,0
Texture	columnar	dendritic, concentric banding	concentric banding, dendritic, massive
Physical properties – volume density [g/cm^3] – porosity [%] – nat. water content [%]	 1,97 59 31	 1,94 61 32	 1,93–1,95 62 32

visible alteration of Mn minerals (black lamina) and Fe (red-brown ones), as well as differentiated growth rate – in the case of manganese minerals it is twice as high as in the case of the iron minerals. Ni and Cu concentrations are associated with laminas of Mn, and Fe minerals are often separated by lamina of volcanic silt. Laminas of Mn and Fe minerals are thicker than laminas observed in the H-type nodules and reach 1.5–2.0 mm. The growth rate of these nodules is estimated to be about 5–15 mm/1,000,000 years (Amann, 1992). This type of nodules occurs on the bottom surface immersed in a semi-liquid layer, usually rest on radiolarian diatomaceous oozes, less frequently on polygenic clays below the CCD.

The HD type is intermediate between the D type and the H one, taking into consideration the form, size and composition. Major manganese mineral is birnessite (7 Å manganite), represented by variable ratios of amorphous and crystalline phases. The Mn/Fe ratio varies between 4 and 5. Nodules are often ellipsoidal, tabular or discoidal (flattened) in shape, with the upper surface being smooth and exposed to the sea water, while the lower surfaces is rough (S-R type) and immersed in the semi-liquid layer. The typical surficial feature of the HD nodules is the presence of ring-shaped bulge, formed at the contact zone of the ocean water and the semi-liquid sediment.

Within the IOM exploration area, additional subtype of diagenetic D1 nodules has been described. It is associated with higher concentrations of Cu than of Ni. What is more, the crusts (C) grown on hard substrata were reported (Kotliński & Stoyanova, 2009).

Distribution of genetic types of polymetallic nodules in the IOM exploration area is shown in Fig. 10.

In the B1 sector nodules of a diameter of 2–4 and > 8 cm are predominant. Among nodules of genetic type H, 2–4 cm size dominate, whereas the HD and D types are represented primarily by the > 8 cm fraction (the domination is more distinct among the nodules of D type). In the northern and central parts of the B2 area nodules which are 2–4 and > 8 cm in size dominate, while in the south nodules 2–4 cm in size prevail. Nodules of H and HD genetic types are represented mainly by the 2–4 cm fraction. Among type D, 4–6 and > 8 cm size nodules dominate, while among type

D1 all fractions show a virtually homogenous distribution. There is no clear relationship between the nodule size distribution and the depth they were found.

Nodule distribution

Although nodules usually occur on the seabed surface (immersed in the semi liquid active sediment layer), they are frequently blanketed by contemporary sediments in the eastern part of the CCZ. This phenomenon is observed at about 70 % of the sites examined within the IOM exploration area. In general, the blanketing extent increases with depth from the north to the south (Abramowski & Kotliński, 2011).

To describe the blanketing intensity quantitatively, an index of blanketing (blanketing coefficient) was developed. It is expressed by a ratio between the area covered by nodules on a template to the area covered by nodules calculated from the photograph of the bottom at the actual sampling station. The lowest parameter values amount to 1 (no blanketing), whereas at some stations the blanketing level of 100 % is observed.

In relation to the morphology, stations with high nodule abundance were found on all types of seafloor morphology. When compared with horst slopes and trough slopes however, it appeared that clearly greatest number was found on flat terrain (undulating plains).

Within the IOM exploration area nodules appear at a depth range of 3,800–4,750 m, with the highest abundance and frequency recorded at the depth range of 4,300–4,500 m. Some regularities can be linked with the critical depths of calcium compensation – CCD and genetic nodule type (Kotliński, 2003, 2011; ISA, 2010a):

- at CCD of about 4,200 m, there is a dominance of small (< 4 cm), spheroidal nodules of hydrogenic (H) type which are characterised by smooth surfaces, higher content of Fe (10.32 %) and Co (0.23 %) as well as relatively lower Mn, Ni and Cu rates;
- between 4,200 and 4,400 m hydro-diagenetic (HD) type nodules with high content of Mn (> 30,5 %), Ni and Cu and relatively lower content of Co (< 0.18 %) are predominant;
- below CCD (> 4,500 m) one can find diagenetic (D) nodules, discoidal and ellipsoidal ones of larger size (6–12 cm) and with rough surfaces.

Tab. 10

Basic physical parameters of nodules in the IOM exploration area in respect to the cruises (values in a counter: min-max, value in a denominator: mean, n = number of analysis).

Cruise	Water content w [%]	Bulk density ρ [g/cm³]	Dry nodule density ρ_d [g/cm³]	Porosity n [%]	Void ratio e	Specific nodule density ρ_s [g/cm³]	Natural water content w_n [%]
2001 n = 227	38–69 47	1.70–2.06 1.95	1.01–1.50 1.33	55–68 60	1.21–2.15 1.53	3.08–3.75 3.35	28–41 32
2004 n = 308	38–63 48	1.77–2.08 1.95	1.09–1.50 1.31	54–69 62	1.18–2.18 1.62	3.13–3.65 3.43	28–39 33
2009 n = 173	36–57 46	1.83–2.06 1.97	1.18–1.51 1.35	53–66 61	1.14–1.96 1.57	2.98–3.68 3.46	27–37 32
2014 n = 205	29–71 47	1.77–2.27 1.97	1.03–1.75 1.34	46–72 62	0.86–2.56 1.62	3.05–3.68 3.49	22–42 32

Tab. 11

Basic physical parameters of nodules in the IOM exploration area in respect to nodule genetic types (Coufal & Dreiseitl, 2008; values: mean of n = 514).

Genetic type	Water content w [%]	Bulk density ρ [g/cm³]	Dry nodule density ρ_d [g/cm³]	Porosity n [%]	Void ratio e	Specific nodule density ρ_s [g/cm³]	Natural water content w_n [%]
D	47	1.95	1.33	61	1.57	3.40	32
D_1	49	1.93	1.30	62	1.64	3.41	33
HD	47	1.94	1.32	61	1.55	3.36	32
H	45	1.97	1.36	59	1.46	3.35	31

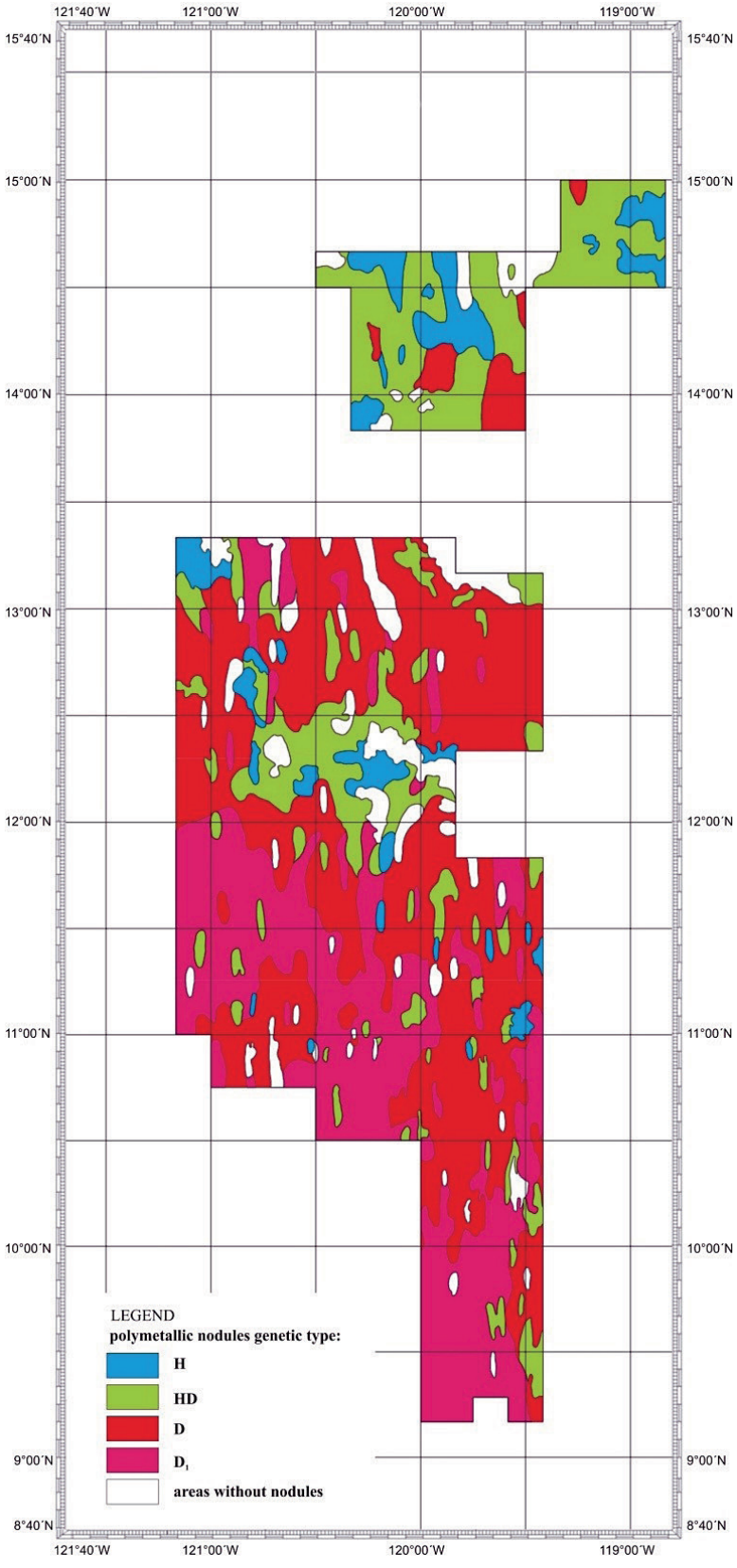


Fig. 10. Distribution of genetic types of polymetallic nodules in the IOM exploration area (H – hydrogenetic, HD – combined, D, D1 – diagenetic type, white color – nodule free areas).

Tab. 12

Nodule uniaxial compression strength in relation to nodule size (Dreiseitl, 2012).

Fraction [cm]	Uniaxial compressive strength [MPa]			Number of trials
	min	max	mean	
0–2	1.80	6.20	3.26	25
2–4	0.38	3.96	1.92	53
4–6	0,24	4.32	1.75	59
6–8	0.24	3.96	1.26	56
8–10	0.33	2.04	0.81	37
10+	0.12	1.48	0.68	17

Generally, in the direction from N to S, the number of H and HD nodules with modal size < 6 cm decreases, while the amount of D-type nodules with a modal size of > 6 cm gradually increases (Kotliński, 2003; Kotliński, 2011). This is reflected also in spatial distribution of metal content.

Geotechnical properties of polymetallic nodules

Physical, mechanical (strength) and technological properties of nodules described below were investigated by IOM in context of future employment of proper mining technology and transportation (Dreiseitl, 2012).

The basic physical properties, which have to be determined on board immediately after the nodules are retrieved from the boxcorer or dredge samplers, are water content and bulk density (volumetric density). In addition, some other properties, such as dry nodule density (drying take place 72 hours at 105 °C), porosity, void ratio, and specific nodule density are calculated. Natural water content (ore based water content, wn) is the ratio of the mass of evaporated water to the mass of wet nodule specimen. While the water content (w) and the natural water content (wn) analysis, the salt content in the sea water present in the nodule pores, assumed as M = 35 ‰, needs to be taken into account. It confirms that the sea water accounts for 1/3 of the total nodule weight, which conclusion may be of major consideration for the loading of cargo ships with nodules. Basic physical parameters of PMN investigated by IOM are presented in Tab. 10 and Tab. 11.

Statistical analysis of physical parameters of nodules shows some relationships in respect to nodule fractions. Small-size nodules are of comparatively low density and high moisture content in relation to larger-size nodules, while the maximum density and minimum water content is observed for nodules of 8–10 cm size-fraction. For nodules of size >10 cm some gradual de-compaction takes place, which is probably related to the increasing age of nodules.

A single mechanical (strength) property, routinely determined in an on-board laboratory is the uniaxial compressive strength, expressed in MPa. The characteristc expresses the amount of stress that needs to be applied to break a nodule. As reported by Dreiseitl (2012), it is not dependent on the nodule genotype, as opposed to the nodule morphotype (spheroidal nodules are harder than discoidal and ellipsoidal ones) and, especially, nodule size (the smaller the nodule, the higher the compressive strength value). Value of the parameter is given in Tab. 12, while Fig. 11 illustrates trends in the uniaxial compressive strength measured during two cruises (2001 and 2004).

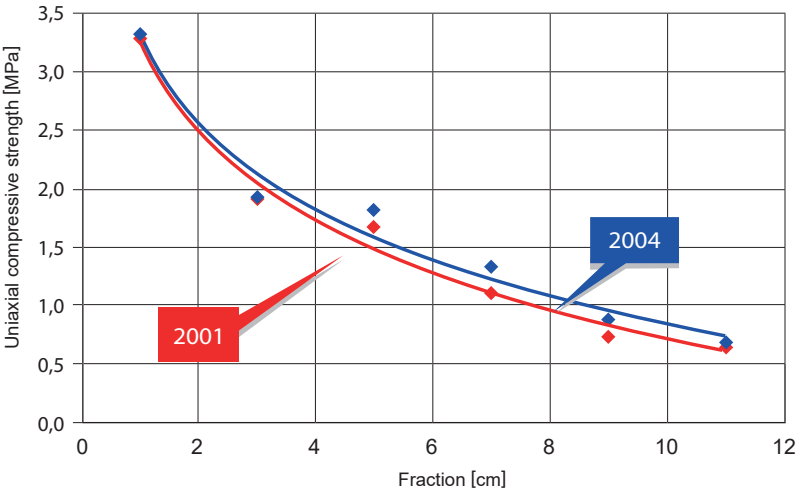


Fig. 11. Uniaxial compression strength of nodule samples obtained during expeditions IOM-2001 and IOM-2004 (Dreiseitl, 2012).

The knowledge on technological properties of nodules is essential for mining and transportation of nodules from

the mine site to an onshore processing plant. The following technological properties were determined in this respect (Dreiseitl, 2012):

– rip off force resistance (kPa);
– nodule apparent density (kg/m^3);
– angle of repose (or slope angle) (°, degree).

The rip off force is the force needed to separate a nodule from the sediment, and is expressed in newtons (N). In practise however, it is the nodule resistance to the rip off force that is being determined. Thus, the area of nodule-sediment contact must be additionally calculated. Therefore, the rip off force resistance is expressed in kPa. The rip off force is determined directly on nodules in the boxcorerr upon retrieval. The characteristic can be of great importance for certain techniques of nodule collection on the sea floor. The analysis shows there is no relationship between nodule morphotype and rip off force resistance, however the maximum values of the rip off force resistance of large nodules (8–10 and 10+ cm) are lower than the maximum values of the medium-sized nodules (4–6 and 6–8 cm). The parameter values in relation to nodule fraction are presented in Tab. 13.

Tab. 13

Rip off force in respect to nodule fraction (IOM-2009 cruise, all morphotypes).

Fraction [cm]	Rip off force resistance [kPa]			Number of trials
	min.	max.	mean	
4–6	0.32	1.78	0.87	34
6–8	0.21	1.72	0.68	72
8–10	0.23	1.16	0.56	26
> 10	0.33	0.84	0.60	5

It is believed that the nodule surface, rough on the bottom and smooth at the top, plays a major role in the resistance, i.e. rough surface increases the force needed for a nodule is ripped off from the sediment when compared with the force necessary to rip off a smooth-surfaced nodule.

The nodule apparent density and angle of repose will be important in loading operations, whereby nodules are loaded onto the transporting vessel. The properties were determined during the processing of the large-volume samples recovered by trawl during IOM-2009 and IOM-2014 cruises (Tab. 14).

The nodule apparent density rapp provides information on the amount (by weight, kg) of nodules that can be places in a 1 m^3 container. The mean apparent density of nodules (cruise IOM-2009, 3 trials) was calculated to be r_{app} = 1,242 kg/m^3. After the container with nodules was shaken and refilled, the maximum apparent density of nodules was r_{appmax} = 1,342 kg/m^3.

The angle of repose was determined as the tangent of the angle α between the height of nodule heap and half-diameter of the heap. The angle obtained for the sample trawled during IOM-2009 cruise was α = 37° and during IOM-2014 cruise α = 31° (Tab. 14).

Tab. 14

Nodule technological parameters – selected results from IOM-2009 and IOM-2014 cruises (mean values).

	Nodule apparent density, max. [kg/m^3]	Angle of repose [stupne]
H11 block (IOM-2009)	1.342	37
H22 block (IOM-2014)	1.229	31

Nodule abundance

Nodule abundance can be estimated in two ways:

– from ground-truth data by simply dividing the weight of recovered nodules by the surface area covered by the open jaws of the sampler (~0.25–0.5 m^2 coverage);
– by estimating the percentage of nodule coverage of the seafloor using a sonar or photography, and then converting this into abundance using calibration factors.

Both methods give slightly different results, which is caused by many factors including the fact that the blanketed nodules are hardly visible in photographs (Kotliński & Stoyanova, 2009), or the areas examined were of different sizes. Rühlemann et al. (2011) reported correlation between the backscatter values in the second method with the size of nodules rather than with their number.

Nodule abundance is usually given in units of kg/m^2 and mostly refers to wet samples. So far, analysis of spatial distribution of nodule abundance within the CCZ shows its great variability (Morgan, 2009). The nodule abundance within the IOM exploration area varies significantly between 0.1–28.4 kg/m^2.

Description of the deposit

Prospective ore bearing fields for nodule mining have been delineated within the B1 and B2 sectors where wet nodule abundance reaches not less than 10 kg/m^2 and the slope inclination angles do not exceed 7°. The total area amounts to about 33,900 km^2 (Fig. 12). The topography of the seabed has a significant influence on the contours,

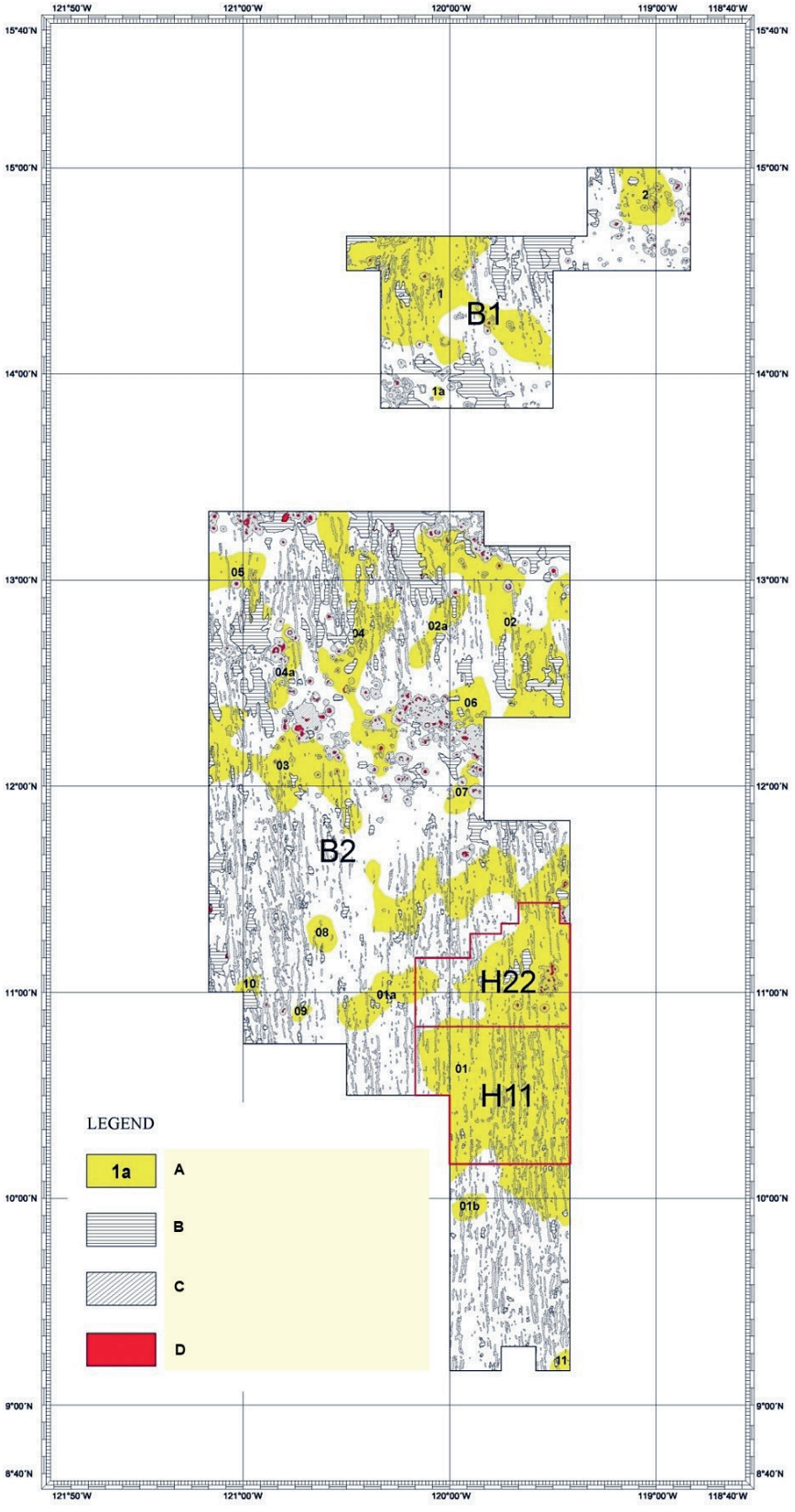


Fig. 12. Ore areas of the IOM exploration area (A – areas with average nodule abundance min. 10 kg/m^2, B – seabed areas with a slope over 7°, C – nodule free areas, D – micro-areas with a high nodule abundance).

sizes and forms of ore deposits. The contours of ribbon-like deposits have a width ranging from 2 to 10 km and reach up to several tens of kilometres in length, generally following the contours of depressions and ridges. Similarly, the mantle-like deposits have widths reaching 70 km and lengths of up to 120 km, and are characterized by large differences in their sizes and variations (Kotliński, 2003).

Within the boundaries of the B2 area, two exploration blocks were delineated: H11 and H22, within the H11 and H22 exploration blocks ore areas have been outlined, which form exploitable blocks: H22_NE, H22_MID, H11_PR2, H11_PR3 and H22_NW. The most promising one is H22_NE, consisting of 4 ore bodies: RZ_09, RZ_10, RZ_11 and RZ_12, an example of ribbon-like ore deposit. The total area of ore bodies is 625.3 km^2. The density of sampling grid is 1 station/31 km^2. The water depth at the sample sites ranged from 4,249 to 4,501 m. The sample-based average PMN abundance is 15.7 kg/m^2(wet conditions). The diagenetic type of PMN is prevalent. Nodules blanketing coefficient ranges from 0 (no blanketing) to 1.6.

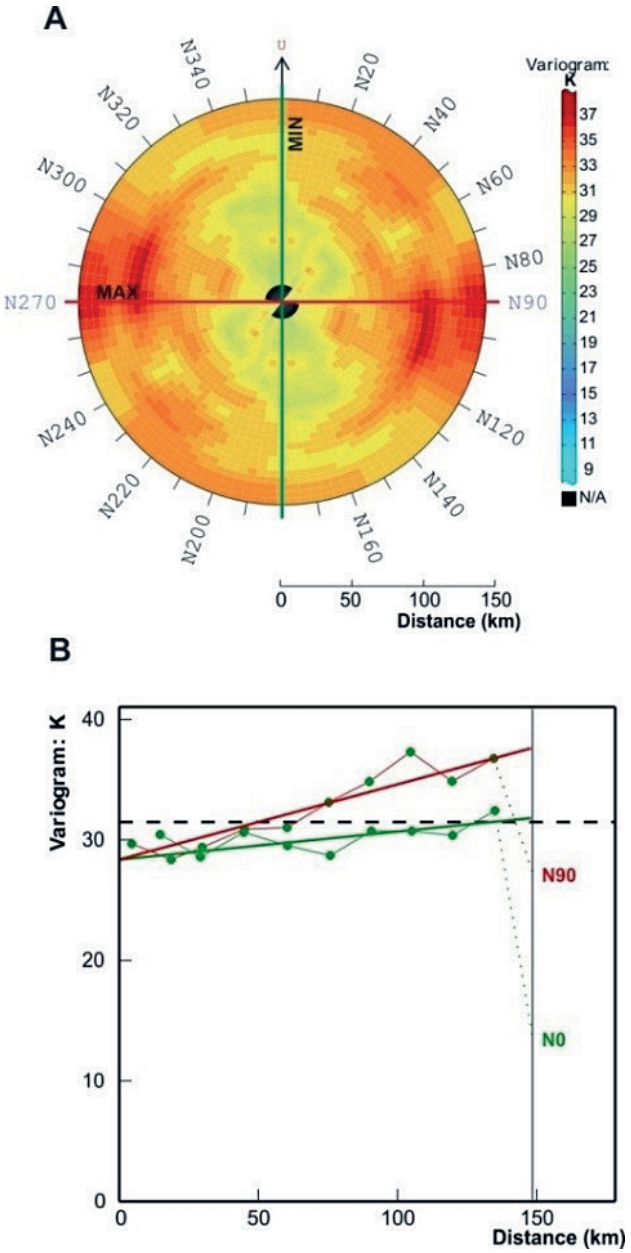


Fig. 13. Directional semivariogram map (A) and semivariogram models (B) for the maximum (red solid line) and minimum (green solid line) variability of nodule abundance in the IOM exploration area (combined data from the B1 and B2 sectors) (Szamałek et al., 2016).

Estimation of resources

The polymetallic nodule resources were estimated in two stages. During the first stage (2007), the overall resources were estimated for both of the exploration sectors B1 and B2, by two working groups (Mucha et al., 2007; Shanov et al., 2007). Both working groups carried out the estimation independently focusing on the resources of polymetallic nodules and selected metals: Mn, Ni and Mo (Group 1) and Co, Cu and Zn (Group 2). The results of this estimate were based on data obtained during cruises up to 2004, which focused on regional research. During the second stage (2011, 2015), the resources of nodules and major metals (Co, Cu, Mn and Ni) were estimated within the exploration blocks H11 and H22 in the central part of sector B2. The data source were expeditions organized in 2009 and 2014 and subsequently the resources were estimated (Mucha et al., 2011; Mucha et al., 2015). In 2016, mineral resources were classified according to the CRIRSCO system, and included in the project summary, provided in the technical report (Szamałek et al., 2016).

Only nodules located in the surface layer to a depth of about 10–15 cm are included in the estimation of resources. Deeper buried nodules, which also occur in the IOM exploration area, were not taken into account, due to the assumed mining methods. Due to the high variability (usually an order of magnitude higher than the variability of the metal content), the nodule abundance, given in kg/m^2, is considered to be a key parameter in estimating the mineral resources. The way nodules are placed on the seabed (in the surface layer), defines the deposit as two-dimensional, to which the methodology of resources estimation was adapted.

Estimation method

The resources of polymetallic nodules and metals contained in them were estimated separately in the B1 and B2 exploration areas, and in the H11 and H22 exploration blocks. The estimation of polymetallic nodules, metal resources contained in them and the mean grades of metals within the exploration blocks were accomplished with the

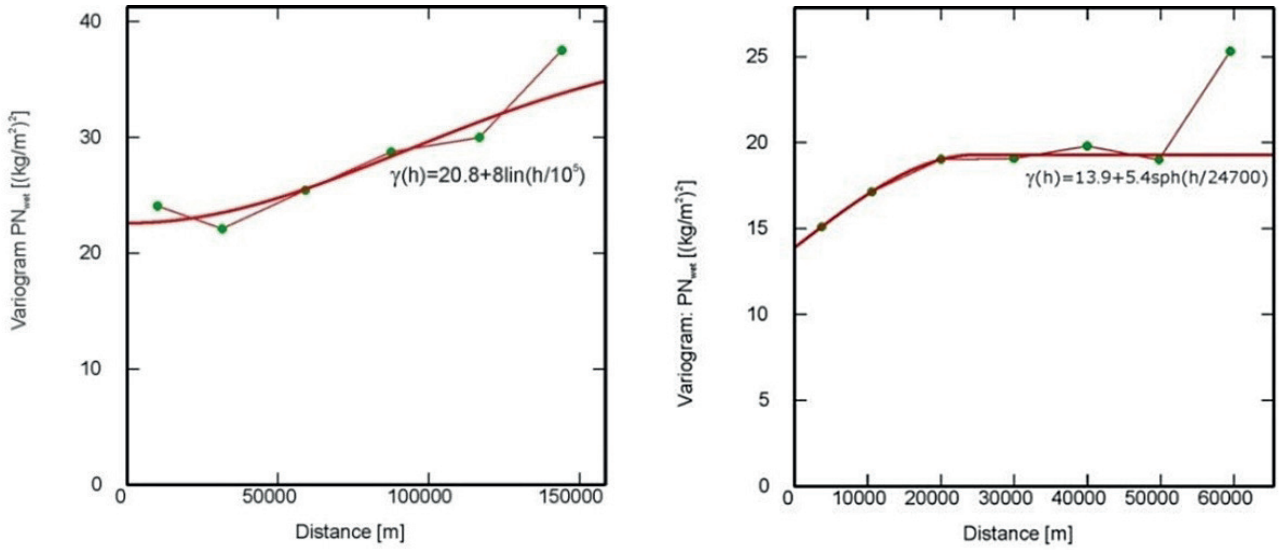


Fig. 14. The empirical omnidirectional semivariograms (green points) of nodule abundance and metal grades, and their spherical models (solid red lines) for data from the H11 (left) and H22 (right) exploration blocks (Szamałek et al., 2016).

geostatistical method of ordinary block kriging (Journel & Huijbregts, 1978; Matheron, 1963) supported by Yamamoto correction (Yamamoto, 2005). Prior to the estimation, the structures of spatial variability of deposit parameters (nodule abundance and metal grades) were modelled using the variography (directional and omnidirectional semivariograms). The estimation was carried out for basic 500 x 500 m calculation blocks located within ore bodies, with the exclusion of barren zones, submarine volcanic zones and zones where the ocean-floor slope exceeded 7°.

The structural geostatistical description of variability of nodule abundance illustrated by directional semivariogram maps for combined data from the B1 and B2 exploration areas reveal weak parameter anisotropy at the large scale of observation, especially for distances over 50 km and strong local variability represented by high nugget effect (Fig. 13). The minimum nodule variability direction is almost aligned north to south, while the maximum variability direction is orthogonal to it and almost east to west. The orientation towards the minimum variability direction is generally parallel to the elongation of particular ore bodies.

In the ordinary kriging procedure the equations of empirical semivariogram models were applied (Fig. 14). The estimation of resources for each calculation block involved the abundance and metal grade values derived from eight closest sampling stations in the search neighbourhood. The total resources of the exploration areas and blocks were obtained by summation of values estimated for basic calculation blocks. Modelling correctness was verified with the cross-validation procedure (Isaaks & Srivastava, 1989).

The average values of nodule abundance and metal contents for H11 and H22 exploration blocks are given in Tab. 15. The conversion factor from wet to dry nodules is 0.7. The values of the standard error of estimation of sources for the cut-off value 10 kg/m^2 in the basic calculation blocks are relatively low and reach about 8 % for sector B1, 3 % for sector B2 and 5 % for H11 and H22 exploration blocks.

Tab. 15

Mean values of polymetallic nodule abundances and metal grades in the H11 and H22 exploration blocks, calculated in 500 x 500 m basic blocks for cut-off abundance PNwet = 10 kg/m^2 (Mucha et al., 2011; Mucha et al., 2015).

Parameter	H11	H22
Nodule abundance PN_{dry} (dry nodules) PN_{wet} (wet nodules)	**8,86 [kg/m^2]** **12,65 [kg/m^2]**	**8,30 [kg/m^2]** **12,20 [kg/m^2]**
Cobalt (Co)	0,16 [%]	0,17 [%]
Copper (Cu)	1,29 [%]	1,29 [%]
Manganese (Mn)	31,74 [%]	31,04 [%]
Nickel (Ni)	1,31 [%]	1,30 [%]

The abundance/tonnage curves for H11 and H22 exploration blocks are shown in Fig. 15 and Fig. 16.

An example of the nodule abundance map in the H11 exploration blocks is shown in Fig. 17. The nodule abundance and metal contents were estimated in basic calculation blocks with dimensions of 500 x 500 m. Nodule free areas, volcanic zones and areas where the slope of the ocean floor exceeds 7 ° were excluded from the estimation.

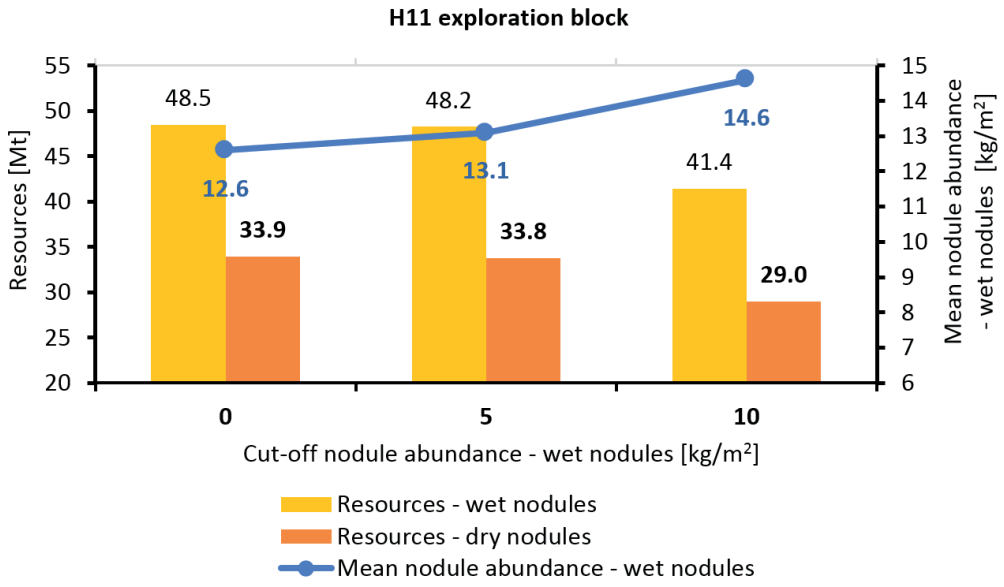


Fig. 15. Nodule Abundance – Tonnage graphs for H11 exploration block.

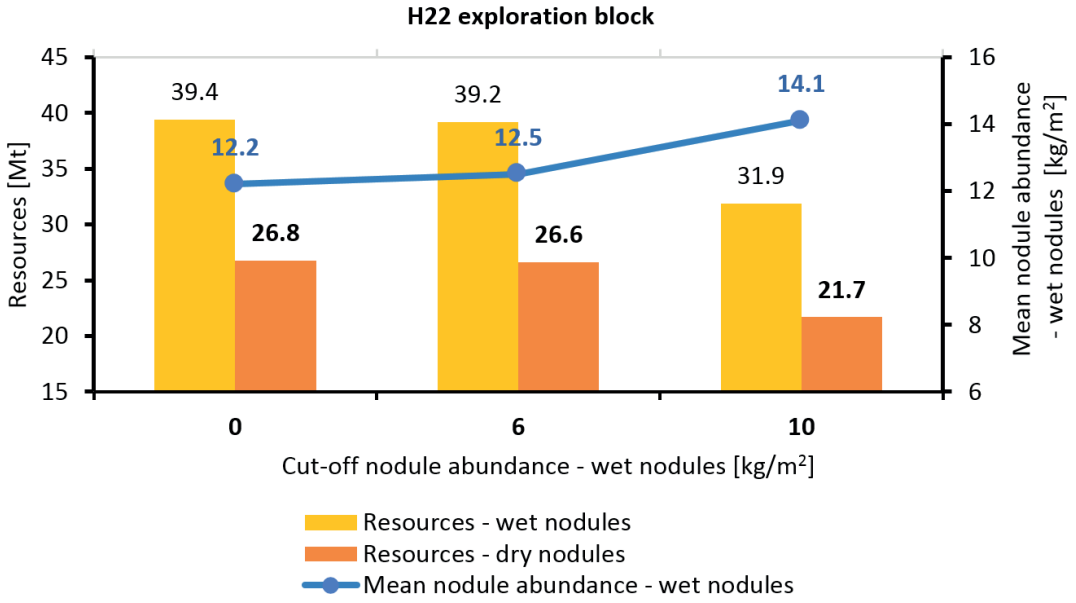


Fig. 16. Nodule Abundance – Tonnage graphs for H22 exploration block.

Resources classification

According to the CRIRSCO directives (Committee for Mineral Reserves International Reporting Standards), the resources of polymetallic nodules can be categorized as "inferred" in the B1 and B2 exploration areas and as "indicated" in the H11 and H22 exploration blocks. Such categorization is justified by different mean sampling intervals within exploration areas and exploration blocks. In the B1 and B2 exploration areas, the mean sampling intervals are 11 and 15 km, respectively. On the contrary, in the H11 and H22 exploration blocks, the mean sampling interval is about 7 km each (Szamałek et al., 2016).

Mineral resource estimate for the IOM exploration area is presented in Tab. 16. The mineral resource estimate at an abundance cut-off of 10 kg/m^2 (wet conditions) is the selected base case scenario considering mining operation. The effective date for the estimate is June 2016. No mineral reserves were estimated at this stage of the project development.

At the current stage of geological prospection, the main factors controlling the accuracy of resource estimates

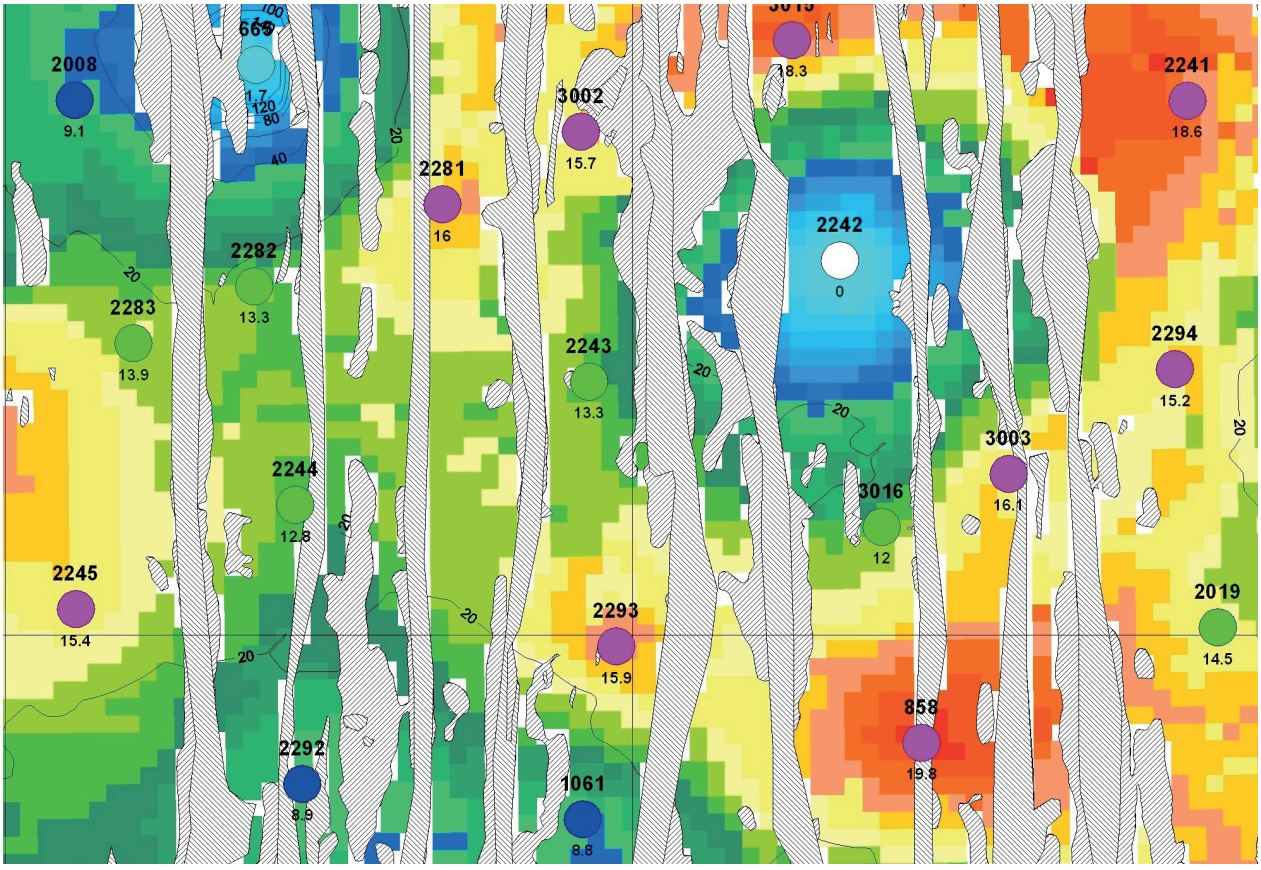


Fig. 17. Section from the nodule abundance map in H11 exploration block. Circular marks represent sampling points using box-corer, particular calculation blocks with 500 x 500 m dimensions are color-coded: cold colors represent low abundances, warm colors high abundances. Blue shades 0–8 kg/m^2, green 8–14 kg/m^2, yellow and red 14–22 kg/m^2. Hatched areas represent areas excluded from the resources estimation: areas with a slope above 7° and nodule free (Mucha et al., 2011).

Tab. 16

Estimation and classification of resources in the IOM exploration area (cut-off value of wet nodules abundance = 10 kg/m^2) (Szamałek et al., 2016).

Resource category (according to CRIRSCO standards)	Abundance, wet conditions [kg/m^2]	Mn [%]	Ni [%]	Cu [%]	Co [%]	Resources, wet condition [mil. t]
Measured	–	–	–	–	–	–
Measured total						–
Indicated (H11 block)	14.6	31.74	1.31	1.29	0.16	41.4
Indicated (H22 block)	14.1	31.04	1.30	1.29	0.17	31.9
Indicated total						**73.3**
Inferred (B1 sector)	13.4	27.84	1.21	0.90	0.21	62.6
Inferred (B2 sector)	13.1	31.53	1.32	1.24	0.18	242.9
Inferred total						**305.5**

of polymetallic nodules are (Szamałek et al., 2016):

- high variability of nodule abundances (coefficient of variation v = 60 %),
- high contribution of random component in the total variability of nodule abundances observed,
- high mean sampling intervals, which are: about 11 km in the B1 area, about 15 km in the B2 area and about 7 km in both the H11 and H22 block.

At the scales of all exploration blocks, the accuracy of resource estimates of polymetallic nodules can be accepted as satisfactory (standard error of about 5 %). At the scale of smaller areas and a mean abundance of wet nodules of about 12 kg/m^2, the expected standard error can be around 10 %. However, for blocks with an area of about 1 km^2, the standard error of the estimate may be significant (over 20 %). For this reason,

in the period of the contract extension after 2016, it was planned to concentrate the sampling points density in the block H22_NE, which was selected for a detailed survey.

The improvement of accuracy of resource estimates, which is particularly important for small fragments of ore bodies, can be expected if:

- more advanced geostatistical methods are applied,
- wider applications of modern photo profiling methods are implemented, which would evaluate nodule abundances based upon images of the sea bottom.

The accuracy of Cu, Co, Mn and Ni grade estimates is highly satisfying in areas of any size due to low variability of metal contents resulted from stable chemical composition of polymetallic nodules. For the future re-categorization of nodule resources into nodule reserves, it is necessary to determine the relationships between the amounts of resources at various cut-off abundances as well as between the mean and the cut-off abundances at various sizes of mining blocks (e.g. areas corresponding to monthly, quarterly or annual production levels).

Conclusions

IOM holds licence over a polymetallic nodule deposit in the CCZ under a contract for exploration of polymetallic nodules signed with the International Seabed Authority. Legal framework for mining and environmental regulations, as a fundamental condition for future deep sea mining activities, is under the development by the ISA.

IOM has sufficient samples of adequate quality and authenticity to define Inferred and Indicated Mineral Resources. The effective date for the estimate is June 2016. Metals of value are manganese, nickel, cobalt, copper and zinc. Other metals of potential value (Mo, Fe, Li, REE) have not been estimated, but in the future, based on processing technology development, could provide added value to the project. Long-term geological survey and exploration confirmed that deposit is widespread and consistent in case of grades – nodule abundance varies more than metal grades. The accuracy of Cu, Co, Mn and Ni grade estimates is highly satisfying in areas of any size, due to low variability of metal contents resulted from stable chemical composition of polymetallic nodules. Mineral Resources were estimated at various nodule abundance cut-offs. Selected base scenario is an abundance cut-off of 10 kg/m^2 (in wet condition).

Indicated Resources in exploration blocks H11 and H22 were selected for the planned preliminary economic assessment. Due to the low degree of verification, Inferred Resources, estimated in the remaining area of sectors B1 and B2, will not be included in the economic assessment. Future activities of IOM will focus on a detailed survey of selected blocks and increasing the category of resources/reserves. Geological data, together with other data obtained during the technological research of mining and processing methods, as well as environmental research, form the basis for the commercial model of deposit utilization in the form of a (pre)feasibility study.

Acknowledgement

Author expresses his thanks to IOM General Director Tomasz Abramowski and IOM experts Ivo Dreiseitl and Jozef Franzen for providing data and consultations. Besides these experts the work of Igor Modlitba in the field of engineering geology is worth to mention. Author is grateful to Dušan Kúšik and Pavel Bačo (State Geological Institute of Dionýz Štúr, Slovakia) for reviewing the primary manuscript.

References

Abramowski, T. & Kotliński, R., 2011: Współczesne wyzwania eksploatacji oceanicznych kopalin polimetalicznych. *Gór. Geoinż. (Kraków), 4, 1, 41–62.*

Amann, H., 1992: The environmental impact of deep-sea mining. Action 1. Polymetallic nodules and their environment. *Research analysis for BGR by THETIS Technology GmbH, Hannover, 19–234.*

Andreev, S. I., 1994: Mietallogienija żeliezomargancewych obrazowanij Tichogo okieana. *VNII Okiengieologija, Niedra, St.-Peterburg, 40–190.*

Anikeeva, L. L, Andreev, S. L, Kazmin, Yu. B., Korsakov, O. D., Egiazarov, B. Kh., Lygina, T. I. & Mirchink, I. M., 1984: Morphology of manganese nodules. In: Manganese nodules of the World Ocean. *Moscow, Nedra, 62–104.*

Beiersdorf, H., von Stackelberg, U. & Wiedicke-Hambach, M., 2003: Scientific challenges related to the development of a geological model for the manganese nodule occurrences in the Clarion-Clipperton zone (Equatorial North Pacific Ocean). In: Establishment of a geological model of polymetallic deposits in the Clarion-Clipperton Fracture Zone of the equatorial North Pacific Ocean. *Proc. Int. Seabed Authority's Workshop held 13–20 May, 2003 in Nadi, Fiji International Seabed Authority (ISA), Kingston, 175–200.*

Burns, R. G. & Burns, V. M., 1977: Mineralogy of manganese nodules. In: Glasby, G. P. (Ed.): Marine Manganese Deposits. *N. Y., Amsterdam, Elsevier, 15, 185–248.*

Coufal, R. & Dreiseitl, I., 2008: Koncepcja podziału dna oceanicznego w strefie wydobywczej Clarion-Clipperton w aspekcie właściwości geologiczno-inżynierskich. XVI seminarium naukowe z cyklu Regionalne problemy ochrony środowiska, Geotechnika w projektach regionalnych Unii Europejskiej na obszarze estuariowym, Szczecin – Praha, 25–33.

Cronan, D. S., 1977: Deep-sea nodules: Distribution and geochemistry. In: Glasby, G. P. (Ed.): Marine Manganese *Deposits. Amsterdam, Elsevier, 15, 11–44.*

Dreiseitl, I. & Bednarek, R., 2011: Physical properties of polymetallic nodules and deep sea sediments, as determined

with different analytical techniques. *Proc. ISOPE – Ocean Mining Symposium, Maui, H.I., U.S.A.*

Dreiseitl, I. & Kondratenko, A., 2012: Geotechnical research in the exploration area of Interoceanmetal, Minerals of the Ocean – 6 & Deep Sea Minerals and Mining – 3, int. conf. *VNII Okeangeologia, Sankt Petersburg, Russia.*

Dreiseitl, I., 2011: The strength characteristics of deep seabed sediment. *Proc. Underwater Mining Institute conf., Hilo, H. I., U.S.A.*

Dreiseitl, I., 2012: Geotechnical properties of polymetallic nodules in the Interoceanmetal (IOM) exploration area. *Proc. Underwater Mining Institute conf., Tongji University, Shanghai, China.*

Dreiseitl, I. & Kondratenko, A., 2013: Geoacoustic and photo-profiling as remote techniques of choice in nodule field exploration. *In: Proc. Underwater Mining Institute conf., Rio de Janeiro, Brazil.*

Franzen, J. & Baláž, P., 2012: Rare Earth Elements in the Polymetallic Nodules – a New Challenge. *Proc. 22th International Offshore and Polar Engineering Conference, Rhodes, Greece, June 17–22, 112–116*.

Halbach, P. & Jahn, A., 2016: Concentrations and metal potentials of REEs in marine polymetallic nodule and Co-rich crust deposits. Deep sea mining value chain: organization, technology and development. *West Pomerania Deep Sea Mining Conference, 18–19 January 2016, IOM, Szczecin, 119–131.*

Halbach, P., Scherhag, I. C., Hebisch, U. & Marchig, V., 1981: Geochemical and Mineralogical Control of Different Genetic Types of Deep-Sea Nodules from the Pacific Ocean. *Miner. Depos., 16, 59–84.*

Halbach, P., Giovanoli, R. & von Borstel, D., 1982: Geochemical processes controlling the relationship between Co, Mn and Fe in early diagenetic deep-sea nodules. *Earth Planet Sci. Lett., 60, 226–236.*

Halbach, P, Friedrich, G. & von Stackelberg, U., 1988: The manganese nodule belt of the Pacific Ocean, Geological Environment Nodule Formation and Mining aspects. *Stuttgart, Enke, 7–254.*

Halbach, P., 1986: Cobalt-rich and platinum bearing manganese crusts – nature, occurrence and formation. In: Johnson, C. J. and Clark, A. L. (Eds.): Pacific mineral resources – physical, economic and legal issues. *Proc. of the Pacific Marine Mineral Resources Training Course, Honolulu, 137–160.*

Haynes, B. W., Law, S. L., Barron, S. C., Kramer, G., W., Maeda, R. & Magyar, M. J., 1985: Pacific Manganese Nodules: Characterization and Processing. *Bull. 679 /U.S. Dept. of the Interior Bureau of Mines, Bull, 1–43.*

Hein, J. R. & Koschinsky, A., 2014: Deep-ocean ferromanganese crusts and nodules. In: Holland, H. D. & Turekian, K. K. (Eds.): Geochemistry of Mineral Deposits. *Treatise Geochem., 13, Elsevier, Oxford, 273–291.*

Hein, J. R., Mizell, K., Koschinsky, A. & Conrad, T. A., 2013: Deep-ocean mineral deposits as a source of critical metals for high- and green-technology applications: Comparison with land-based resources. *Ore Geol. Rev., 51, 1–14.*

Hein, J., 2012: Prospects for Rare Earth Elements from Marine Minerals. *ISA Briefing Paper 02/12.*

ISA, 2010a: A Geological Model of Polymetallic Nodule Deposits in the Clarion Clipperton Fracture Zone. In: Morgan, Ch. (Ed.): A Geological Model of Polymetallic Nodule Deposits in the Clarion Clipperton Fracture Zone. *ISA Technical Study No. 6. International Seabed Authority, Kingston, Jamaica, 1–75.*

ISA, 2010b: Prospector's Guide for Polymetallic Nodule Deposits in the Clarion Clipperton Fracture Zone. In: Morgan, Ch. (Ed.): A Geological Model of Polymetallic Nodule Deposits in the Clarion Clipperton Fracture Zone. *ISA Technical Study No. 6. International Seabed Authority, Kingston, Jamaica, 1–105.*

Isaaks, E. H. & Srivastava, R. M., 1989: An Introduction to Applied Geostatistics. *New York, Oxford University Press, 1–561.*

Journel, A. G. & Huijbregts, Ch. J., 1978: Mining Geostatistics. *London, Academic Press, 1–600.*

Kotliński, R. A. & Stoyanova, V., 2009: Relationship between nodule coverage, morphology and distribution in the Eastern Clarion-Clipperton Zone. Presentation from The workshop on the finalization of the Geological Model of the Clarion--Clipperton Fracture Zone (CCZ) is scheduled for 14–17 December 2009 at the Authority's headquarters in Kingston. https://ran-s3.s3.amazonaws.com/isa.org.jm/s3fs-public/documents/EN/Workshops/2009/VStoyanova2.pdf.

Kotliński, R. A. & Tkatchenko, G., 1997: Preliminary results of IOM environmental research. In: Proc. int. symposium on environmental studies for deep-sea mining. *Tokyo, Metal Mining Agency Japan, 35–44.*

Kotliński, R. A., Parizek, A. & Rezek, K., 1997: Polymetallic nodules – a possible source of Rare Earth Elements. *Proc. 2nd ISOPE Ocean Mining Symposium, Seul, Korea 1997, 50–56.*

Kotliński, R. A., 1999: Metallogenesis of the World's ocean against the background of oceanic crust evolution. *Spec. Pap., 4. Warszawa, Polish Geol. Inst., 1–59*.

Kotliński, R. A., 1998: Surowce metaliczne. In: Depowski, S., Kotliński, R., Rühle E. & Szamałek, K. (Eds.): Surowce mineralne mórz i oceanów. *Warszawa, Scholar, 125–184.*

Kotliński, R. A., 1999: Metallogenesis of the World's ocean against the background of oceanic crust evolution. Spec. Pap., 4. *Warszawa, Pol. Geol. Inst., 1–59.*

Kotliński, R. A., 2003: Relationships Between Nodule Genesis and Topography In The Eastern Area Of The C-C region – Meeting of Scientists for the Preparation of a Programme of Work for the Development of a Geological Model of the Clarion-Clipperton Fracture Zone. *Int. Seabed Authority, Nadi, Fiji, 2003, 203–221.*

Kotliński, R. A., Yubko, V. & Stoyanova, V., 2009: Effects of the structural-tectonic and volcanic processes on formation of polymetallic nodules in the CCZ. Presentation from The workshop on the finalization of the Geological Model of the Clarion-Clipperton Fracture Zone (CCZ). Authority's headquarters in Kingston, Jamaica.

Kotliński, R. A., 2010: Sediments in the Eastern CCZ. Prospector's Guide for the Clarion-Clipperton Zone Polymetallic Nodule Deposits. In: Morgan, Ch. (Ed.): Development of a Geological Models for the Clarion--Clipperton Zone Polymetallic Nodule Deposits ISA. *Jamaica, 2, 5–16.*

Kotliński, R. A., 2011: Polymetallic Nodule Deposits in the Clarion Clipperton Fracture Zone – a source of raw materials in the future (in Polish). *Gór. Geoinż., 35, 4, 1, 195–214.*

Mackových, D., Lučivjanský, P. & Pramuka, S., 2015: Determination of matrix composition of polymetallic nodules on samples taken in the cruise iom-2014, including ree and noble elements. Final report. *Manuscript. Spišská Nová Ves, archive SGIDŠ.*

Matheron, G., 1963: Principles of Geostatistics. *Econ. Geol., 58, 1246 – 1266.*

Meylan, M. A., 1974: Field description and classification of manganese nodules. In: Andrews, J. E. et al.: Ferromanganese deposits of the ocean floor. *Cruise report Mn-74-01 R/V Moana Wawe, Hawaii, Inst. Geophys. Rep. HIG – 74–79, Honolulu, 158–168.*

Morgan, Ch., 2009: Geological Model Project Implementation. Presentation from The workshop on the finalization of the Geological Model of the Clarion-Clipperton Fracture Zone (CCZ) is scheduled for 14–17 December 2009 at the Authority's headquarters in Kingston. https://ran-s3.s3.amazonaws.com/isa.org.jm/s3fs-public/documents/EN/Workshops/2009/Implementation_CM.pdf.

Morgan, Ch., 2012: A Geological Model of Polymetallic Nodule Deposits in the Clarion Clipperton Fracture Zone. *ISA Briefing Paper 01/12, 1–12.*

Moritani, T., Maruyama, S., Nohara, M., Matsumoto, K., Ogitsu, T. & Moriwaki, H., 1977: Description, classification and distribution of manganese nodules. *Geol. Surv. Jpn., Cruise Rep., 8, 136–158.*

Mucha, J. & Wasilewska, M., 2007: Estimation of polymetallic nodule resources of the IOM's exploration area and its nickel, manganese and molybdenum contents using a geostatistical method for available geological data processing (in Russian). *Report, IOM, Szczecin.*

Mucha, J., Wasilewska-Błaszczyk, M. & Yubko, V., 2011: Estimation of polymetallic nodule resources of and its nickel, manganese copper and cobalt contents using the geostatistical method of processing based on the IOM geological data. *Report, IOM, Szczecin.*

Mucha, J., Wasilewska-Błaszczyk, M. & Wójtowicz, J., 2015: Evaluation of the resources of polymetallic nodules and contained metals in the H22 exploration block, and in ore deposits distinguished within the block. *Report, 1–31, IOM, Szczecin.*

Piper, D. & Blueford, R., 1982: Distribution, mineralogy and texture of Manganese nodules and their relation to sedimentation at Domes Site A in the equatorial North Pacific. *Deep Sea Res., 29, 8a, 927–952.*

Rühlemann, C., Kuhn, T., Wiedicke, M., Kasten, S., Mewes, K. & Picard, A., 2011: Current Status of Manganese Nodule Exploration in the German License Area. *Proc. 9th ISOPE Ocean Mining Symp., Maui, Hawaii, USA.*

Sea-floor mining, 2014. In: Marine Resources – World Ocean Review 3. *Opportunities Risks, 54–95.* https://worldoceanreview.com/wp-content/downloads/wor3/WOR3_english.pdf.

Shanov, S., Boikova, A. & Radulov, A., 2007: Estimation of the resources of polymetallic nodules of the IOM exploration area and their content of copper, cobalt and zinc using a geostatistical method for processing the geological data available in IOM. *Report, IOM, Szczecin, 1–48.*

Stackelberg, von U. & Beiersdorf. H., 1991: The formation of manganese nodules between the Clarion and Clipperton fracture zones southeast of Hawaii. *Mar. Geol., 98, 411–423.*

Szamałek, K., Damrat, M., Frydel, J., Kaulbarsz, D., Kramarska, R., Relisko-Rybak, J., Mucha, J. & Wasilewska-Blaszczyk, M., 2016: Technical Report on the Interoceanmetal Joint Organization polymetallic nodules project in the Pacific Ocean Clarion-Clipperton Fracture Zone. *Pol. Geol. Inst. – Nation. Res. Inst., AGH Univ. Sci. Technol., Internal IOM report.*

Usui, A., Nishimura, A., Tanahashi, M. & Terashima, S., 1987: Local variability of manganese facies on small abyssal hills of the Central Pacific Basin. *Mar. Geol., 74, 237–275.*

Yamamoto, J. K., 2005: Correcting the smoothing effect of ordinary kriging estimates. *Mathem. Geol., 37, 1, 69–94.*

Výsledky prvej fázy geologického prieskumu hlbokomorských polymetalických konkrécií v prieskumnom území Spoločnej organizácie Interoceanmetal (2001 – 2016)

Spoločná organizácia Interoceanmetal (IOM) vykonáva geologický prieskum v prieskumnom území v oblasti zlomového pásma Clarion-Clipperton (CCZ) vo východnej časti Tichého oceánu. Činnosti súvisiace s prieskumom a využívaním nerastného bohatstva morského dna v medzinárodných vodách (za hranicami národnej jurisdikcie štátov) je pod administratívnym dozorom Medzinárodnej organizácie pre morské dno (MOMD), ktorá bola zriadená na kontrolu dodržiavania *Dohovoru OSN o morskom práve* (1982) a *Dohody o uplatňovaní časti XI* uvedeného dohovoru (1994). Organizácia MOMD má v súčasnosti 168 členských štátov vrátane Slovenska a Európskej únie ako celku.

MOMD vydáva záväzné právne dokumenty, ktorými reguluje vykonávanie prieskumu a budúceho využívania morského dna. Zmluva s MOMD poskytuje exkluzívne právo na prieskum územia a uzatvára sa na obdobie 15 rokov s možnosťou predĺženia o ďalšie 5-ročné obdobia. Vykonávateľ prác je povinný predkladať MOMD ročné správy o činnosti. IOM zavŕšil činnosti spojené s 15-ročnou zmluvou v roku 2016, v súčasnosti je kontrakt predĺžený do roku 2021.

Prieskumné územie organizácie Interoceanmetal je spoločné pre všetkých 6 členských krajín: Bulharsko, Kuba, Česká republika, Poľsko, Ruská federácia a Slovensko. Deliť sa bude len prípadný zisk alebo krajina bude

môcť predať svoj podiel v spoločnom podniku. Preto sa plánuje transformácia IOM z prieskumnej organizácie na formu akciovej spoločnosti.

Okrem geologického prieskumu IOM pracuje na výskume technológie dobývania a úpravy hlbokomorských polymetalických konkrécií (PMK), ako aj na environmentálnom výskume.

Lokalita

V rámci pásma Clarion-Clipperton (CCZ) vo východnej časti Tichého oceánu sa prieskumné práva IOM vzťahujú na územie s rozlohou 75 000 km^2 (obr. 1). Prieskumné územie sa v roku 2016 skladalo z dvoch sektorov (B1 a B2) a v rámci sektora B2 boli vyčlenené dva prieskumné bloky, H11 a H22 (tab. 1, obr. 2).

Metodika prieskumu

Z viacerých metód zameraných na prieskum a vzorkovanie polymetalických konkrécií morského dna boli počas expedícií IOM využité nasledujúce dištančné metódy:

Batymetria

Batymetria slúži na meranie hĺbky a mapovanie morfológie dna s využitím multilúčového sonaru (*multibeam bathymetry*) a zároveň poskytuje informácie o charaktere morského dna na základe intenzity odrazeného signálu (*backscatter*). Zariadenie je inštalované na prieskumnom plavidle.

Geoakustické profilovanie

Geoakustické profilovanie sonarom bočného skenovania (*side-scan sonar*) slúži na detailné mapovanie profilu dna v šírke zhruba 2 km a získanie akustického profilu dna do hĺbky okolo 100 m (obr. 3). Pomáha identifikovať oblasti pokrytia konkréciami, druhy sedimentov, ako aj reliéf dna a potenciálne prekážky, ktoré môžu limitovať budúcu ťažbu. Zariadenie je vlečené za prieskumným plavidlom 80 až 120 m nad morským dnom.

Fotoprofilovanie

Foto- a videoprofilovanie (obr. 4, obr. 5) poskytuje informácie na analýzu pokrytia dna konkréciami (jednotlivé snímky dna) a identifikáciu zón s výskytom PMK, ako aj identifikáciu prekážok pre potenciálnu ťažbu (súvislé videozáznamy). Zariadenie je vlečené za prieskumným plavidlom asi 4 m nad morským dnom, jednotlivé snímky pokrývajú zhruba 5 m^2 morského dna.

Kontaktné metódy predstavujú odber vzoriek konkrécií a sedimentov morského dna:

- vzorkovanie PMK a sedimentov pomocou zariadenia *box-corer*, ktorým sa získava vzorka s rozmermi 0,5 x 0,5 x 0,5 m,
- vzorkovanie sedimentov pomocou zariadenia *gravity-corer*, ktorým sa získava jadrová vzorka sedimentu do hĺbky 4 m,
- odoberanie veľkokapacitných vzoriek PMK *vlečnou sieťou*, jedným odberom je možné získať do 1 000 kg suroviny.

Laboratórne chemické analýzy a geotechnické merania sa robili štandardnými metódami. Základné analýzy a merania vyžadujúce okamžité spracovanie vzoriek sa vykonávali na palube prieskumného plavidla počas trvania expedície.

Geotechnické merania

Geotechnické merania fyzikálnych a mechanických vlastností sedimentov (napr. obsah vody, objemová hmotnosť, odpor odtrhnutia konkrécie zo sedimentu, pevnosť v šmyku, penetračný odpor, mechanická pevnosť) a polymetalických konkrécií (vlhkosť, objemová hmotnosť) sa vykonávali v palubných laboratóriách prieskumného plavidla. Merania sedimentov sa robili na neporušených vzorkách priamo vo vzorkovacom zariadení (*box-corer*) vyrezávaním reznými prstencami v geochemicky aktívnej vrstve (priemer jadrovej vzorky 50 mm, výška 25 mm) a v podložných sedimentoch (priemer 70 mm a výška 50 mm). V závislosti od množstva sedimentu vo vzorkovnici sa testovali hĺbkové intervaly 2 – 5, 10 – 15, resp. 25 – 30 cm. Vzorky PMK určené na analýzu sa vyberali z prevládajúcich morfologických typov a frakcií. Stanovenie parametrov fyzikálnych vlastností konkrécií sa uskutočnilo v súlade s *Metodickými odporúčaniami pre štúdium fyzikálno-mechanických vlastností kobaltovo-mangánových kôr svetového oceánu* (Andreev, 1994).

Laboratórne analýzy

Analýzy sa vykonávali v palubných a pozemných laboratóriách. Obsah kovu v odobratých vzorkách bol stanovený rôznymi metódami vrátane atómovej absorpčnej spektroskopie a röntgenovej fluorescencie. Štandardné metódy a zariadenia boli použité na určenie obsahu pórovej vody v sedimente (centrifúga, polykarbonátové filtračné zariadenie s vákuovou pumpou), hodnoty pH a Eh (elektródy, kalibrovaný pH-meter/ionometer), obsahu opálu SiO_{2am} (spektrofotometria), obsahu kovov v sedimente (atómová absorpčná spektroskopia), obsahu As (inverzná voltamperometria), obsahu kalcitu a dolomitu, organického uhlíka, koncentrácie dusitanov, dusičnanov, fosfátov a kremičitanov v pórovej vode (špeciálne laboratórne merania a spektrofotometria) a obsahu kovov v pórovej vode (inverzná voltamperometria). Všetky merania boli vykonané s použitím certifikovaných metodík a štandardných noriem.

Geotechnické merania sedimentov a konkrécií zahŕňali určenie objemovej hustoty, obsahu vody, hmotnosti sušiny, pórovitosti, čísla pórovitosti a špecifickej hustoty (s použitím piknometrickej metódy).

Výsledky

Prezentované výsledky zahŕňajú údaje relevantné na odhad zásob a zdrojov v skúmanej oblasti, plánovanie

potenciálnej ťažby a úpravy suroviny, ako aj hodnotenie dosahov na životné prostredie.

Prehľad vykonaných expedícií 2001 – 2016

Pred podpisom zmluvy o prieskume medzi MOMD a IOM v roku 2001 sa uskutočnilo 21 vedeckovýskumných expedícií do oblasti CCZ. V prvej fáze kontraktu (2001 – 2016) sa realizovali 4 expedície. Práce sa vykonávali v súlade s programami činností na päťročné obdobia, schválenými MOMD. Práce zahŕňali geologický prieskum zameraný na hustotu uloženia PMK, pokrytie plochy dna konkréciami, určenie obsahu kovov a chemického zloženia PMK a sedimentov morského dna, štúdium ich geotechnických vlastností, ako aj zber základných oceánografických a meteorologických údajov a údajov o životnom prostredí.

Výsledky prieskumu sa sumarizovali po jednotlivých expedíciách v správach o komplexnom geologicko-environmentálnom výskume, v polročných správach na zasadania Rady IOM a v ročných správach pre MOMD. Prehľad a výsledky doterajších prieskumných prác boli zhrnuté v technickej správe (Szamalek et al., 2016).

Topografia morského dna

Ešte pred začiatkom 15-ročného zmluvného obdobia (1999) IOM vykonal batymetrické mapovanie celého prieskumného územia (sektory B1 a B2). Výsledkom meraní je batymetrická mapa morského dna zostavená v mierke 1 : 200 000 s izobatovými intervalmi 25 m.

Litológia a stratigrafia

Skúmané územie je tvorené vulkanickým podložím (bazalty) a prevažne ílovito-kremičito-vápenatými sedimentmi. Morské sedimenty v oblasti CCZ reprezentuje zmes karbonátov (hlbokomorské karbonátové kaly – bahná), červenohnedých ílov a kremičitých sedimentov (kremičité hlieny a kremičito-ílovité bahná). Litofácie vykazujú jednosmerný gradientový trend zmeny od prevládajúcich karbonátových sedimentov na jv. okraji zóny až po prevládajúce červenohnedé íly a kremičité sedimenty na zsz. okraji zóny (Kotliński a Stoyanova, 2009). Sedimentárne pokrytie sa vyznačuje postupným poklesom veku sedimentov od neskorej kriedy po kvartér a postupným znižovaním ich hrúbky smerom na východ od zhruba 300 do 100 m (Kotliński, 2011). Rýchlosť sedimentácie v oblasti neprekračuje 10 mm/1 000 rokov. Podiel kremičito-ílových zložiek sedimentov sa zvyšuje od miocénu, zmeny litodynamických podmienok však spôsobujú pravidelnú aktiváciu eróznych procesov na morskom dne (ISA, 2010b).

Sedimenty morského dna v prieskumnej oblasti IOM možno na základe genézy a zloženia rozdeliť na štyri litostratigrafické jednotky (Kotliński, 2010):

- F_M I (oligocén – miocén) – najnižšia litofácia pozostávajúca z biogénneho vápnitého bahna, hrúbka je asi 0,7 m, obsah amorfného oxidu kremičitého je 1,36 – 7,75 %;
- F_M II (miocén) – litofácia reprezentovaná amorfnou rádioláriovou kremičitou hlinkou, sedimenty sú biogénne, pelagické a detritické, čiastočne sú produktom halmyrolýzy a erózie bazaltov, hrúbka je asi 2,6 m, obsah amorfného oxidu kremičitého je 0,9 – 16,3 %;
- F_{Cl} III (miocén – pliocén) – litofácia zahŕňa zeolitovú hlinku alebo červenohnedú hlinku a hustejšie zeolitové kôry, celková hrúbka je 4 m, z toho hrúbka zeolitovej vrstvy zhruba 2,7 m, obsah amorfného oxidu kremičitého je 0,48 – 8,8 %;
- F_{Cl} IV (pleistocén – holocén) – litofácia pozostáva z kremičitého hlinitého ílu, diatómového ílu a vápenatého kremičitého ílu, jeho horná vrstva s hrúbkou zhruba 0,4 m do hĺbky prechádza do svetlejšieho sedimentu, ktorý je biogénneho a detritického pôvodu, celková hrúbka je viac ako 5 m.

Predpokladá sa, že litostratigrafické jednotky F_M I a F_M II predstavujú formáciu Marqueasas (oligocén a miocén), sedimenty litofácií F_{Cl} III a F_{Cl} IV predstavujú formáciu Clipperton (pliocén – holocén). Maximálna hrúbka príslušných litostratigrafických jednotiek zistená vzorkovacím zariadením a vybrané chemicko-fyzikálne vlastnosti sedimentov dna v prieskumnom území IOM sú uvedené v tab. 2. Sedimentárna pokrývka v prieskumnej oblasti IOM dosahuje hrúbku okolo 100 m (Dreiseitl a Kondratenko, 2012). Najvyššiu vrstvu sedimentárneho profilu, ktorá je geochemicky aktívnym prostredím na tvorbu polymetalických konkrécií, predstavuje jemný kremičito-silikátový íl s hrúbkou 1 – 15 cm. Sedimenty tejto vrstvy obsahujú 3,0 – 28,6 % amorfného oxidu kremičitého, vyznačujú sa zníženou objemovou hmotnosťou a zvýšenou vlhkosťou.

Akustické profily morského dna (do hĺbky okolo 100 m) poskytujú údaje na identifikáciu geoakustických komplexov. Interpretácia seizmických akustických profilov viedla k rozlíšeniu nasledujúcich geoakustických jednotiek vo východnej časti CCZ (Kotliński a Tkatchenko, 1997):

A – horná akusticky priehľadná vrstva (sedimentárna jednotka kvartérneho až neskoromiocénneho veku),
B – horná stratifikovaná (akusticky polopriehľadná) vrstva (sedimentárna jednotka od neskorého miocénu do skorého miocénneho veku),
C – dolná akusticky transparentná vrstva (sedimentárna jednotka skorého miocénneho veku),
F – skalné podložie (tholeiitický čadič).

Geoakustické komplexy A, B, C a F identifikované na základe údajov sonaru (obr. 6) zodpovedajú uvedeným seizmickým akustickým jednotkám. Hrúbka komplexu A dosahuje 10 až 20 m, čo súvisí s rozmanitosťou topografie dna oceánu, ako aj hlbokomorskými prúdmi ovplyvňujúcimi procesy erózie.

Interpretácia ôsmich staníc odberu vzorky pomocou zariadenia *gravity-corer* (expedícia IOM-2001) vo forme profilu je znázornená na obr. 7. Siedma vzorkovnica narazila na odkryv bazaltu (bez odberu vzorky).

Charakteristika sedimentov

Chemické a fyzikálne vlastnosti sedimentov majú rozhodujúci význam pri výbere optimálnej metódy budúcej

ťažby (technológia zberu konkrécií a pohybu kolektora po morskom dne) s ohľadom na environmentálne monitorovanie a ochranu morského prostredia. Výsledky meraní fyzikálnych vlastností sú prezentované v tab. 3. Atterbergove limity (kritický obsah vody v jemnozrnnej pôde) pre rôzne typy sedimentov v prieskumnej oblasti IOM (okrem kôry, ktorú nie je možné týmto spôsobom testovať) sú uvedené v tab. 4. Výsledky potvrdzujú vysoko plastickú a kvapalnú konzistenciu analyzovaných hlbokomorských sedimentov.

Mechanické (pevnostné) vlastnosti sedimentov, ktorých charakteristiky je nevyhnutné poznať pri plánovaní budúcej banskej činnosti, sú uvedené v tab. 5 a 6. Odhaduje sa, že rozdiel medzi hodnotami parametrov pevnosti sedimentu určenými v palubnom laboratóriu a *in situ* je približne 28 – 32 % (Dreiseitl, 2011), pretože hlbokomorské sedimenty strácajú svoje vlastnosti po vyzdvihnutí na palubu v akomkoľvek type vzorkovacieho zariadenia.

Fyzikálne a mechanické parametre kremičitých sedimentov vo vrchných vrstvách hlbokomorských sedimentov závisia od obsahu opálu (SiO_{2am}) v sedimente. Hodnoty objemovej hustoty, ako aj pevnosť v šmyku sú nepriamo úmerné obsahu SiO_{2am} v sedimente.

Redoxný potenciál (Eh) sedimentov v prieskumných blokoch bol stanovený na palube plavidla pomocou platinových elektród. Analýzy ukazujú, že nízke hodnoty E_h (< 450 mV) geochemicky aktívnej vrstvy majú za následok neprítomnosť konkrécií v dôsledku redukcie Mn^{4+}, ktorý prechádza do pórovej vody a zostáva rozpustený vo vrstve sedimentu. Naproti tomu, zistil sa vysoký výskyt konkrécií tam, kde Eh dosahoval vysoké hodnoty (> 500 mV).

Hodnoty pH v sedimentoch prieskumného bloku H22 namerané počas expedície v roku 2014 sa pohybovali od slabo alkalických (7,5 – 7,8) po neutrálne (7,1 – 7,5), čo zodpovedá hodnotám pH vo vrstvách sedimentu v prieskumnom bloku H11 nameraným v roku 2009 (Kotliński, 2010) v rozsahu od slabo alkalických (7,6) po neutrálne (pH 7,14). Vo všeobecnosti vrchné vrstvy sedimentu vykazujú relatívne zvýšené hodnoty pH.

Polymetalické konkrécie

Všeobecný model tvorby konkrécií

Polymetalické konkrécie v skúmanom území vystupujú na oceánskom dne a spravidla ležia v polotekutej povrchovej vrstve. Pomerne často sú pokryté tenkou vrstvou nekonsolidovaných sedimentov. Konkrécie tvorí jadro, na ktorom narastajú koncentrické vrstvy hydroxidov a oxidov železa a mangánu. Okrem Mn a Fe sú hlavnými kovovými prvkami v konkréciách aj Cu, Ni a Co. Výskyt vysokej koncentrácie konkrécií v oblasti CCZ je výsledkom komplexných procesov pôsobiacich na regionálnej a lokálnej úrovni.

Na základe spôsobu formovania možno kovy obsiahnuté v konkréciách rozdeliť na tri skupiny:

- železo sa vyskytuje vo vodách oceánu vo forme koloidných častíc oxyhydroxidov železa, zdrojom je rozpúšťanie vápenatých schránok pod zónou CCD (ISA, 2010a),
- kobalt sa akumuluje vplyvom hydrogénnych procesov (Halbach, 1986),
- mangán, nikel a meď sú závislé od biogeochemického cyklu, všeobecne akceptovaný model (ISA 2010a) rozdeľuje proces akumulácie mangánu, niklu a medi na 4 fázy: 1. prvá fáza zahŕňa transport kovov do oceánu zo súše (zvetrávanie), z vulkanogénneho oceánskeho hrebeňa East Pacific Rise (EPR) a z atmosférických zdrojov. Kovy sú na povrchu jemných častíc sedimentov transportované v suspenzii oceánskymi prúdmi; 2. častice konzumuje zooplanktón a kovy sú koncentrované vo fekálnych mikropeletách (najmä Mn) a v schránkach odumretého planktónu klesajú na morské dno; 3. pelety sú biologicky prepracované bentickou faunou a degradované bakteriálnymi metabolickými procesmi. Následkom toho sa uvoľňujú rozpustné katióny kovov – počas prvotnej diagenézy sa pórová voda vo vrchnej vrstve polotekutého sedimentu stáva suboxickou, zintenzívňuje proces a lúhuje kovy. Vďaka tomu je silne obohatená o ióny kovov; 4. posledná fáza zahŕňa tvorbu konkrécií, keď sa v najvrchnejšej vrstve vytvárajú mangánové minerály (todorokit, birnessit), ktorých intersticiálne vrstvy dokážu zachytávať kovy ako meď a nikel (Morgan, 2012).

Proces tvorby konkrécií v oblasti CCZ ovplyvňuje šesť hlavných faktorov (ISA, 2010b):

a) zdroj (dostupnosť) kovov – vo všeobecnosti dostupnosť kovov z morskej vody a sedimentov dna nie je obmedzená;
b) nevyhnutná prítomnosť jadra – jadrá konkrécií predstavujú fragmenty starých konkrécií, spevnených sedimentov, vulkanoklastických hornín, schránok živočíchov, zubov rýb a pod. (v podstate všetky materiály, ktoré sú o niečo tvrdšie ako sediment morského dna, môžu slúžiť ako jadrá na tvorbu konkrécií);
c) antarktická spodná voda (AABW) – tento prúd, resp. vodná masa sa považuje za zdroj kyslíka a materiálov, z ktorých sa formovali jadrá konkrécií, najmä počas stredného až neskorého miocénu;
d) polotekutá povrchová vrstva – vrstva na povrchu dna, ktorá má rozhodujúci význam pri tvorbe konkrécií, poskytujúca stavebné prvky a chemické prostredie na ich rast;
e) bioturbácia – mechanizmus, ktorý zabraňuje rýchlemu prekrytiu konrécií sedimentmi morského dna;
f) interná stratigrafia konkrécií – výsledok meniacich sa podmienok v geologickej histórii hlbokomorských bazénov.

Poloha vznikajúcej konkrécie v rámci polotekutej povrchovej vrstvy dna je rozhodujúcim faktorom pri zásobovaní kovovými iónmi. V závislosti od polohy konkrécie počas jej rastu sa rozlišujú tri typy konkrécií:

- v polotekutej povrchovej vrstve – diagenetický typ D, nazývaný aj typ R (*rough*) kvôli charakteristickému drsnému povrchu konkrécií;
- na rozhraní morskej vody a polotekutej povrchovej vrstvy – zmiešaný typ hydrogenetických a diagenetických procesov (typ HD), nazývaný aj typ R + S (*rough-smooth*) kvôli zmiešanej morfológii ich povrchu;

– nad morským dnom na povrchových sedimentoch dna – hydrogenetický typ H, nazývaný aj typ S (*smooth*) kvôli charakteristickému hladkému povrchu konkrécií.

Proces rastu konkrécií je ovplyvnený vzdialenosťou od vulkanogénnych zdrojov kovov (Hein et al., 2013). V blízkosti Východopacifického chrbta (*East Pacific Ridge* – EPR) je najpravdepodobnejšia tvorba hydrogenetického typu konkrécií, s rastúcou vzdialenosťou sa jeho podiel znižuje a postupne ho nahrádzajú konkrécie tvorené diagenetickými procesmi.

Rýchlosť rastu polymetalických konkrécií v oblasti CCZ predstavuje 1 až 10 mm za 1 milión rokov (Beiersdorf et al., 2003). Priemerná rýchlosť rastu konkrécií typu H je približne 1 mm za 1 milión rokov, zatiaľ čo konkrécie typu D rastú rýchlosťou približne 5 až 15 mm za 1 milión rokov (Amann, 1992; Kotliński, 1998). Niektorí autori uvádzajú, že konkrécie typu D môžu rásť až 100 mm za 1 milión rokov (Sea-floor mining, 2014). Malá rýchlosť rastu naznačuje, že konkrécie vyžadujú stabilné podmienky prostredia po dlhý čas, aby dosiahli niekoľkocentimetrovú veľkosť. Aj keď sa akumulácia sedimentov v tejto oblasti považuje za nízku (niekoľko milimetrov za tisíc rokov), je o tri rády vyššia ako rast konkrécií.

Mineralogické zloženie

Minerálne zloženie polymetalických konrécií pozostáva z kryštalických minerálnych fáz (najmä oxidov mangánu) a amorfných minerálnych fáz (hlavne hydratovaných oxidov železa) v rôznych pomeroch v závislosti od hydrogenetických alebo diagenetických procesov tvorby konrécií.

Hlavnými minerálmi mangánu sú (Burns a Burns, 1977; Usui et al., 1987; Halbach et al., 1988; Kotliński, 1998; 2003):

– todorokit (10 Å manganit, busserit), ktorý sa pravdepodobne tvorí z rozpusteného mangánu v pórových vodách počas diagenézy,
– birnessit (7 Å manganit),
– vernadit (δ-MnO_2, birnessit s nepravidelnou štruktúrou), slabo kryštalizovaný hydrogenetický oxid Fe-Mn.

Hlavným minerálom železa je amorfný oxyhydroxid železa ô-FeO (OH), ktorý môže zahŕňať goethit, ferroxyhit, lepidokrokit, akageneit, hematit alebo ferrihydrit (Kotliński, 1999; Hein a Koschinsky, 2014). V konkréciách sa okrem toho nachádzajú mikroskopické detritické kremičitany, živce, plagioklasy, kremeň a phillipsit (Kotliński, 1998). Ako akcesorické minerály sa vyskytujú aragonit, apatit, amorfný oxid kremičitý (opál), pyroxény, amfiboly, barit, spinely, rutil, anatas a ílové minerály (chloritany, illit, montmorillonit) (Cronan, 1977; Piper a Blueford, 1982; Halbach et al., 1982; Andreev, 1994; Kotliński, 1998). Ílové minerály a zeolity sa väčšinou vyskytujú v jadrách konkrécií, niekedy ako rozptýlené zhluky. Obsah SiO_2 a Al_2O_3 v konkréciách zvyčajne dosahuje 25 až 30 %. Zriedkavo sa objavujú kalcitové bioklasty (napr. *Foraminifera*) vyplnené apatitom (Kotliński, 1998).

Chemické zloženie

Konkrécie z oblasti CCZ sa vyznačujú vysokým plošným výskytom (hustotou uloženia udávanou v kg/m^2) a obsahom kovov (hlavne Mn, Ni, Cu, Co, Mo, Zn a vzácnych zemín) v porovnaní s ostatnými oceánskymi konkrécionosnými oblasťami (Kotliński, 1998; Kotliński, 2011). Obsah prvkov v konkréciách závisí od podielu hydrogenetických alebo diagenetických procesov na tvorbe konkrécií. Konkrécie, v ktorých prevláda todorokit, sú zvyčajne bohaté na Mn, Ni, Cu a Zn, zatiaľ čo konkrécie, v ktorých prevláda vernadit, sú bohaté na Fe, Co a Pb. Priemerné hodnoty obsahu hlavných kovov sa v rámci prieskumného územia IOM pohybujú v tomto rozmedzí: Mn 27,64 – 31,55 %, Ni 1,22 – 1,30 %, Cu 0,93 – 1,30 % a Co 0,16 – 0,20 %.

S rastúcou hĺbkou výskytu konkrécií (generálne v severo-južnom smere) sa zvyšuje obsah Mn a Cu, zatiaľ čo obsah Ni a Co klesá. Vyšší obsah Co je charakteristický pre genetické typy H a D v severnej časti oblasti. Zvýšený obsah Mn, Cu a Ni bol zaznamenaný v konkréciách genotypu D v centrálnej časti oblasti, v južnom smere možno pozorovať aj nárast obsahu Mn (Abramowski a Kotliński, 2011). Železo spolu s mangánom tvoria hlavnú zložku polymetalických konkrécií. Priemerný obsh Fe v konkréciách v oblasti CCZ je takmer 6 %.

Výsledky komplexnej chemickej analýzy spoločnej vzorky (10 kg) odobratej vlečnou sieťou v priekumnom bloku H22 sú uvedené v tab. 7. Na stanovenie Ni, Cu a oxidov sa použila röntgenová spektrometria, AES-ICP sa použil na stanovenie Co a prvkov vzácnych zemín (tab. 8), gravimetria sa použila na stanovenie celkovej síry a straty žíhaním. Obsah drahých kovov Pt, Pd, Au a Ag bol nižší ako detekčný limit použitých analytických metód (AAS-F, ETA-AAS, ICP-MS).

V CCZ konkrécie obsahujú aj ďalšie kovy s potenciálnym ekonomickým významom, ako sú Mo, Zn, V, Zr, Li a REE, ktoré môžu byť vedľajšími produktmi ťažby (Hein, 2012; Hein a Koschinsky, 2014; Halbach a Jahn, 2016). Obsah Mo je v rozmedzí 0,048 – 0,058 %, Zn 0,124 – 0,168 %, V 0,045 %, Zr 0,036 – 0,077 % a Li 131 ppm (Hein et al., 2013). Obsah vzácnych zemín (REE) je vo všeobecnosti nižší ako na ložiskách na súši, ale v absolútnych číslach predstavuje omnoho väčšie minerálne zdroje. Navyše, zastúpenie ťažkých vzácnych zemín (HREE), ktoré majú väčší ekonomický význam ako ľahké vzácne zeminy (LREE), je v hlbokomorských ložiskách podstatne vyšší ako na ložiskách na súši (26 % z celkového obsahu REE v porovnaní s 1 % na súši) (Hein, 2012; Hein et al., 2013; Halbach a Jahn, 2016). Obsah REE súvisí s genetickým typom: hydrogenetické – najvyšší obsah, diagenetické – najnižší obsah (Kotliński et al., 1997). Navyše, hlbokomorské ložiská nie sú kontaminované rádioaktívnymi prvkami ako Th a U. Vybrané hodnoty obsahu REE v konkréciách z prieskumného územia IOM sú prezentované v tab. 8.

Klasifikácia polymetalických konkrécií

Polymetalickú konkréciu spravidla tvorí jadro a koncentricky narastené vrstvy hydroxidov a oxidov železa

a mangánu. Jadrom môžu byť zvyšky vulkanoklastického materiálu, litifikované sedimenty, bioklasty alebo fragmenty starších konkrécií.

Hlavné morfologické typy konkrécií v oblasti CCZ sú diskoidné (D), elipsoidné (E), sféroidné (S), tabuľovité (T), polyjadrové (P), hroznovité (b), nepravidelné (I) a fragmenty (f).

Morfológia konkrécií je podmienená ich genézou, minerálnym zložením, veľkosťou, vekom, ako aj zdrojmi prvkov (Kotliński, 1998, obr. 8). Konkrécie majú najčastejšie nasledujúce textútry: koncentrické pásikavé, dendritické, masívne a stĺpcovité. Vrstvy sú často popretínané inými vrstvami, čo svedčí o hiátoch pri raste konkrécií. Konkrécie sú často popraskané, väčšinou radiálne alebo tangenciálne. Praskliny sú následkom vnútorného pnutia, ktoré sa vyskytuje v procesoch dehydratácie a rekryštalizácie počas rastu vrstiev konkrécií, alebo sú následkom diagenetických procesov. Zvyčajne sú vyplnené ílovými minerálmi alebo rekryštalizovanými Mn minerálmi (Kotliński, 1998). Veľkosť konkrécií v oblasti CCZ sa pohybuje od mikroskopických častíc po pelety s priemerom viac ako 20 cm.

Na klasifikáciu konkrécií sa používa viacero klasifikácií berúcich do úvahy ich veľkosť, tvar, zloženie a počet jadier, hrúbku kôry, ako aj minerálne a chemické zloženie (napr. Meylan, 1974; Moritani et al., 1977; Anikeeva et al., 1984; Halbach et al., 1981; Stackelberg a Beiersdorf 1991; Haynes et al., 1985; Kotliński, 1998). Klasifikácia prijatá MOMD pre oblasť CCZ (ISA, 2010b) definuje tri hlavné typy konkrécií vzhľadom na ich povrchovú morfológiu:

- typ S (hladký povrch, *S-smooth*),
- typ R (drsný povrch, *R-rough*),
- type S-R (kombinovaný povrch).

Tieto hlavné typy zodpovedajú trom hlavným genetickým typom: hydrogenetický (H), diagenetický (D) a hydrogeneticko-diagenetický (HD). Genetické typy sú charakterizované rozdielnym mineralogickým a chemickým zložením a rôznym podielom prírastku Mn (tab. 9, obr. 9).

Konkrécie typu H majú relatívne nízky priemerný obsah Mn, Ni a Cu a v porovnaní s typmi HD a D sú obohatené o Fe a Co, zaznamenaný bol aj vyšší obsah prvkov vzácnych zemín (Kotliński et al., 1997, 1999). Hlavné minerálne zložky predstavujú mikrokryštály vernaditu a goetitu. Pomer Mn/Fe, jeden z najdôležitejších parametrov pri určovaní genotypu konkrécií, je obvykle nižší ako 4. Majú hladký povrch (typ S), sú zvyčajne sféroidné alebo nepravidelne sféroidné, veľkosť je menšia ako priemer 4 cm. Jadrá konkrécií väčšinou predstavuje sopečné sklo, ktoré sa neskôr halmyrolýzou transformujú na ílové minerály (zeolity), prítomné sú aj fragmenty bioklastov. V okolí jadra sa vrstvy minerálov Mn a Fe striedajú s ílovými minerálmi. Konkrécie sú často popraskané a vyznačujú sa prítomnosťou sekundárnych žíl naplnených ílovými alebo mangánovými minerálmi. Miera rastu je asi 1 mm/1 mil. rokov. Konkrécie typu H sa zvyčajne vyskytujú na vápenatých kaloch nad zónou CCD (*Carbonate Compensation Depth* – hĺbka karbonátovej kompenzácie).

Konkrécie typu D vykazujú vyšší obsah Mn, Ni, Cu a Zn a nižší obsah REE. Hlavnými minerálmi mangánu sú todorokit a birnessit. Pomer Mn/Fe je vyšší ako 5. Konkrécie sú zvyčajne diskoidné alebo elipsoidné, s veľkosťou 6 až 12 cm (alebo viac). Vyznačujú sa silne diferencovanou alebo asymetrickou štruktúrou s drsným povrchom (typ R). Jadrá sú zvyčajne reprezentované fragmentmi starších konkrécií alebo bioklastov. Vykazujú masívnu, radiálnu, dendritickú alebo kolomorfnú štruktúru a vyznačujú sa prítomnosťou radiálnych trhlín. Vyznačujú sa aj zreteľne viditeľnou zmenou minerálov Mn (čierne vrstvy) a Fe (červenohnedé vrstvy), ako aj rozdielnou rýchlosťou rastu – v prípade minerálov Mn je dvakrát vyššia ako v prípade minerálov Fe. Koncentrácia Ni a Cu je spojená s vrstvami Mn a minerály Fe sú často oddelené vrstvou vulkanického kalu. Vrstvy minerálov Mn a Fe sú hrubšie ako tie, ktoré boli pozorované v konkréciách typu H, a dosahujú 1,5 až 2,0 mm. Odhaduje sa, že rýchlosť rastu týchto konkrécií je 5 až 15 mm/1 000 000 rokov (Amann, 1992). Tento typ sa vyskytuje na povrchu dna, ponorený do polotekutej vrstvy, obyčajne spočívajúcej na rádiolárových kremelinových kaloch alebo polygénnych íloch pod zónou CCD.

Konkrécie typu HD sú zmiešaný (prechodný) typ medzi H a D, a to vzhľadom na formu výsyktu, ako aj veľkosť a zloženie. Hlavným minerálom mangánu je birnessit (7 Á manganit) s premenlivým pomerom amorfnej a kryštalickej fázy. Pomer Mn/Fe sa pohybuje medzi 4 a 5. Konkrécie majú často elipsoidný, tabuľovitý alebo diskoidálny (sploštený) tvar, horný povrch je hladký a vystavený morskej vode, zatiaľ čo spodná časť je drsná a ponorená do polotekutej vrstvy. Typickým znakom je prítomnosť prstencového vydutia, vytvoreného v kontaktnej zóne medzi morskou vodou a polotekutým sedimentom.

V prieskumnej oblasti IOM bol opísaný dodatkový podtyp diagenetických konkrécií D1. Charakterizuje ho vyššia koncentrácia Cu ako Ni. Okrem toho boli opísané kôry (C – *crusts*) vystupujúce na tvrdých substrátoch (Kotliński a Stoyanova, 2009).

Distribúcia genetických typov polymetalických konkrécií v prieskumnom území IOM je znázornená na obr. 10.

V sektore B1 prevládajú konkrécie s priemerom 2 až 4 cm (dominuje genetický typ H) a viac ako 8 cm (dominuje genetický typ HD a D). V severnej a strednej časti sektora B2 prevládajú konkrécie s veľkosťou 2 – 4 cm a viac ako 8 cm, zatiaľ čo v južnej časti s veľkosťou 2 – 4 cm. Genetické typy H a HD sú zastúpené hlavne frakciou 2 – 4 cm. Genotyp D charakterizujú najmä konkrécie s priemerom 4 – 6 cm a viac ako 8 cm, zatiaľ čo genotyp D1 vykazuje prakticky homogénne rozdelenie frakcií. Medzi veľkosťou konkrécií a hĺbkou ich výskytu nebola preukázaná jednoznačná závislosť.

Priestorová distribúcia konkrécií

Konkrécie zvyčajne vystupujú na povrchu morského dna (ponorené do polotekutej aktívnej vrstvy sedimentu), často sú však prekryté sedimentmi. Prekrytie sedimentmi sa vyskytuje na približne 70 % skúmaných miest v prieskumnej oblasti IOM. Všeobecne sa rozsah prekrytia

zväčšuje s hĺbkou a v smere zo severu na juh (Abramowski a Kotliński, 2011).

Na kvantitatívny opis rozsahu pokrytia sa používa parameter index pokrytia, ktorý je vyjadrený pomerom medzi plochou pokrytia konkréciami na laboratórnej šablóne (štvorcovej sieti) vo vzťahu k ploche pokrytia konkréciami vypočítanej z fotografie dna na mieste odberu vzorky (stanici). Najnižšia hodnota parametra je 1 (bez pokrytia). Na niektorých staniciach sa pozoruje 100 % pokrytie konkrécií sedimentom.

Pokiaľ ide o morfológiu dna, vzorky s vysokým výskytom konkrécií sa našli na všetkých morfologických typoch morského dna. V porovnaní s výskytom na svahoch hrastí a priekop sa však najväčší výskyt zistil na rovnom alebo mierne zvlnenom teréne.

V rámci prieskumného územia IOM sa konkrécie vyskytujú v hĺbkovom rozsahu 3 800 – 4 750 m, s najvyššou hustotou uloženia a frekvenciou výskytu zaznamenanou v hĺbkovom rozsahu 4 300 – 4 500 m. Analýza súvisiaca s hĺbkou ukazuje, že priemerná hustota uloženia sa postupne zvyšuje až do hĺbky 4 500 m (najväčšia hustota uloženia je v hĺbke 4 300 – 4 500 m) a s hĺbkou viac ako 4 500 m sa výrazne znižuje. Niektoré zákonitosti výskytu môžu súvisieť s kritickou hĺbkou kompenzácie uhličitanov (CCD), ako aj s genetickým typom konkrécií (ISA, 2010a; Kotliński, 2003, 2011):

- pri hĺbke okolo 4 200 m dominujú malé (< 4 cm) sféroidné konkrécie hydrogenetického typu (H) s hladkým povrchom, vyšším obsahom Fe (10,32 %) a Co (0,23 %) a relatívne nižším obsahom Mn, Ni a Cu;
- v hĺbke medzi 4 200 a 4 400 m prevládajú konkrécie hydrogeneticko-diageneticého typu (HD) s vyšším obsahom Mn (> 30,5 %), Ni a Cu a relatívne nižším obsahom Co (< 0,18 %);
- pod hranicou CCD (< 4,500 m) sa vyskytujú konkrécie diagenetického typu (D), diskoidné a elipsoidné, s veľkosťou 6 – 12 cm a drsným povrchom.

Všeobecne v smere zo S na J klesá výskyt konkrécií typu H a HD s modálnou veľkosťou < 6 cm, zatiaľ čo výskyt konkrécií typu D s modálnou veľkosťou > 6 cm sa postupne zvyšuje (Kotliński, 2003; Kotliński, 2011). Prejavuje sa to aj v priestorovom rozložení obsahu kovov v rámci prieskumnej oblasti.

Geotechnické vlastnosti polymetalických konkrécií

Fyzikálne, mechanické a technologické vlastnosti polymetalických konkrécií sa v rámci prieskumnej činnosti IOM skúmajú s cieľom poskytnúť informácie a údaje na výber vhodnej ťažobnej technológie (Dreiseitl, 2012).

Základné fyzikálne vlastnosti konkrécií, ktoré sa stanovujú v lodnom laboratóriu, sú obsah vody (vlhkosť) a objemová hmotnosť. Okrem toho sa vypočítavajú ďalšie parametre, ako je objemová hmotnosť suchých konkrécií (sušenie prebieha 72 hodín pri teplote 105 °C), pórovitosť, koeficient pórovitosti a merná hmotnosť. Prirodzený obsah vody w_n je pomer hmotnosti odparenej vody k hmotnosti vzorky mokrej konkrécie. Pri analýze obsahu vody (w) a prirodzeného obsahu vody (w_n) sa musí brať do úvahy obsah soli v morskej vode prítomnej v póroch konkrécie (predpokladaný M = 35 ‰). Merania potvrdzujú, že morská voda predstavuje 1/3 celkovej hmotnosti konkrécií, čo je potrebné brať do úvahy pri kalkuláciách transportu. Základné fyzikálne parametre konkrécií sú uvedené v tab. 10 a 11.

Štatistická analýza fyzikálnych parametrov konkrécií preukázala určitú závislosť vo vzťahu k veľkosti (frakcie) konkrécií. Malé konkrécie majú pomerne nízku hustotu a vysoký obsah vody oproti konkréciám väčších rozmerov, zatiaľ čo maximálnu hustotu a minimálny obsah vody pozorujeme v konkréciách s veľkosťou 8 – 10 cm. Konkrécie s veľkosťou > 10 cm sa postupne rozpadajú, čo pravdepodobne súvisí s ich narastajúcim vekom.

Jediným parametrom pevnostnej charakteristiky určovaným priamo v palubnom laboratóriu bola jednoosová pevnosť v tlaku vyjadrená v MPa. Táto vlastnosť vyjadruje tlak, ktorý je potrebné vyvinúť na deštrukciu konkrécie. Ako uvádza Dreiseitl (2012), nezávisí od genotypu konkrécie, ale od jej morfotypu (sféroidné konkrécie sú tvrdšie ako diskoidálne a elipsoidálne), a najmä od jej veľkosti (čím menšia konkrécia, tým je potrebný väčší tlak). Hodnota parametra je uvedená v tab. 12. Obrázok 11 znázorňuje trendy v jednoosovej pevnosti v tlaku merané počas 2 expedícií (2001 a 2004).

Znalosť technologických vlastností konkrécií je nevyhnutná pri ich ťažbe aj preprave z miesta ťažby do spracovateľského závodu na pevnine. V rámci výskumu na vzorkách z prieskumnej oblasti IOM sa určujú nasledujúce technologické vlastnosti (Dreiseitl, 2012):

- merná sila odtrhnutia (kPa),
- sypná hmotnosť (kg/m^3),
- uhol prirodzenej sklonitosti, resp. svahový uhol (°, stupeň).

Merná sila odtrhnutia je sila potrebná na oddelenie konkrécie od sedimentu. V praxi sa však určuje odpor proti odtrhávacej sile. Dodatočne sa musí vypočítať plocha kontaktu konrécie so sedimentom. Preto je odpor sily pri odtrhnutí vyjadrený v kPa. Merná sila odtrhnutia sa určuje na konkréciách v *box-coreri* hneď po jeho vyzdvihnutí z morského dna. Táto vlastnosť môže byť dôležitá pri určovaní techniky zberu konkrécií z morského dna. Analýza IOM preukázala, že neexistuje žiadny vzťah medzi morfotypom konkrécie a mernou silou odtrhnutia, ale maximálne hodnoty mernej sily odtrhnutia pri veľkých konkréciách (8 – 10 a 10+ cm) sú nižšie ako maximálne hodnoty mernej sily odtrhnutia pri stredne veľkých konkréciách (4 – 6 a 6 – 8 cm). Hodnoty parametra vo vzťahu k veľkosti (frakcii) konkrécií sú uvedené v tab. 13.

Predpokladá sa, že povrch konkrécie hrá hlavnú úlohu v odpore proti vytrhnutiu, t. j. drsný povrch zvyšuje silu, ktorou je konkrécia vyťahovaná zo sedimentu v porovnaní so silou, ktorá je potrebná na vytiahnutie konkrécie s hladkým povrchom.

Sypná hmotnosť a svahový uhol uloženia konkrécií budú dôležitými parametrami pri nakladacích a prekladacích operáciách (ťažobné plavidlo/transportné plavidlo/skladovanie/pozemná preprava). Parametre sa zisťovali spracovaním veľkoobjemových vzoriek získaných pomocou

vlečnej siete počas expedícií IOM-2009 a IOM-2014 (tab. 14).

Sypná hmotnosť r_{app} poskytuje údaj o množstve (hmotnosti) konkrécií, ktoré sa vojde do nádoby s objemom 1 m^3. Priemerná sypná hmotnosť konkrécií (expedícia IOM-2009, 3 skúšky) bola vypočítaná na r_{app} = 1,242 kg/m^3. Po utrasení a doplnení nádoby konkréciami bola maximálna sypná hmotnosť stanovená na r_{appmax} = 1,342 kg/m^3.

Svahový uhol bol stanovený ako dotyčnica uhla α medzi výškou haldy konkrécií a polomerom haldy. Svahový uhol v prípade vzorky získanej vlečnou sieťou počas expedície IOM-2009 bol stanovený na 37° a počas expedície IOM-2014 na 31° (tab. 14).

Hustota uloženia

Hustota uloženia PMK na morskom dne (kg/m^2) sa dá odhadnúť dvomi spôsobmi:

- z výsledkov vzorkovania *box-corerom* – vydelením hmotnosti získaných konkrécií plochou pokrytou otvorenými čeľusťami vzorkovača (0,25 m^2);
- využitím snímok sonaru alebo fotografií s aplikáciou kalibračných faktorov.

Obe metódy poskytujú mierne odlišné výsledky. Je to spôsobené viacerými faktormi, najmä tým, že konkrécie zasypané sedimentmi sú na fotografiách ťažšie identifikovateľné (Kotliński a Stoyanova, 2009), ako aj faktom, že hodnotené oblasti majú rôznu veľkosť. V druhej metóde korelujú hodnoty *backscattera* (intenzity zvukovej vlny odrazenej od morského dna) viac s parametrom veľkosti konkrécií ako s ich počtom (Rühlemann et al., 2011).

Hustota uloženia sa udáva v kg/m^2 a obvykle sa vzťahuje na mokré vzorky. Analýza priestorového rozloženia hustoty uloženia v rámci CCZ poukazuje na jeho veľkú variabilitu (Morgan, 2009). Hustota uloženia PMK v prieskumnom území IOM sa pohybuje v rozmedzí 0,1 – 28,4 kg/m^2.

Priestorový opis ložiska

Perspektívne konkrécionosné polia na budúcu ťažbu boli vymedzené v rámci sektorov B1 a B2 v oblastiach s priemernou hustotou uloženia vyššou ako 10 kg/m^2 a sklonom morského dna max. 7°. Ich celková plocha bola odhadnutá na 33 900 km^2 (obr. 12). Topografia morského dna má rozhodujúci vplyv na kontúry, veľkosť a tvary rudných telies ložiska. Rudné telesá predstavujú pretiahnuté šošovky (pásy) a zložené šošovkovité tvary s šírkou 2 – 10 km a dĺžkou až niekoľko desiatok kilometrov, kopírujúc okraje podmorských depresií a chrbtov. V oblastiach s väčšími rovnými plochami dosahujú rudné polia šírku až do 70 km a dĺžku do 120 km. Líšia sa rozsahom i tvarom (Kotliński, 2003).

V hraniciach sektora B2 boli vyčlenené dva prieskumné bloky: H11 a H22. V rámci týchto prieskumných blokov boli identifikované oblasti rudných polí H22_NE, H22_MID, H11_PR2, H11_PR3 and H22_NW. Najperspektívnejšie rudné pole H22_NE pozostáva zo štyroch rudných telies: RZ_09, RZ_10, RZ_11 a RZ_12. Predstavuje typické pásmové ložisko tvorené šošovkovitými pretiahnutými rudnými poľami. Celková plocha rudných telies tu dosahuje 625 km^2. Hustota vzorkovania dosiahla hodnotu 1 stanica (*box-corer*)/31 km^2. Hĺbka dna tu dosahuje od 4 249 do 4 501 m. Priemerná hustota uloženia mokrých PMK bola na základe vzorkovania stanovená na 15,7 kg/m^2. Prevažuje diagenetický typ konkrécií, index pokrytia sedimentom sa pohybuje od 1 (žiadne prisypanie konkrécií sedimentom) do 1,6.

Výpočet zásob a zdrojov

Zdroje polymetalických konkrécií sa odhadovali v dvoch etapách. Počas prvej etapy (2007) boli na odhadnutie zdrojov v sektoroch B1 a B2 vytvorené dve pracovné skupiny (Mucha et al., 2007; Shanov et al., 2007). Obe pracovné skupiny vykonali odhad nezávisle, so zameraním na zdroje polymetalických konkrécií a vybraných kovov: Mn, Ni a Mo (skupina 1) a Co, Cu a Zn (skupina 2). Výsledky tohto odhadu boli založené na údajoch získaných počas expedícií do roku 2004, ktoré sa orientovali na regionálny prieskum. Počas druhej etapy (2011, 2015) boli odhadnuté zdroje konrécií a hlavných kovov (Co, Cu, Mn a Ni) v rámci prieskumných blokov H11 a H22 v centrálnej časti sektora B2. Zdrojom údajov boli expedície organizovaná v rokoch 2009 a 2014 a následne boli vypočítané zdroje (Mucha et al., 2011, 2015). V roku 2016 boli minerálne zdroje prvýkrát klasifikované podľa systému CRIRSCO a v rámci súhrnného dokumentu uvedené v technickej správe (Szamałek et al., 2016).

Do výpočtu zásob a zdrojov sú zahrnuté len konkrécie ležiace na morskom dne nachádzajúce sa v povrchovej vrstve do hĺbky okolo 10 – 15 cm. Hlbšie pochované konkrécie, ktoré sa v oblasti prieskumného územia IOM taktiež vyskytujú, neboli vo výpočte zohľadnené vzhľadom na predpokladané dobývacie metódy. Vzhľadom na vysokú variabilitu (zvyčajne rádovo vyššiu, ako je variabilita obsahu kovov) za kľúčový parameter pri odhade minerálnych zdrojov polymetalických konkrécií sa považuje hustota uloženia uvádzaná v kg/m^2. Spôsob uloženia konkrécií na morskom dne, resp. v povrchovej vrstve definuje ložisko ako dvojrozmerné. Tomu je prispôsobená metodika odhadu minerálnych zásob a zdrojov.

Metodika výpočtu

Množstvo polymetalických konkrécií a kovov obsiahnutých v nich bolo odhadnuté osobitne v sektoroch B1 a B2 a v prieskumných blokoch H11 a H22. Odhad množstva polymetalických konkrécií a kovov obsiahnutých v nich a priemerný obsah kovov v rámci blokov sa robil geoštatistickou metódou bežného blokového krigingu (Journel a Huijbregts, 1978; Matheron, 1963) s aplikáciou Yamamotovej korekcie (Yamamoto, 2005). Pred odhadom boli štruktúry priestorovej variability parametrov ložiska (hustota uloženia a obsah kovov) modelované pomocou smerových a všesmerových semivariogramov. Výpočet sa uskutočnil pre základné výpočtové bloky s rozmermi 500 x 500 m umiestnené v rudných telesách s vylúčením zón bez výskytu konkrécií, podmorských vulkánov a oblastí, kde sklon dna oceánu presahoval 7°.

Štrukturálny geoštatistický opis variability hustoty uloženia, ilustrovaný smerovou semivariogramovou mapou

pre kombinované údaje zo sektorov B1 a B2, indikuje slabú anizotropiu parametrov pri veľkom rozsahu pozorovaní, najmä pri vzdialenostiach väčších ako 50 km, a silnú lokálnu variabilitu, predstavovanú výrazným nugetovým efektom (obr. 13). Minimálna variabilita je v smere S – J, maximálna v smere V – Z. Minimálna variabilita súvisí so smerom uloženia rudných telies. Pri krigingu boli použité rovnice empirických modelov semivariogramu (obr. 14). Odhad zdrojov pri každom výpočtovom bloku zahŕňal hustotu uloženia a obsah kovov, odvodené z ôsmich najbližších vzoriek. Celkové zdroje sektorov a blokov boli vypočítané súčtom hodnôt v základných výpočtoých blokoch. Správnosť modelovania sa overila pomocou krížovej validácie (Isaaks a Srivastava, 1989).

Priemerné hodnoty hustoty uloženia a obsahu kovov v prieskumných blokoch H11 a H12 sú uvedené v tab. 15. Prepočítavací koeficient z mokrých konkrécií na suché je 0,7. Hodnoty štandardnej chyby odhadu pri výpočte zdrojov pri medznej hodnote 10 kg/m^2 v základných výpočtových blokoch sú pomerne nízke a dosahujú okolo 8 % v sektore B1, 3 % v sektore B2 a 5 % v prieskumných blokoch H11 a H22.

Krivky hustoty uloženia/tonáže v prieskumných blokoch H11 a H22 sú na obr. 15 a 16.

Príklad znázornenia hustoty uloženia PMK v prieskumných blokoch je na obr. 17. Hustota uloženia a obsah kovov boli odhadnuté v základných výpočtových blokoch s rozmermi 500 x 500 m. Z výpočtu boli vylúčené oblasti bez výskytu konkrécií, vulkanických zón a oblastí, kde svah oceánskeho dna prekračuje 7°.

Klasifikácia zásob

Podľa smerníc CRIRSCO (*Committee for Mineral Reserves International Reporting Standards* – Výbor pre medzinárodné štandardy vykazovania minerálnych zásob) boli zdroje polymetalických konkrécií kategorizované v sektoroch B1 a B2 ako odvodené (*inferred*) a v prieskumných blokoch H11 a H22 ako indikované (*indicated*). Takáto kategorizácia je odôvodnená rôznymi priemernými intervalmi vzorkovania v rámci prieskumných sektorov a blokov. V prieskumných sektoroch B1 a B2 sú priemerné intervaly odberu vzoriek 11, respektíve 15 km. V prieskumných blokoch H11 a H22 je priemerný interval vzorkovania približne 7 km (Szamalek et al., 2016).

Výsledky odhadu zásob a zdrojov v prieskumnom území IOM sú uvedené v tab. 16. Predložený variant výpočtu zohľadňuje medznú hodnotu (*cut-off*) hustoty uloženia PMK 10 kg/m^2 (v mokrom stave) a predstavuje základný scenár odhadu zásob a zdrojov na potenciálnu ťažobnú činnosť. Stav zásob a zdrojov sa vzťahuje na dátum jún 2016. V tejto fáze vývoja projektu boli odhadnuté len zdroje nerastnej suroviny. Odhad v kategórii zásob sa predpokladal po ďalšej expedícii, zahustení vzorkovania a novom výpočte.

V súčasnej fáze geologického prieskumu rozlišujeme nasledujúce hlavné faktory ovplyvňujúce presnosť odhadu zdrojov polymetalických konkrécií:

- vysoká variabilita početnosti konkrécií (koeficient variácie v = 60 %),
- významný podiel náhodnej zložky v celkovej pozorovanej variabilite početnosti,
- vysoké priemerné vzdialenosti odberu vzoriek (zhruba 11 km v sektore B1, 15 km v sektore B2 a 7 km v prieskumných blokoch H11 a H22).

Presnosť celkového odhadu zdrojov polymetalických konkrécií v prieskumnej oblasti možno považovať za uspokojivú (štandardná chyba asi 5 %). Pri menších plochách (rádovo stovky km^2 – napr. rudné telesá a rudné polia) môže byť očakávaná štandardná chyba okolo 10 %. V prípade blokov s rozlohou asi 1 km^2 však môže byť štandardná chyba odhadu významná (viac ako 20 %). Preto bolo v období predĺženia kontraktu po roku 2016 naplánované zahustenie vzorkovacích bodov v prieskumnom bloku H22, ktorý bol vybraný na detailný prieskum.

Zvýšenie presnosti odhadov zdrojov, najmä v menších oblastiach, akými sú rudné telesá, možno dosiahnuť (Szamalek et al., 2016):

- použitím pokročilých geoštatistických metód,
- aplikáciou moderných metód analýzy fotografií morského dna s použitím nepriameho vyhodnotenia hustoty uloženia PMK na základe snímok morského dna (táto metóda nevyžaduje dodatočné vzorkovanie oceánskeho dna).

Záver

IOM mal v roku 2016 spracované dostatočné množstvo vzorkového materiálu požadovanej kvality na klasifikáciu minerálnych zdrojov v kategóriách odvodené zdroje (*Inferred Resources*) a indikované zdroje (*Indicated Resources*). Využiteľnými kovmi sú mangán, nikel, kobalt, meď a zinok. Ostatné kovy s potenciálnou hodnotou (Mo, Fe, Li a REE) neboli do roku 2016 predmetom výpočtu zásob a zdrojov, v budúcnosti však môžu (v závislosti od dostupnosti využiteľných technológií) predstavovať pridanú hodnotu projektu. Geologický prieskum potvrdil, že presnosť odhadov obsahu kovov je uspokojivá v oblastiach akejkoľvek veľkosti, a to vďaka nízkej variabilite ako dôsledku stabilného chemického zloženia polymetalických uzlín. Variabilita je podstatne vyššia v prípade hustoty uloženia konkrécí, ktorá sa mení s veľkosťou hodnotenej oblasti. Nerastné zdroje boli vypočítané pri rôznych medzných hodnotách hustoty uloženia PMK. Zvoleným základným scenárom je medzná hodnota 10 kg/m^2 (vo vlhkom stave).

Na plánované predbežné ekonomické hodnotenie boli vybrané indikované zdroje (*Indicated Resources*) v prieskumných blokoch H11 a H22. Vzhľadom na nízky stupeň overenia do ekonomického hodnotenia nebudú vstupovať odvodené zdroje (*Inferred Resources*) vypočítané vo zvyšnej oblasti sektorov B1 a B2. Budúce aktivity v oblasti prieskumu IOM budú zamerané na detailný prieskum vybraných blokov a zvýšenie kategórie zdrojov/zásob. Geologické údaje spolu s ostatnými dátami získanými pri technologickom výskume ťažobných a spracovateľských metód, ako aj pri environmentálnom výskume predstavujú základ tvorby komerčného modelu využitia ložiska formou štúdie využiteľnosti.

Doručené / Received: 5. 6. 2021
Prijaté na publikovanie / Accepted: 30. 6. 2021

Mineralia Slovaca, Web ISSN 1338-3523, ISSN 0369-2086
53 (2021), 37 – 46, © Authors 2021. CC BY 4.0

Upper Cretaceous limestone olistoliths in the Rázová Formation (Horné Belice Group), Považský Inovec Mts. (Western Carpathians)

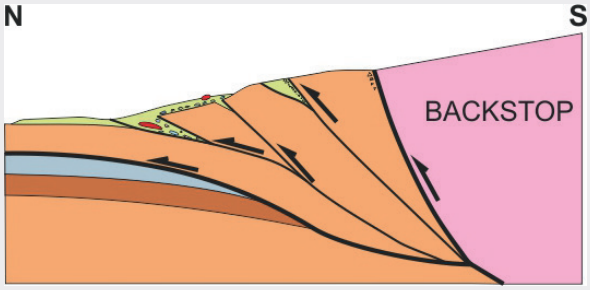
Ondrej Pelech[1], Daniela Boorová[1], Jozef Hók[2] and Miloš Rakús[1†]

[1] State Geological Institute of Dionýz Štúr, Mlynská dolina 1, SK-817 04 Bratislava
[2] Comenius University in Bratislava, Natural Sciences Faculty, Department of Geology and Paleontology, Ilkovičova 6, SK-842 15 Bratislava
[†] Deceased 23 May 2005

Abstract: The Horné Belice Group of the Považský Inovec Mts. represents a tectonic mélange containing numerous native and exotic olistoliths that accumulated on the outer Tatric active margin during the stacking of the Western Carpathian Middle Group of Nappes. Thin-section samples of the pelagic limestones from 3 different olistoliths located on the NE slopes of the Humienec elevation point in the Rázová Formation were studied and analysed. Two limestone samples represent foraminifera biomicrite (foraminifera wackestone). The sample HR1 contained *Globotruncana* cf. *linneiana* (d´ Orbigny), *Globotruncana* cf. *arca* (Cushman), *Globotruncana ventricosa* White, *Globotruncana* sp., *Globotruncanita stuartiformis* (Dalbiez), *Globotruncanita subspinosa* (Pessagno), *Falsomarginotruncana* cf. *desioi* (Gandolfi), *Muricohedbergella* sp. and *Heterohelix* sp. The sample PI4 contained *Globotruncana ventricosa* White, *Globotruncana* sp., *Globotruncanita* cf. *subspinosa* (Pessagno), and most commonly form *Globotruncanita calcarata* (Cushman), *Globotruncanella havanensis* (Voorwijk), *Muricohedbergella* cf. *monmouthensis* (Olsson) and *Heterohelix* sp. Microfauna from both samples points to late Campanian age of the pelagic limestones. New results confirm diachronity of Rázová and Hranty formations (at least during Campanian) and tectonic activity leading to formation of the olistoliths after Campanian.

Key words: biostratigraphy, foraminifera, Late Cretaceous, tectonic mélange, Tatricum, Western Carpathians

Graphical abstract



Highlights

- The Horné Belice Group represents tectonic mélange containing numerous intrabasinal and exotic olistoliths that accumulated due to thrusting on the outer Tatric active margin during the Late Cretaceous
- Samples from grey pelagic limestone olistoliths from the Rázová Formation contain globotruncanid planktonic foraminifera indicating Campanian age
- New results confirm diachronity of Rázová and Hranty formations during Campanian and tectonic activity leading to formation of the olistoliths after Campanian

Introduction

The Tethyan orogenic belts often contain zones of mélanges and/or disrupted formations typical for chaotic structure formed by various sedimentary and tectonic processes (e.g. Festa et al., 2010, 2012). In the Western Carpathians such formations are very common in the Meliaticum and Pieniny Klippen Belt (e.g. Mock et al., 1998; Plašienka, 2018).

The Považský Inovec Mts. (Fig. 1) is unique among the Core mountains Belt of the Western Carpathians due to the presence of the Late Cretaceous sediments which are located in different structural positions, overlying the Tatric tectonic unit, or folded and sheared between the particular Tatric thrust slices (Kullmanová & Gašpariková, 1982; Havrila & Vaškovský, 1983; Plašienka et al., 1994; Havrila in Pristaš et al., 2000; Pelech et al., 2016a, b; Pelech et al., 2017a; Figs. 1–3). The Upper Cretaceous formations represent very unique syn-orogenic sediments which are due to their character and structural position comparable to typical tectonic mélange (Fig. 6). The numerous olistoliths are large enough to be shown in geological map at a scale 1 : 50 000 (Ivanička et al., 2007). The formations of Late Cretaceous age are the most widespread in the northern portion of the mountain range – in the so-called Selec Block (sensu Maheľ, 1986), where they were discovered

by Kullmanová & Gašpariková (1982) and later together with other Jurassic formations formally included into the Belice Succession (Plašienka et al., 1994). Continuation of detailed geological mapping later proved that concept of the Belice Unit is incorrect and was abandoned. The Upper Cretaceous formations of the Belice Succession were redefined as the Horné Belice Group (Rakús in Ivanička et al., 2011). The sediments of the Horné Belice Group (Fig. 3) are divided into the Rázová Formation ("grey flysch" of Coniacian – late Campanian age) and the Hranty Formation ("red flysch" of Campanian – ?Maastrichtian age). Both formations contain blocks/olistoliths of various rocks, including underlying micaschists, Permian basalts and different sediments of Mesozoic age, ranging from the Early Triassic to Late Cretaceous (Ivanička et al., 2011) and forming tectonic mélange (sensu Festa et al., 2019). The composite sedimentary sequence assembled from the more or less exotic material of different blocks/olistoliths in the Upper Cretaceous syn-orogenic "flysch" was defined as the Humienec Succession (Plašienka et al., 1994) and considered as former sedimentary cover of the Selec Block crystalline basement. It should be, however, noted that Selec Block contains apart of crystalline basement also an autochthonous sedimentary cover, the so-called Selec Succession ranging from Late Carboniferous to Early Jurassic (Ivanička et al., 2007, 2011). The relationship between Selec Succession and Humienec Sucession is not straightforward. Both have several common members (Late Paleozoic volcanites, Triassic quartzites and carbonates), and the composite sequence of the Humienec Succession could represent continuation of the Selec Succession (e.g., Jurassic radiolarites, metamorphosed Albian and Upper Cretaceous pelagic limestones; Hók et al., 2006).

Two distinct types of Upper Cretaceous pelagic limestones are known from the olistoliths in the Rázová Formation. The first type is represented by the so-called Svinica Marlstone – pelagic, clayey often pink laminated limestones containing Turonian foraminifera (Plašienka et al., 1994; Putiš et al., 2008) found in the wider area of Humienec elevation point (609.0 m a. s. l.), SW of Mníchova Lehota village. The second type represents fragments up to blocks (max. 0.5 m in diameter) of light grey massive fine-grained limestones occurring on the northern slope of the Humienec elevation point. The aforementioned limestones were due to the lithological appearance formerly considered as calpionellid limestones since similar calpionellid limestones occur as blocks in the Horné Belice Group at the Belice locality (NE of Selec village). Thin section study, however, revealed that limestones yielded upper Campanian foraminifera (Rakús et al., 2006). Research has, however, not been published as Miloš Rakús succumbed to a serious illness. Therefore, localization and detailed biostratigraphic documentation were missing. The main aim of this paper is to provide a more detailed knowledge including localization, lithological description and biostratigraphic evaluation of the Upper Cretaceous limestone olistoliths.

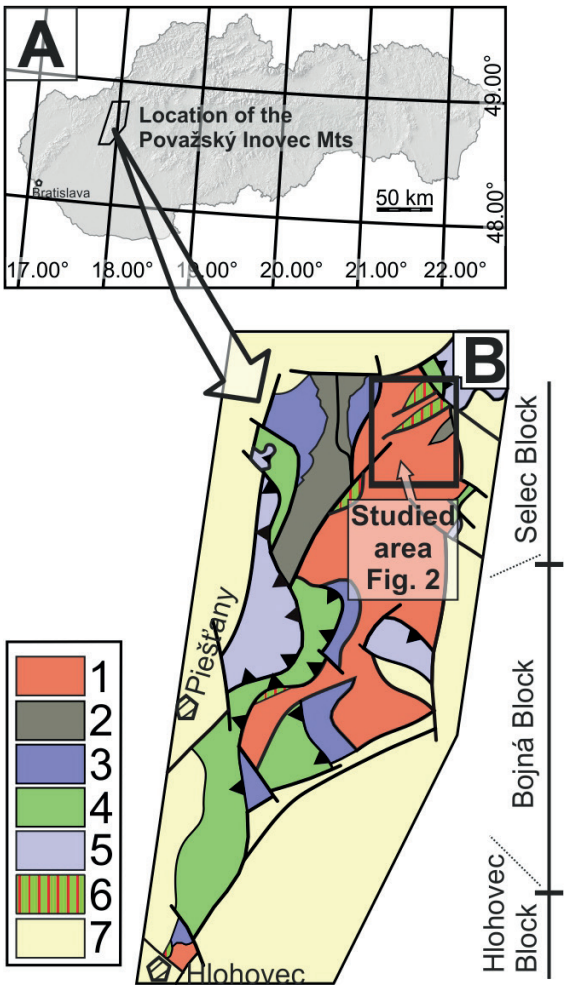


Fig. 1. Location of the investigated area within Slovakia (A) and Považský Inovec Mts. (B). 1 – Tatric Crystalline basement (Carboniferous); 2 – Tatric Kálnica Group (Upper Carboniferous – Permian); 3 – Tatric Mesozoic sedimentary cover successions; 4 – Fatricum; 5 – Hronicum; 6 – Horné Belice Group (Late Cretaceous sediments); 7 – Cenozoic sediments. Tectonic map modified from Bezák et al. (2011).

Methods

The work is based partly on the results of older geological mapping performed for the preparation of the geological map of Považský Inovec 1 : 50 000 (Ivanička et al., 2007, 2011) and later geological mapping (Pelech et al., 2016b). New rock samples from olistoliths were obtained during field research in 2020 from the Rázová Fm. The samples were processed by standard methods. Additional 4 covered thin-sections were studied. Planktonic foraminifera zones were classified according to Caron (1975), Robaszynski et al. (1984) and Sliter (1989). A combined classification

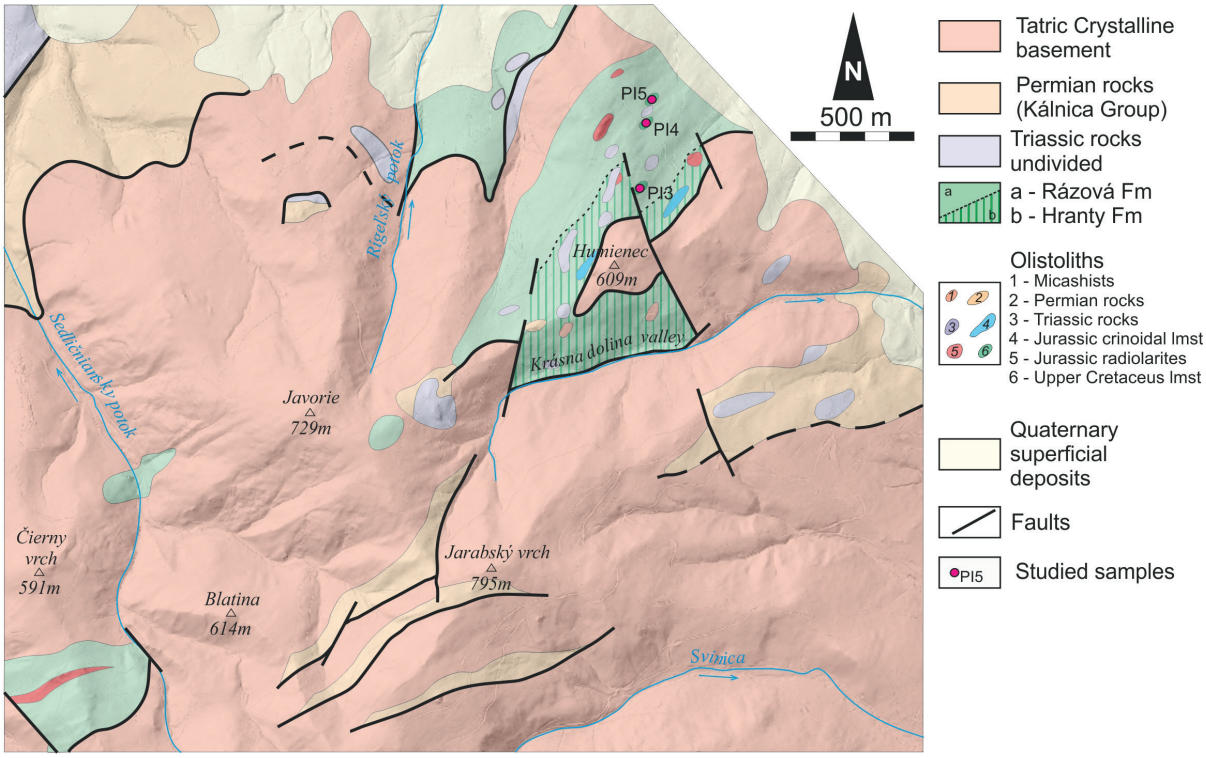


Fig. 2. Geological map of the wider area of the Humienec elevation point (609 m a.s.l.) with the marked studied outcrops and localities (for details see Tab. 1). [Background Relief model DMR 5.0 courtesy of Geodesy, Cartography and Cadastre Authority of the Slovak Republic, geological map based on Ivanička et al. (2007) and Pelech et al. (2016b)].

of Folk (1959, 1962) and Dunham (1962) was used to describe the carbonate microstructures.

Results

The area to the NW of the Humienec elevation point (609.0 m a. s. l.; Fig. 2) is poorly exposed. The limestone olistoliths are situated within the grey quartz-carbonate sandstones and claystones (or shales) of the Rázová Formation (grey "flysch") which does not form natural exposures. The observed olistoliths form blocks up to 0.5 m in diameter and represent varied lithology. At the site PI4 ("under the spring", Fig. 2, Tab. 1) various blocks including Triassic Gutenstein type limestones, grey crinoidal limestones similar to the Trlenská Formation and particularly the studied pale grey clayey limestones (sample PI4) are present. This site was the place where blocks were originally found by M. Rakús (sample HR1, Rakús et al., 2006).

Other localities include isolated blocks of grey-green clayey limestones with slaty cleavage resembling the Svinica Marlstone (in the forest road cut near lumber logs stockpile at site PI3), as well as an isolated block of fine-grained massive pale grey to pinkish limestone (sample PI5; Fig. 2, Tab. 1), which could be also possibly correlated with Svinica Marlstone.

The age of studied olistoliths was determined, based on planktonic foraminifera recognized in the thin-sections.

The sample HR1 (Tab. 1) from the original material of Miloš Rakús collected in 2005 has been revised. Microstructurally, it represents foraminifera biomicrite (foraminifer wackestone) with observed deformation and directional arrangement of allochems. Significantly recrystallized planktonic foraminifera represent *Globotruncana* cf. *linneiana* (D´ Orbigny) (Fig. 5B), *Globotruncana* cf. *arca* (Cushman), *Globotruncana ventricosa* White (Fig. 5C), *Globotruncana* sp. (Fig. 5E), *Globotruncanita stuartiformis* (Dalbiez) (Fig. 5A), *Globotruncanita subspinosa* (Pessagno) (Fig. 5D), *Falsomarginotruncana* cf. *desioi* (Gandolfi) (Fig. 5F), *Muricohedbergella* sp. and *Heterohelix* sp. The foraminifera community indicates the middle to lower part of the late Campanian. Most likely it represents the Globotruncana ventricosa zone. Other microfossils are represented by irregularly "scattered" prisms of *Inoceramus* sp. Indeterminable recrystallized biodetritus and authigenic quartz are present as well.

The sample PI4 gathered during the field investigation in 2020 (for localization see Fig. 2 and Tab.1) represents limestone with deformed and partly recrystallized components. Microstructuraly, it is a foraminifera biomicrite (foraminifera wackestone). Locally, there are more pronounced recrystallized domains of the matrix formed by

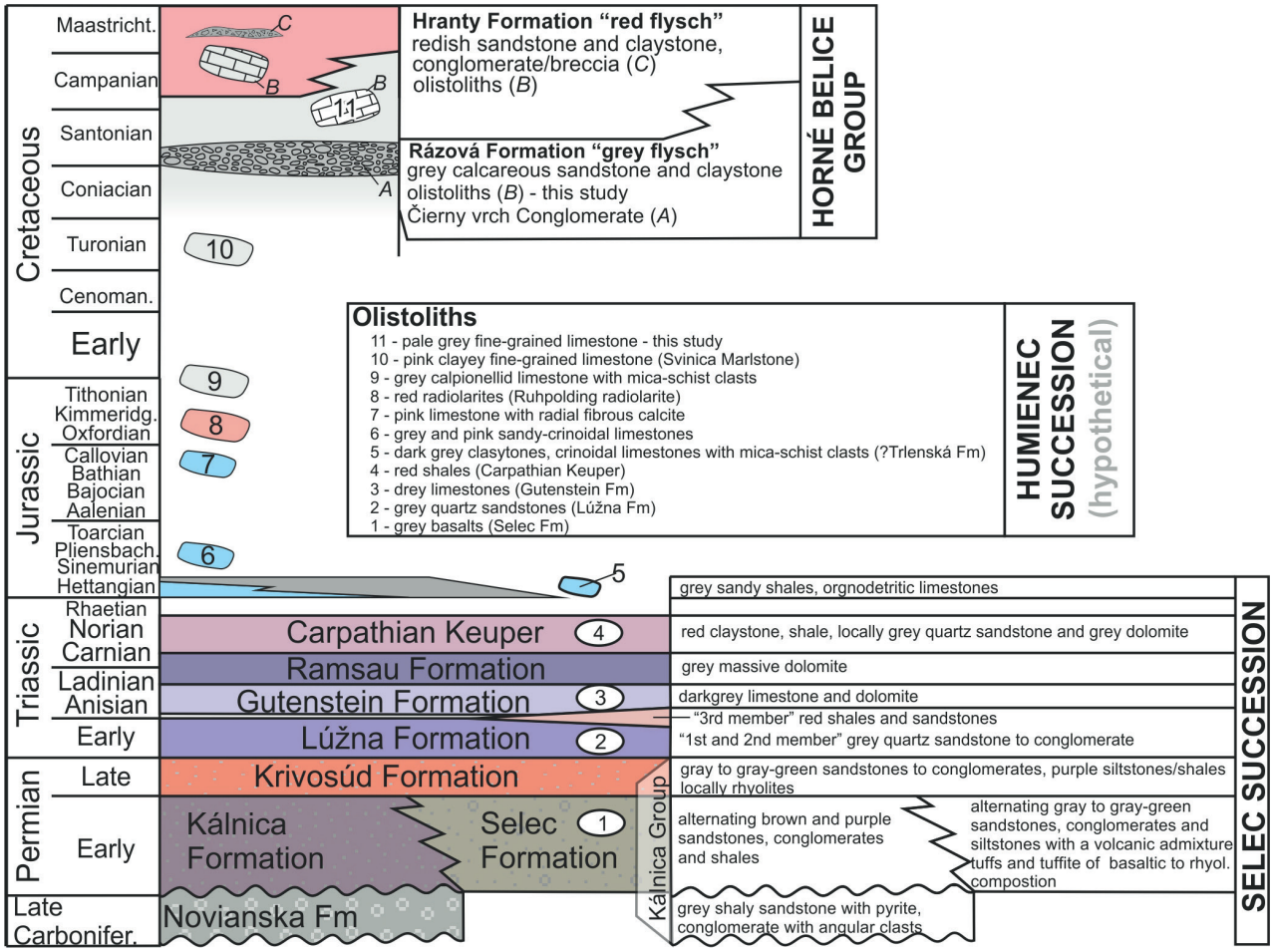


Fig. 3. Lithostratigraphic scheme of Selec Succession (Late Paleozoic – Early Jurassic), composite sequence of hypothetical Humienec Succession (from olistoliths) and Horné Belice Group (lithostratigraphy according to Olšavský, 2008; Ivanička et al., 2011; Pelech et al., 2016b).

a pseudosparite with micrite/microspartite residues, which gives the sediment a "schlieren" character. Microfossils are significantly recrystallized; the planktonic foraminifers dominate. Foraminifera tests are commonly amputated or represented only by fragments. Tests are usually filled with crystalline calcite. Foraminifera form sporadically small accumulations (clusters) (Fig. 5H). Identified microfauna is represented by the *Globotruncana ventricosa* White, *Globotruncana* sp., *Globotruncanita* cf. *subspinosa* (Pessagno), and most commonly form *Globotruncanita calcarata* (Cushman) (Fig. 5G), *Globotruncanella havanensis* (Voorwijk) (Fig. 5I), *Muricohedbergella* cf. *monmouthensis* (Olsson) and *Heterohelix* sp. The community of planktonic foraminifera represents the Zone Globotruncanita calcarata, which indicates the late Campanian. Other preserved organic detritus is mostly recrystallized, only rarely small fragment of bivalve was observed. Exceptionally, an authigenic quartz and mica are present. A brown substance probably representing insoluble clay and opaque minerals is concentrated on the foliation surfaces.

The oldest rock type of the studied olistoliths is represented by massive grey limestone samples PI5A and PI5B. The limestone is recrystallized with signs of ductile deformation and stylolites. Microstructurally, it is radiolaria-foraminifera biomicrite/biomicrosparite (radiolaria-foraminifera wackstone) gradually passing into microsparite/micrite (mudstone). Allochems are poorly sorted, irregularly arranged, more or less directionally oriented. The material was obviously redeposited. Recrystallized fossils are represented by the *Spumellaria* type radiolarians filled by crystalline calcite, echinoderm, lamellibranchiata and possibly also brachiopod fragments. Other fossil fragments include sponge spicules, rare aptychus fragments, an ammonite shell and, last but not least, sporadic poorly preserved planktonic foraminifera. The presence of rare one keel forms represented by the *Parathalmanninella* sp., or *Rotalipora* sp., as well as *Praeglobotruncana* sp. and *Muricohedbergella delrioensis* (Carsey) has been identified. Benthic foraminifera are represented by rare fragments of the nodosaride forms. Due to the poor preservation and ambiguity of their

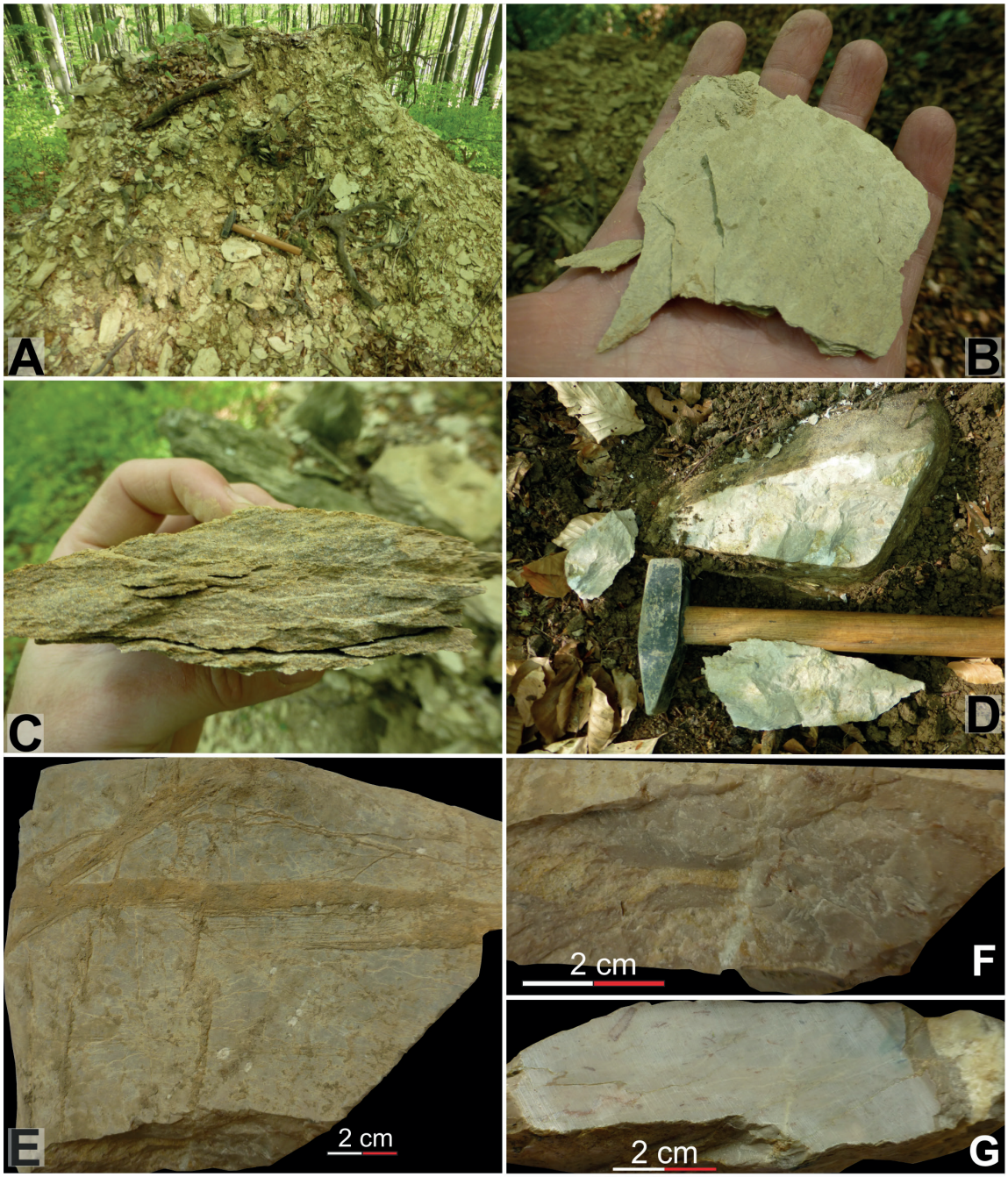


Fig. 4. A – Rock debris of the Rázová Fm. in the roots of uprooted tree at the PI4 site ("under the spring"); B – Detail of the calcareous shales of the Rázová Fm., site PI4; C – Quartz-carbonate sandstones of the Rázová Fm. with visible deformation, probably due to emerging cleavage, site PI4; D – Loose blocks of pale grey Upper Cretaceous limestones, site PI4; E–G – Detail on the sample PI4 – grey to pink pelagic limestone; E – Weathered sample; F – Fresh surface; G – Polished section.

identification, observed community most likely represents Cenomanian age. Both authigenic and clastic quartz are rarely present. The presence of Fe-minerals was also observed. Despite the limestone samples PI5A and B macroscopically strongly resemble Campanian limestones described above, their stratigraphic range is different and suggests possible correlation with Svinica Marlstone.

Discussion

Various both native/intrabasinal (originating from Selec Succession) and exotic blocks (originating from hypothetical Humienec Succession) in the Upper Cretaceous sediments of the Horné Belice Group are considered olistoliths of pre-existing and/or contemporary

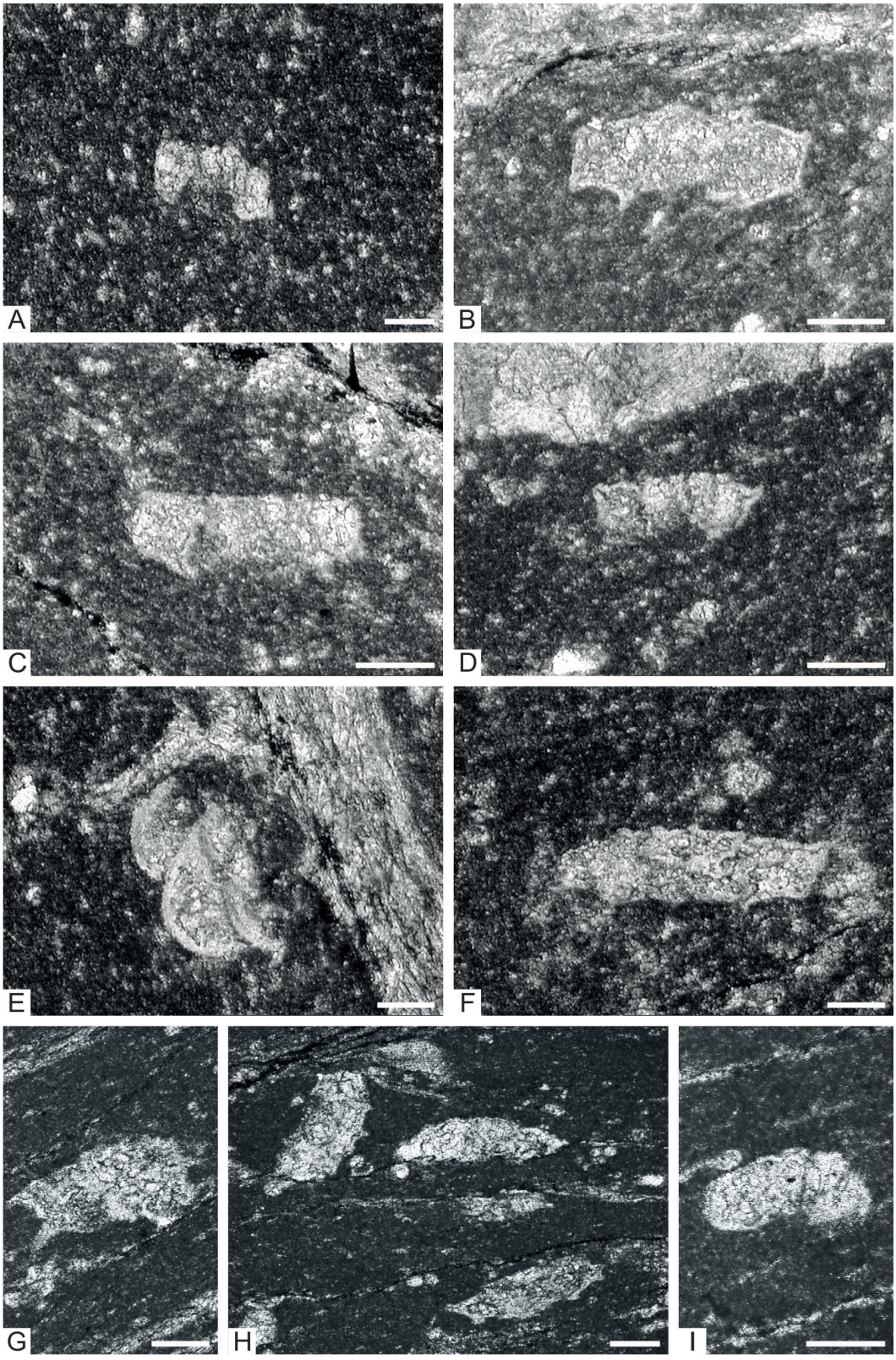


Fig. 5. Photomicrographs showing planktonic foraminifera from studied olistoliths. A–F sample HR1; G–I sample PI4. A – *Globotruncanita stuartiformis* (Dalbiez); B – *Globotruncana* cf. *linneiana* (d'Orbigny); C – *Globotruncana ventricosa* White; D – *Globotruncanita subspinosa* (Pessagno); E – *Globotruncana* sp.; F – *Falsomarginotruncana* cf. *desioi* (Gandolfi); G –*Globotruncanita calcarata* (Cushman); H – Group of recrystallized foraminifera of Calcarata Zone; I – *Globotruncanella havanensis* (Voorwijk). Scale 100 μm.

Tab. 1
An overview of important outcrops and studied sites.

Sample	Latitude (N, Y)°	Longit. (E, X)°	Lithology and locality description	Lithostratigraphy
Pl3	48.815145	18.070117	grey-green laminated limestone, forest road cut (Svinica Marlstone olistolith)	Rázová Fm
Pl4 & HR1	48.817752	18.069885	olistolith of grey fine-grained Campanian limestone, "under the spring"	Rázová Fm
Pl5	48.819024	18.070630	olistolith of grey fine-grained limestone (?Svinica Marlstone)	Rázová Fm

formations that were eroded, or tectonically dismembered (e.g. boudinaged) in the hinterland and later transported by gravity mass movements into the sedimentary basin (Fig. 6) during folding and thrusting. Therefore, the age of olistoliths cannot be younger than the age of the strata in which they are found. The youngest age of olistoliths most probably represents the onset of thrusting and destruction of the former Late Cretaceous basin overlying Tatricum in the Považský Inovec Mts. as well as in the adjacent western portion of the Strážovské vrchy Mts. (boreholes SBM-1 Soblahov and P-1 Peťovka; Kullmanová & Maheľ, 1969; Maheľ & Kullmanová, 1975; Kullmanová, 1978; Gašpariková, 1980; Maheľ, 1985).

Studied olistoliths are located in the Rázová Formation, formerly considered Coniacian – Santonian in age (Plašienka et al., 1994; Ivanička et al., 2007, 2011). Indications that the Rázová and Hranty formations coexisted together during the Campanian has sporadically appeared also earlier (Kullmanová, 1978; Pelech et al., 2016a). The confirmation of the Campanian age of the limestone olistoliths suggests that stratigraphic range of the Rázová Formation is wider. It follows that the lateral transition between the Rázová and Hranty formations existed during the Campanian and their contact is (at least partly) diachronous. Paleocurrent directions from both formations, however, differ (Plašienka et al., 1994). While the mass transport deposits (sandy turbidites and conglomerates) of the Rázová Fm. were transported generally from South to North, the sandy turbidites of the Hranty Fm. were transported from NW to SE, S and SW. The sedimentary sequence of the Horné Belice Group than can represent mixing of two sources, or two distinct submarine fans. The coarse-grained debris flow sediments of the Hubina Fm. in the Bojná Block were transported generally from the South (Pelech et al., 2017a). The paleocurrent data are, however, very sparse.

The studied olistoliths are included into the hypothetic (composite) sequence of the Humienec Succession (Fig. 3) in accordance with the previous interpretations of Rakús (in Ivanička et al., 2011; Hók et al., 2006). Unlike previous research, we consider correct to include the Svinica Marlstones to the Humienec Succession as well.

The new knowledge is in accordance with known ages of other Upper Cretaceous rocks occurrences in the Považský Inovec Mts. The sedimentation in the Hlohovec Block (southern portion of the Považský Inovec Mts.) terminated in Campanian. The age of Hubina Formation, the youngest documented Tatric sediments in the Bojná Block (central portion of the Považský Inovec Mts.), is middle Turonian – Santonian (Pelech et al., 2017a). The age of similar sediments in the borehole SBM-1 Soblahov Coniacian – Campanian (Kullmanová, 1978; Gašpariková, 1980) possibly up to Eocene (Maheľ & Kullmanová, 1975). It can be deduced, that the end of sedimentation of the Horné Belice Group is younging in general direction from south to north. This is in accordance with the process of gradual movement of the Middle Group of Nappes (sensu Hók et al., 2014, 2019).

There exist also other interpretations of the structure of Horné Belice Group and they are described in paper Pelech et al. (2016b). The Upper Cretaceous sediments are often included into the so-called Belice Unit (Plašienka et al., 1994, 2017). According to aforementioned papers it represents a continuous sedimentary succession ranging from the uppermost Middle Jurassic to Maastrichtian. The Belice Unit is often considered to be a remnant of Vahic oceanic crust, exhumed to the surface by out-of-sequence thrusting. The validity of this interpretation has been discussed by Pelech et al. (2017b). Other rarer interpretations include works of Leško et al. (1988) and Putiš et al. (2008). It should be noted, that we cannot completely exclude, that the blocks of Campanian limestones are not olistoliths and represent another thrust sheet, which is not seen in the field due to poor outcrop conditions. However, such an interpretation is, due to knowledge of structure of the wider area, mentioned here only as an unlikely alternative.

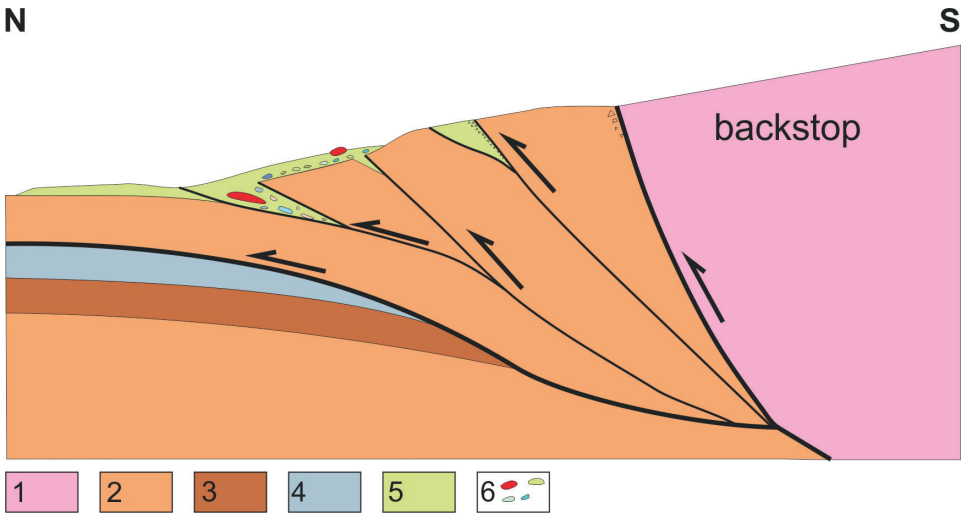


Fig. 6. Scheme showing structural position of the Upper Cretaceous Horné Belice Group tectonic mélange between the thrust sheets of the mica-schist basement of the Selec Block. 1 – Crystalline basement of Bojná Block (acting as a backstop); 2 – Mica-schists basement rocks of the Selec Block; 3 – Upper Paleozoic Kálnica Group; 4 – Selec Succession: Mesozoic sedimentary cover of the Selec Block; 5 – Upper Cretaceous Horné Belice Group; 6 – Olistoliths.

Conclusions

The Horné Belice Group of the Selec Block of the Považský Inovec Mts. is represented by mass transport deposits that accumulated on the outer active margin of the Tatric unit during the main nappe-stacking event of the Internal Western Carpathians since the Turonian. The evolution of the basin was marked by formation of olistoliths that were deposited in the Rázová and Hranty formations. The sedimentary sequence of the Upper Cretaceous Horné Belice Group thus represents a typical tectonic mélange.

Two analysed samples (PI4 and HR1) from grey pelagic limestone olistoliths (Fig. 3) situated in Rázová Fm. at the northeastern slopes of the Humienec elevation point (Fig. 2, Tab. 1) yielded foraminifera fauna of Globotruncana ventricosa and Globotruncanita calcarata zones indicating middle to late Campanian age (Fig. 5). The Upper Cretaceous limestones are included in to the hypothetical (composite) Humienec Succession. New findings suggest that the deposition of the Rázová Formation continued at least until the period of the latest Campanian. The relationship of the Rázová Formation with the Hranty Formation is diachronous.

At the same time, it can be assumed that the tectonic activity that caused deformation and folding of the Horné Belice Group together with the crystalline basement rocks postdates the late Campanian. New findings are in good agreement with process of gradual termination of deposition in the Horné Belice Group which started in the Campanian in the Hlohovec Block (southern portion of the Považský Inovec Mts.) and lasted until the Maastrichtian in the north (Selec Block) or possibly to Eocene, according to the borehole SBM-1 Soblahov.

Acknowledgements

This research was funded by the geological task of the Ministry of Environment of the Slovak Republic No. 01 02 *Geological map of the Považský Inovec Mts. and SE part of the Trenčianska kotlina Basin at scale 1 : 50 000* and by the Slovak Research and Development Agency under contract No. APVV-17-0170. The paper benefited from constructive reviews of Andrzej Ślączka and Milan Havrila.

References

Bezák, V., Biely, A., Elečko, M., Konečný, V., Mello, J., Polák, M. & Potfaj, M., 2011: A new synthesis of the geological structure of Slovakia – the general geological map at 1 : 200 000 scale. *Geol. Quart., 55, 1, 1–8.*

Caron, M., 1975: Late Cretaceous planktonic foraminifera from the Northwestern Pacific: Leg 32 of the Deep Sea Drilling Project. *Initial Rep. Deep Sea Drill. Proj., 32, 719–724.*

Dunham, R. J., 1962: Classification of carbonate rocks according to depositional texture. In: Ham, W. E. (ed.): Classification of carbonate rocks. A symposium. *Amer. Assoc. Petrol. Geol. Mem., 1, 108–171.*

Festa, A., Pini, G. A., Dilek, Y., Codegone, G., Vezzani, L., Ghisetti, F., Lucente, C. C. & Ogata, K., 2010: Peri-Adriatic mélanges and their evolution in the Tethyan realm. *Int. Geol. Rev., 52, 4–6, 369–403.*

Festa, A., Dilek, Y., Pini, G. A., Codegone, G. & Ogata, K., 2012: Mechanisms and processes of stratal disruption and mixing in the development of mélanges and broken formations: rede fining and classifying mélanges. *Tectonopysics, 568–569, 7–24.*

Festa, A., Pini, G. A., Ogata, K. & Dilek, Y., 2019: Diagnostic features and field-criteria in recognition of 4 tectonic,

sedimentary and diapiric mélanges 5 in orogenic belts and exhumed subduction-accretion complexes. *Gondw. Res., 74, 7–30.*

Folk, R. L., 1959: Practical classificaion of limestones. *Amer. Assoc. Petrol. Geol. Bull., 43, 1–38.*

Folk, R. L., 1962: Spectral subdivision of limestone types. In: Ham, W. D. (ed.): Classification of carbonate rocks. A symposium. *Amer. Assoc. Petrol. Geol. Mem., 1, 62–84.*

Gašpariková, V., 1980: Doplnenie mikrofauny z pestrých slieňov vo vrte SBM-1 Soblahov. *Geol. Práce, Spr., 74, 205–206.*

Havrila, M. & Vaškovský, I., 1983: Vysvetlivky ku geologickej mape mezozoika južnej časti Považského Inovca. *Manuscript. Bratislava, archive St. Geol. Inst. D. Štúr (n. 57032), 112 p.*

Hók, J., Rakús, M., Olšavský, M., Havrila, M., Ivanička, I. & Boorová, D., 2006: Nové poznatky o geologickej stavbe severnej časti Považského Inovca. In: Kováč, M. a Dubíková, K. (ed.): Nové metódy a výsledky v geológii Západných Karpát. Zborník 2006. *Bratislava,Univerzita Komenského, 57–66.*

Hók, J., Šujan, M. & Šipka, F., 2014: Tektonické členenie Západných Karpát – prehľad názorov a nový prístup. *Acta Geol. Slov., 6, 2, 135–143.*

Hók, J., Pelech, O., Teťák, F., Németh, Z. & Nagy, A., 2019: Outline of the geology of Slovakia (W. Carpathians). *Miner. Slov., 51, 1, 31–60.*

Ivanička, J., Havrila, M., Kohút, M. (eds.), Olšavský, M., Hók, J., Kováčik, M., Madarás, J., Polák, M., Rakús, M., Filo, I., Elečko, M., Fordinál, K., Maglay, J., Pristaš, J., Buček, S., Šimon, L., Kubeš, P., Scherer, S. & Zuberec, J., 2007: Geologická mapa Považského Inovca a jv. časti Trenčianskej kotliny, M = 1 : 50 000. *Bratislava, St. Geol. Inst. D. Štúr.*

Ivanička, J., Havrila, M., Kohút, M. (eds.), Olšavský, M., Havrila, M., Hók, J., Kováčik, M., Madarás, J., Polák, M., Rakús, M., Filo, I., Elečko, M., Fordinál, K., Maglay, J., Pristaš, J., Buček, S., Šimon, L., Kubeš, P., Scherer, S. & Zuberec, J., 2011: Vysvetlivky ku geologickej mape regiónu Považský Inovec a jv. časť Trenčianskej kotliny, M = 1 : 50 000. *Bratislava, St. Geol. Inst. D. Štúr, 389 p.*

Kullmanová, A., 1978: Výskyt pestrých slieňov vrchnej kriedy vo vrte SBM-1 Soblahov. *Geol. Práce, Spr., 71, 157–160.*

Kullmanová, A. & Maheľ, M., 1969: Záverečná správa za vrt Peťovka P-1, čiastková záverečná správa. Názov úlohy v perspektívnom pláne: Výskum mezozoika centrálneho a bradlového pásma Západných Karpát. *Manuscript. Bratislava, archive St. Geol. Inst. D. Štúr (arch. no. 24157), 19 p.*

Kullmanová, A. & Gašpariková, V., 1982: Vrchnokriedové sedimenty v severnej časti pohoria Považský Inovec. *Geol. Práce, Spr., 78, 85–95.*

Leško, B., Šutora, A. & Putiš, M., 1988: Geology of the Považský Inovec Horst based on geophysical investigation. *Geol. Zbor. Geol. Carpath., 39, 2, 195–216.*

Maheľ, M., 1985: Geologická stavba Strážovských vrchov. *Bratislava, Geol. Inst. D. Štúr, 207 p.*

Maheľ, M., 1986: Geologická stavba československých Karpát – Paleoalpínske jednotky. *Bratislava, Veda, 503 p.*

Maheľ, M. & Kullmanová, A., 1975: Výskum mezozoika Strážovskej hornatiny – štruktúny vrt SBM-1 Soblahov, čiastková záverečná správa za roky: 1969–1975. Regionálny výskum mezozoika Západných Karpát. *Manuscript Bratislava, archive St. Geol. Inst. D. Štúr (arch. no. 35434), 29 p.*

Mock, R., Sýkora, M., Aubrecht, R., Ožvoldová, L., Kronome, B., Reichwalder, P. & Jablonský, J., 1998: Petrology and stratigraphy of the Meliaticum near the Meliata and Jaklovce villages, Slovakia. *Slovak Geol. Mag., 4, 4, 223–260.*

Olšavský, M., 2008: Litostratigrafia a sedimentogenéza vrchnopaleozoických súvrství v severnej časti Považského Inovca. *Miner. Slov., 40, 1–16.*

Pelech, O., Józsa, Š., Kohút, M., Plašienka, D., Hók, J. & Soták, J., 2016a: Structural, biostratigraphic and petrographic evaluation of the Upper Cretaceous red marlstones and underlying granitoids from the borehole HPJ-1 Jašter near Hlohovec (Považský Inovec Mts., Slovakia). *Acta Geol. Slov., 8, 1, 27–42.*

Pelech, O., Hók, J., Havrila, M. & Pešková, I., 2016b: Structural position of the Upper Cretaceous sediments in the Považský Inovec Mts. (Western Carpathians). *Acta Geol. Slov., 8, 1, 43–58.*

Pelech, O., Hók, J. a Józsa, Š., 2017: Turonian–Santonian sediments in the Tatricum of the Považský Inovec Mts. (Internal Western Carpathians, Slovakia). *Aust. J. Earth Sci., 110, 1, 19–33.*

Pelech, O., Hók, J., Havrila, M. & Pešková, I., 2017b: Reply to Comment on "Structural position of the Upper Cretaceous sediments in the Považský Inovec Mts. (Western Carpathians)". *Acta Geol. Slov., 9, 1, 39–43*.

Plašienka, D., 2018: The Carpathian Klippen Belt and types of its klippen – an attempt at a genetic classification. *Miner. Slov., 50, 1, 1–24.*

Plašienka, D., Marschalko, R., Soták, J., Peterčáková, M. & Uher, P., 1994: Origin and structural position of Upper Cretaceous sediments in northern Považský Inovec Mts. Part One: Lithostratigraphy and sedimentology. *Miner. Slov., 26, 5, 311–334.*

Plašienka, D., Putiš, M., Soták, J. & Méres, Š., 2017: Are we still far from a reliable solution? *Acta Geol. Slov., 9, 1, 35–38*.

Pristaš, J. (ed.), Elečko, M., Maglay, J., Fordinál, K., Šimon, L., Gross, P., Polák, M., Havrila, M., Ivanička, J., Határ, J., Vozár, J., Tkáčová, H., Tkáč, J., Liščák, P., Jánová, V., Švasta, J., Remšík, A., Žáková, E. & Töröková, I., 2000: Vysvetlivky ku geologickej mape Podunajskej nížiny – Nitrianskej pahorkatiny 1 : 50 000. *Bratislava, St. Geol. Inst. D. Štúr, 250 p.*

Putiš, M., Gawlick, H.-J., Frisch, W. & Sulák, M., 2008: Cretaceous transformation from passive to active margin in the Western Carpathians as indicated by the sedimentary record in the Infratatric unit. *Int. J. Earth Sci. (Geol. Rdsch.), 97, 799–819.*

Rakús, M., Boorová, D. & Hók, J., 2006: Nález vrchnokriedového vápenca v severnej časti Považského Inovca. *Miner. Slov., 38, 2, Geovestník, 18–19.*

Robaszynski, F., Caron, M., Gonzales Donoso, J. M., Wonders, A. A. H. & Eur. Working Group on Plankt. Foram., 1984: Atlas of Late Cretaceous Globotruncanids. *Revue Micropaleont., 26, 3–4, 145–305.*

Sliter, W. V., 1989: Biostratigraphic zonation for Cretaceous planktonic foraminifers examined in thin section. *J. Foraminiferal Res., 19, 1, 1–19.*

Olistolity vápencov vrchnej kriedy v rázovskom súvrství hornobelickej skupiny Považského Inovca (Západné Karpaty)

Považský Inovec je v rámci jadrových pohorí výnimočný kvôli výskytu sedimentov vrchnej kriedy, ktoré sa nachádzajú v odlišných pozíciách v nadloží tektonickej jednotky tatrika, resp. zavrásnené medzi jeho tektonickými šupinami (Kullmanová a Gašpariková, 1982; Plašienka et al., 1994; Havrila in Pristaš et al., 2000; Rakús et al., 2006; Pelech et al., 2016a, 2016b, 2017a, 2017b). Plošne najrozšírenejšie sú v severnej časti pohoria (selecký blok *sensu* Maheľ, 1986), kde boli formálne zahrnuté do belickej sukcesie (*sensu* Plašienka et al., 1994) a neskôr do hornobelickej skupiny (*sensu* Rakús in Ivanička et al., 2011). Sedimenty hornobelickej skupiny sa vnútorne členia na rázovské (koňak – spodný kampán) a hrantské súvrstvie (kampán – ?mástricht). V oboch súvrstviach sa vyskytujú bloky/olistolity hornín podložného kryštalinika, bázických vulkanických hornín (paleozoikum), ako aj sedimentov mezozoika v stratigrafickom rozsahu od spodného triasu do spodnej kriedy (Ivanička et al., 2011). Pre tento kompozitný horninový súbor, ktorý sa považuje za pôvodný sedimentárny obal tatrického fundamentu, zaviedli Plašienka et al. (1994) pomenovanie humienecká sukcesia. Osobitým litostratigrafickým členom humienieckej sukcesie, opísaným z rázovského súvrstvia severného okraja Považského Inovca (Rakús in Ivanička et al., 2007; Rakús in Ivanička et al., 2011), sú úlomky až bloky (max. 0,5 m^3) svetlosivých nevrstevnatých jemnozrnných vápencov vyskytujúce sa na severnom svahu kóty Humienec (609,0). Tieto vápence boli stratigraficky zaradené do stredného kampánu až spodnej časti vrchného kampánu, ale bez náležitej lokalizácie a biostratigrafickej dokumentácie (Rakús et al., 2006). V príspevku uvádzame ich lokalizáciu, litologický opis a biostratigrafické vyhodnotenie (obr. 1 – 3, tab. 1).

Pri stanovení veku vápencov odobraných z olistolitov je určujúci výskyt rekryštalizovaných planktonických foraminifer zistených vo výbrusovom materiáli.

Z opakovaného terénneho zberu materiálu z olistolitov v roku 2020 pochádza vzorka PI4. Jednotlivé komponenty vápenca sú vplyvom tlakového postihnutia usmernené. Z hľadiska mikroštruktúry ide o foraminiferový biomikrit (foraminiferový *wackestone*). Lokálne sa vyskytujú výraznejšie rekryštalizované pasáže základnej hmoty tvorené pseudosparitom so zvyškami mikritu/mikrosparitu, čím sediment nadobúda šmuhovitý charakter.

Mikrofosílie sú výrazne rekryštalizované. Dominujú planktonické foraminifery, ktorých schránky sú bežne amputované, ponorené v základnej hmote, prípadne sa vyskytujú iba ich fragmenty. Sú vyplnené spravidla kryštalickým kalcitom. Foraminifery tvoria sporadicky malé akumulácie (zhluky) (obr. 5H). Identifikované bolo spoločenstvo *Globotruncana ventricosa* White, *Globotruncana* sp., *Globotruncanita* cf. *subspinosa* (Pessagno), najbežnejšie sa vyskytujúca forma *Globotruncanita calcarata* (Cushman) (obr. 5G), *Globotruncanella havanensis* (Voorwijk) (obr. 5I), *Muricohedbergella* cf. *monmouthensis* (Olsson) a *Heterohelix* sp. Spoločenstvo planktonických dierkavcov reprezentuje zónu Globotruncanita calcarata, ktorá indikuje vrchný kampán. Organické zvyšky reprezentuje aj ojedinelý malý úlomok najpravdepodobnejšie lastúrnika. Bežne sa vyskytuje drobný rekryštalizovaný biodetrit, resp. detrit.

Výnimočne je prítomný autigénny kremeň a sľuda. Na plochách foliácie je koncentrovaná hnedá substancia.

Vo vzorke HR1 zo starších zberov M. Rakúsa, ktorá bola podrobená revízii, je rovnako viditeľné tlakové postihnutie vápenca a usmernenie alochémov. Mikroštruktúrne sa zaraďuje k foraminiferovým biomikritom (foraminiferový *wackestone*).

Výrazne rekryštalizované planktonické foraminifery reprezentujú *Globotruncana* cf. *linneiana* (d´ Orbigny) (obr. 5B), *Globotruncana* cf. *arca* (Cushman), *Globotruncana ventricosa* White (obr. 5C), *Globotruncana* sp. (obr. 5E), *Globotruncanita stuartiformis* (Dalbiez) (obr. 5A), *Globotruncanita subspinosa* (Pessagno) (obr. 5D), *Falsomarginotruncana* cf. *desioi* (Gandolfi) (obr. 5F), *Muricohedbergella* sp. a *Heterohelix* sp. Spoločenstvo foraminifer indikuje stredný kampán až spodnú časť vrchného kampánu. Ide najpravdepodobnejšie o zónu Globotruncana ventricosa.

Mikrofosílie zastupujú okrem foraminifer časti, ako aj nepravidelne „roztrúsené“ prizmy schránok lastúrnika *Inoceramus* sp. Prítomný je bližšie neurčený rekryštalizovaný biodetrit, resp. detrit.

Doručené / Received: 20. 5. 2021
Prijaté na publikovanie / Accepted: 30. 6. 2021

Mineralia Slovaca, Web ISSN 1338-3523, ISSN 0369-2086
53 (2021), 47 – 56, © Author 2021. CC BY 4.0

Lithology and position of the Biele Karpaty Unit SE of Lednica (Biele Karpaty Mts., Western Carpathians)

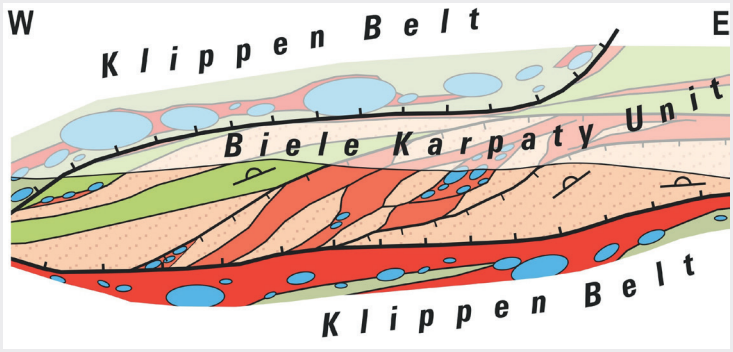
FRANTIŠEK TEŤÁK

State Geological Institute of Dionýz Štúr, Mlynská dolina 1, SK-817 04 Bratislava, Slovakia;
frantisek.tetak@geology.sk

Abstract: Recent geological research and mapping SE of Lednica village brought several new findings important not only for the studied area, but also for understanding the relationship between the Klippen Belt and Flysch Belt at all: (1) The flysch sequence from the base to top is the Ondrášovec, Javorina, Chabová and Bzová mbs. of the Biele Karpaty Unit of Magura Nappe (Campanian to early Eocene). (2) The sequence of the Biele Karpaty Unit is situated in an overturned position with the prevailing strike of the beds 250–360° and dip of the beds 20–50°. (3) The structure is significantly sliced, especially in the zone with the Ondrášovec Mb. The slices of the Biele Karpaty Unit were turned back and then they were back thrust to the SE over Klippen Belt together with the Vršatec slice. (4) So far undescribed group of the Bukovina hill klippen NW from the Dolná Breznica village and a group of klippen NW from Kvašov village have been identified. (5) Six paleocurrent measurements were measured from the Ondrášovec Mb. – 210°, Javorina Mb. – 315° and Chabová Mb. – 2 x 330° and 2 x 10°.

Key words: stratigraphy, back thrust, Klippen Belt, Flysch Belt, Magura Nappe

Graphical abstract



Highlights

- The flysch sequence SE of Lednica village belongs to the Biele Karpaty Unit of Magura Nappe. From the base to top the Ondrášovec, Javorina, Chabová and Bzová mbs. are present.
- The external position of the klippen integrated into the Magura Nappe can be explained by back thrusting.

Introduction

The studied area of the Biele Karpaty Mts. forms a nappe complex of "flysch" formations belonging to the Biele Karpaty Unit of the Magura Nappe and to the complex structure of Klippen Belt of the Western Carpathians (Fig. 1). In the past, the area SE of Lednica village has been processed several times and displayed in geological maps (Maheľ et al., 1962; Salaj et al., 1983; Began et al., 1992, 1993; Mello et al., 2005, 2011). The authors focused more on the study of Jurassic-Lower Cretaceous klippen of Klippen Belt than on the flysch sequences. Salaj et al. (1983) defined the flysch formations in this area as the Kvašov development of the Klape Unit. Within the geological map of the Žilina sheet at a scale of 1 : 200,000 (Maheľ et al., 1962) authors divided the flysch complex of the studied area into the Biele Karpaty Unit (middle to late Eocene) and Klippen Belt (flysch development of Pupov Mb. – Santonian–Campanian) without structural data, between which they distinguished the variegated marls of late Santonian in two places.

The geological map of the Pruské sheet at a scale of 1 : 25,000 (Salaj et al., 1983) is a relatively detailed map. The authors documented position of 8 outcrops, but they did not specify the position of the sequence (top and bottom). Therefore, the authors could not find that the sequence was overturned. The map also omits a group of klippen NW from Dolná Breznica village and NW from Kvašov village, which led to the opinion that the sequence is continuous in a normal position. The authors classified the flysch sequences as the Kvašov development of the Drietoma succession of Klape Unit. In some places of the map, the belt of "variegated marls" is missing or it is incorrectly displayed. The mentioned work represented a base for the compilation of the later maps. Former limitations were later included in the works of Began et al. (1992, 1993) and Mello et al. (2005, 2011).

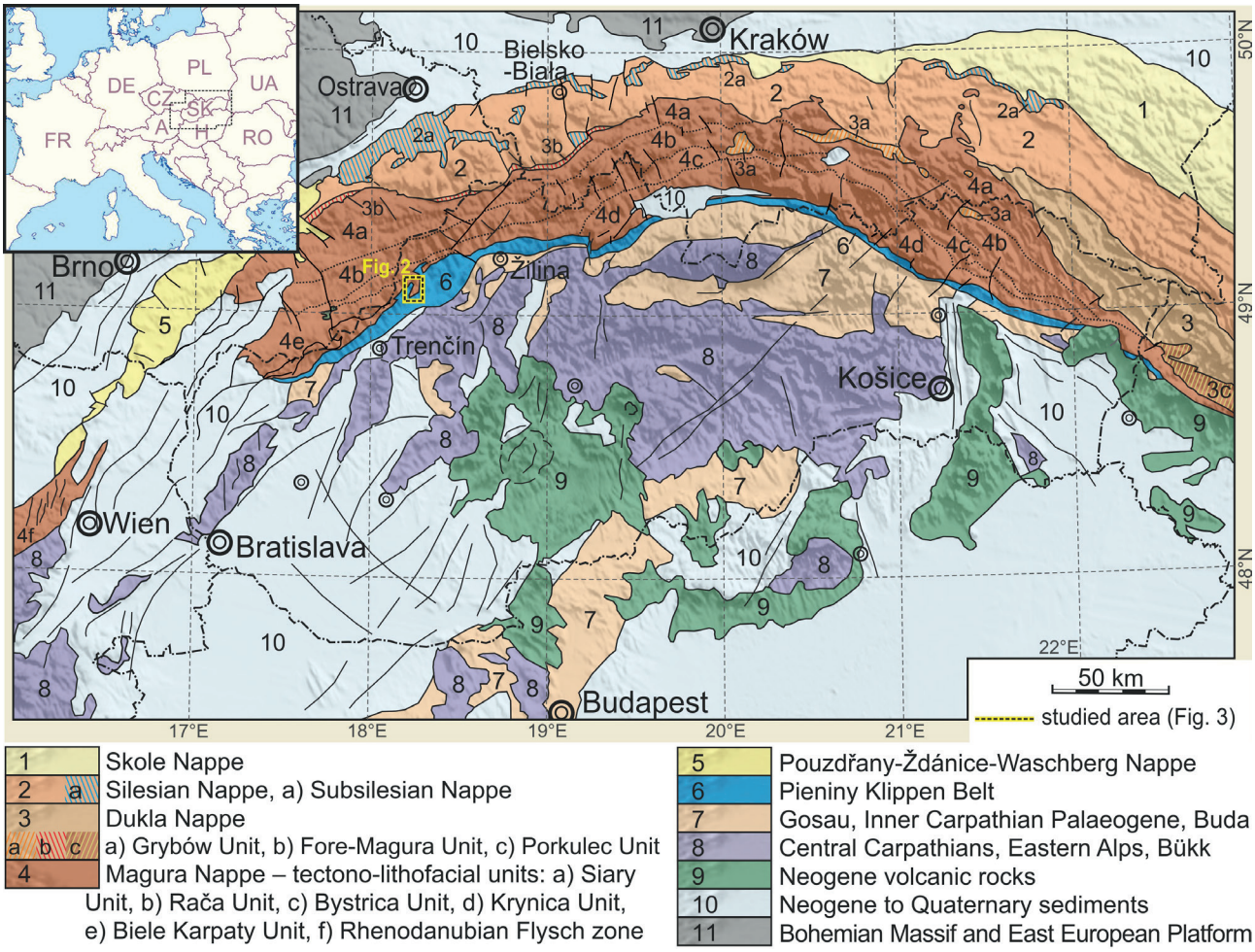


Fig. 1. Schematic geological map of the Western Carpathians with the location of studied area (designated as Fig. 2).

Methodology

The intensive geological research and mapping at a scale of 1 : 25,000 that carried out in the Biele Karpaty Mts. since 2016, intended to compile a new geological map and to solve the geological setting of the area between towns of Nové Mesto nad Váhom and Nemšová (Pešková et al., 2021a). Since 2019, the engineering geological monitoring of slope deformations was tied on previous regional geological research in the area of the Biele Karpaty and Javorníky Mts. The problematic areas of the geological map underwent the reambulation. Also, the area built by the Biele Karpaty Unit and Klippen Belt SE of Lednica was reambulated at a scale of 1 : 10,000. Geological mapping and its evaluation took place without the availability of LIDAR maps (high-resolution relief maps). Rock samples were not petrographically and paleontologically analysed, because the research was focused on the identification, inventory and engineering geological mapping of slope deformations. The advantage of done geological research was its connection to previous detailed research of the Biele Karpaty Mts. and the possibility to mutually compare the areas.

The research results

The geological research in the area SE of Lednica has distinguished four lithostratigraphic units. Although they originally formed a continuous sequence of the Biele Karpaty Unit, the enormously complex geological development of the area caused the tectonic contacts probably of all lithostratigraphic units. The more plastic horizon of the Ondrášovec Mb. rocks was squeezed into the main tectonic zones. The rock sequence can be reconstructed from bottom to top as follows: the Ondrášovec and Javorina mbs. of the Lopeník Fm. and the Chabová and Bzová mbs. of the Svodnice Fm. (Figs. 2 and 3), reaching the age from Campanian to early Eocene (Potfaj, 1993; Pešková et al., 2021b).

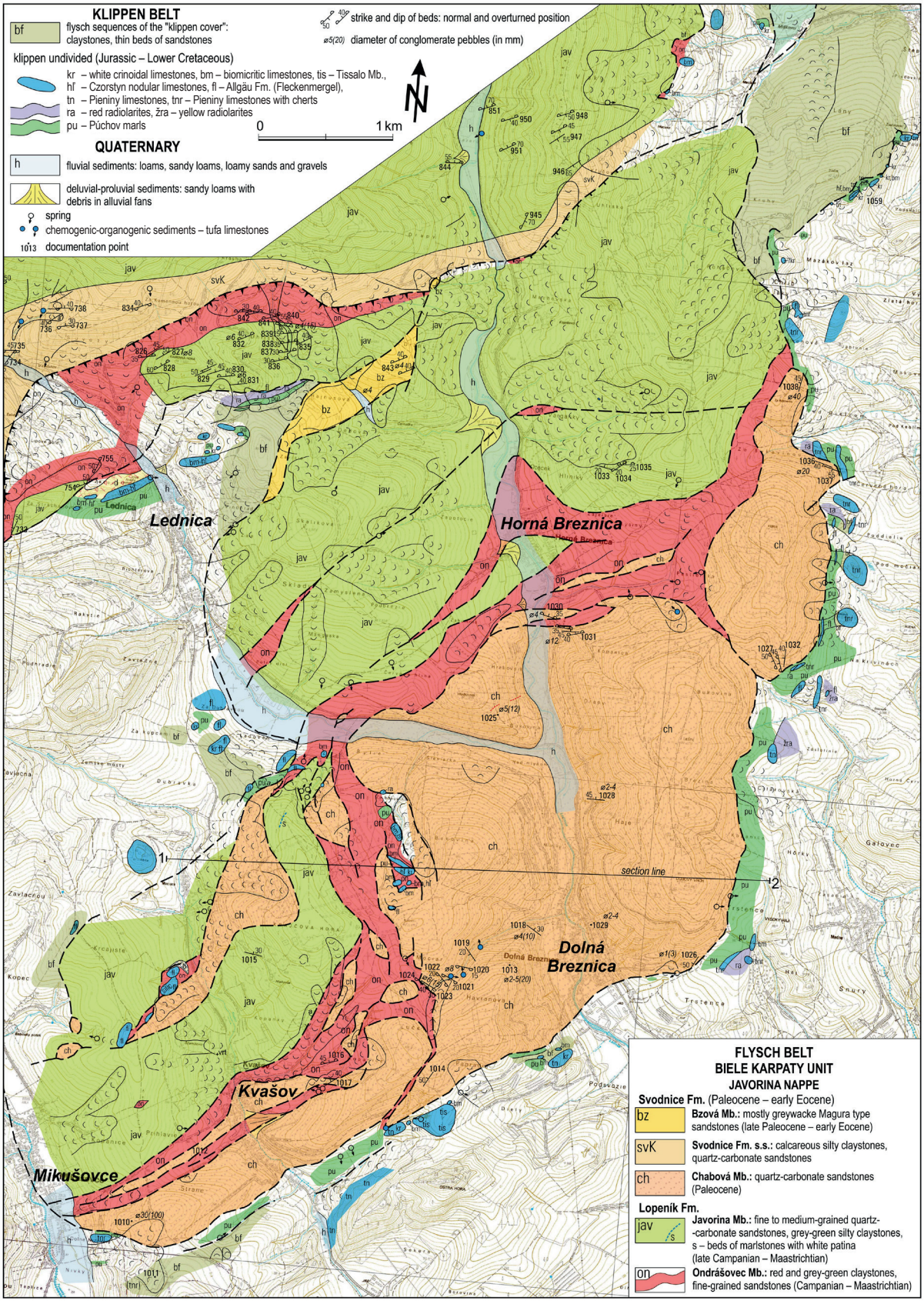


Fig. 2. Geological map of the Biele Karpaty Unit SE of Lednica.

Biele Karpaty Unit

Ondrášovec Mb.

The Ondrášovec Mb. was defined by Potfaj (1993) on the outcrops near the Ondrášovec settlement on the southern slope of the Veľký Lopeník Mt., describing a variegated formation at the base of Javorina Nappe. The member can be characterized as thin-bedded flysch deposits, formed by red and grey-green claystones alternating with thin beds of greenish laminated sandstones with muscovite.

Just one outcrop of Ondrášovec Mb. was observed in the studied area (Fig. 4A). Claystones predominate over sandstones. Light green-grey, grey and red non-calcareous claystones to silty claystones alternate with thin but also thicker beds (4–20 cm) of laminated very fine-grained quartz-carbonate sandstones. All other outcrops were significantly weathered.

The Ondrášovec Mb. is located at the basal plane of the Javorina, Zubák and Vrbovce nappes, it is rheologically plastic and it tends to be significantly deformed and tectonically reduced. The thickness of the member is only a few tens of meters. Tectonic duplexes are assumed to form over a 100 m thick complex in some places. They are a significant and important marker in geological mapping. Based on nannoplankton, Potfaj (1993) indicates a middle Campanian to early Maastrichtian age of the member.

Javorina Mb.

The development of the Javorina Mb. (Potfaj, 1993; Pešková et al., 2021b) is facially diverse. It can vary within areas, tectonic slices or the bed sequence of the Biele Karpaty Unit. In the studied area, the Javorina Mb. can be characterized as a flysch-type formation with a variable proportion of sandstones and claystones known only from several outcrops and character of the deluvium in studied area. Sandstones slightly predominate over claystones. They form 20 to 60 cm thick beds of well-sorted fine-grained, rarely medium-grained, massive or laminated quartz-carbonate sandstones with a higher content of muscovite and coalified plant detritus (Fig. 4B). Green-grey non-calcareous claystones form only thinner layers.

The debris of a solid grey marlstone bed with a white patina was observed in a deluvium on the ridge north of the Kvašov village. Beds of such marlstones to limestones are typical for the higher part of the Javorina Mb. (Potfaj et al., 2014; Pešková et al., 2021b).

The thickness of the Javorina Mb. is significantly tectonically reduced. It does not exceed 400 m in the studied area. Based on nannoplankton, Potfaj (1993) indicates the age of Javorina Mb. as a late Campanian to Maastrichtian.

Chabová Mb.

The member can be characterized as thick-bedded flysch sequence with massive quartz-carbonate sandstones almost without claystones (Potfaj, 1993; Pešková et al., 2021b). In the studied area, Salaj et al. (1983) interpreted it as Jarmuta Mb. in a continuous sequence passing from the Púchov marls. Due to the relatively abundant outcrops, it was possible to verify reliably the overturned position

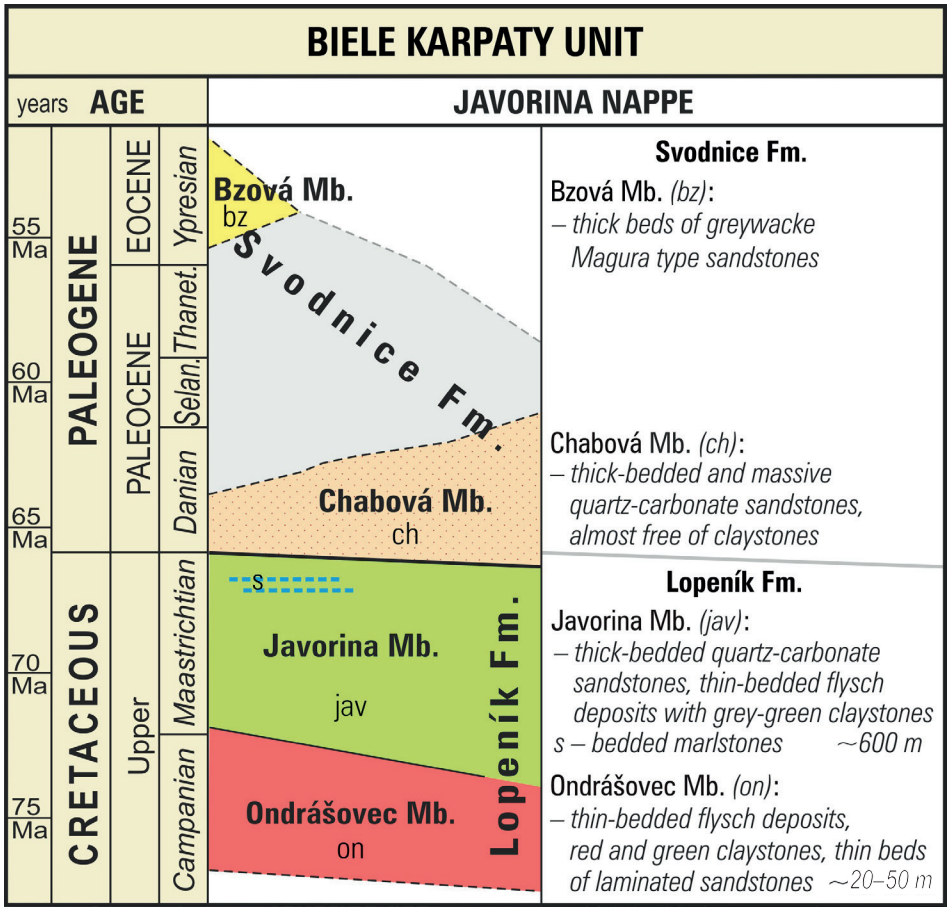


Fig. 3. Lithostratigraphy of the Biele Karpaty Unit SE of Lednica (modified after Pešková et al., 2021b).

of the Chabová Mb., having tectonic contact with the Púchov marls.

There is an absolute predominance of sandstones over claystones in the studied area. The character of the member changes continuously towards the top. The ratio of sandstones to claystones, the thickness of layers and grain size of sandstones are increasing and the lithification of sandstones is weakening towards the top. Fine- to coarse-grained quartz-carbonate sandstones form 40 to 300 cm thick, generally amalgamated, massive structureless beds. The fine-grained parts of the beds show an indistinctive plane lamination. Rapid weathering or disintegration with poorer lithification, rusty coatings to liesegang bands, rusty cracks, absence of clay interlayers, abundant muscovite and coalified plant detritus are the common features of sandstones (Fig. 4C, D). Deluvium is formed by thick yellowish-white sandy loams (Fig. 4E).

Green-grey and grey silty claystones are only up to 5 cm thick. Intraclasts of green claystones are rare in sandstones.

Lenses or layers of fine-grained conglomerates were observed in several places. The pebbles reach a diameter of 2–10 (max. 100) mm. In addition to standard quartz and quartzites, the conglomerates contain metamorphic rocks, granites, porphyries, phyllites, melaphyre pebbles, but carbonate material is predominating over quartz – dolosparite (?Triassic), fossil-free micritic and sparite limestones, calpionella-radiolarian biomicritic limestones of Tithonian and Berriasian and sandstones with Cenomanian orbitolina (*Orbitolina concava* Lamarck, *O. plana* d'Archiac, a.o.; Salaj et al., 1983).

Salaj et al. (1983) determined the age of the member in the studied area based on agglutinated microfauna and orbitoid foraminifers as the late Campanian and Maastrichtian. It can be considered a redeposition based on an analogy with the Chabová Mb. of Biele Karpaty Unit and the age of member classify as Paleocene (Potfaj, 1993; Pešková et al., 2021b).

The thickness of the member does not exceed 500 m in the studied area, or 300 m according to Salaj et al. (1983).

Bzová Mb.

About 1.5 km long tectonic slice, formed by Magura type sandstones, should be included into the Biele Karpaty Unit within the studied area east of the Lednica village. These sandstones represent the youngest sequence of the Svodnice Fm. and in the case of larger accumulation they form the Bzová Mb. within the Biele Karpaty Unit sequence. Magura type sandstones were clearly identified from the debris in the studied area, and especially on the several outcrops with over 1.5 m thick graded beds of coarse- to medium-grained greywacke sandstones. Weathered sandstones are brown, usually with scattered larger grains with a diameter of 1–(4) mm (paraconglomerate) and with water-escape structures. Their age is middle to late Paleocene based on nannoplankton from Bzová area (Potfaj, 1993) and thickness reaches up to 300 m in the studied area.

Klippen Belt

The aim of geological research and mapping was not a detailed research of the Klippen Belt, but especially the flysch sequence of the Biele Karpaty Unit. Nevertheless, the research revealed several unpublished data. Red and pinkish marls with globotruncana to red claystones of the Púchov Fm. form an almost continuous belt around the Biele Karpaty Unit sequence in the studied area (Fig. 4F). Púchov marls are accompanied with the flysch sequence of the klippen cover in particular between Lednica and Mikušovce villages (Fig. 2). Spotted marls of the Tissalo Mb. occur between Kvašov and Dolná Breznica villages. Mentioned Cretaceous members form the cover of smaller irregularly distributed klippen, built by various Jurassic-Lower Cretaceous lithofacies. Klippen build by spotted limestones of Allgäu Fm. (Fleckenmergel), white crinoidal limestones, red and yellow radiolarites, biomicritic and nodular Czorsztyn limestones and Pieniny limestones with or without cherts were observed (Fig. 2).

Two groups of klippen tectonically incorporated between the slices of the Biele Karpaty Unit were found NW from Kvašov and NW from Dolná Breznica. Klippen are built by most of the above mentioned lithofacies, including the Púchov marls. The southeastern edge at the junction of Biele Karpaty Unit with the Klippen Belt is bordered by the Púchov marls (Fig. 4F). This boundary line is sharp and the Púchov marls or klippen were not found folded into the Chabová Mb. along this border.

Paleocurrent analyses

Six paleocurrent measurements were done during geological research (Fig. 5). They do not represent a statistically sufficient set, but with the support of the knowledge of the neighbouring Biele Karpaty Unit paleogeography, it is possible to draw certain conclusions (Fig. 5). The SW (210°) paleotransport direction of the Ondrášovec Mb. corresponds to the predominant paleotransport direction of the thin-bedded facies during the latest Cretaceous in the direction parallel to the Magura Basin elongation (Teťák et al., 2019).

The paleotransport direction of the Javorina Mb. to the NW (315°) is in accordance with the knowledge of



Fig. 4. A: Ondrášovec Mb. – weathered variegated claystones and thin beds of sandstones (road cut east from Kvašov, documentary point 1016); **B:** Javorina Mb. – bedding plane with flute casts (d. p. 1035); **C, D:** Weathered and disintegrating sandstone of Chabová Mb. (d. p. 1018, 1037); **E:** Excavation of at least 4 m thick deluvium of weathered sandstones of Chabová Mb. (Dolná Breznica, d. p. 1029); **F:** Red Púchov marls in the road cut (d. p. 1032).

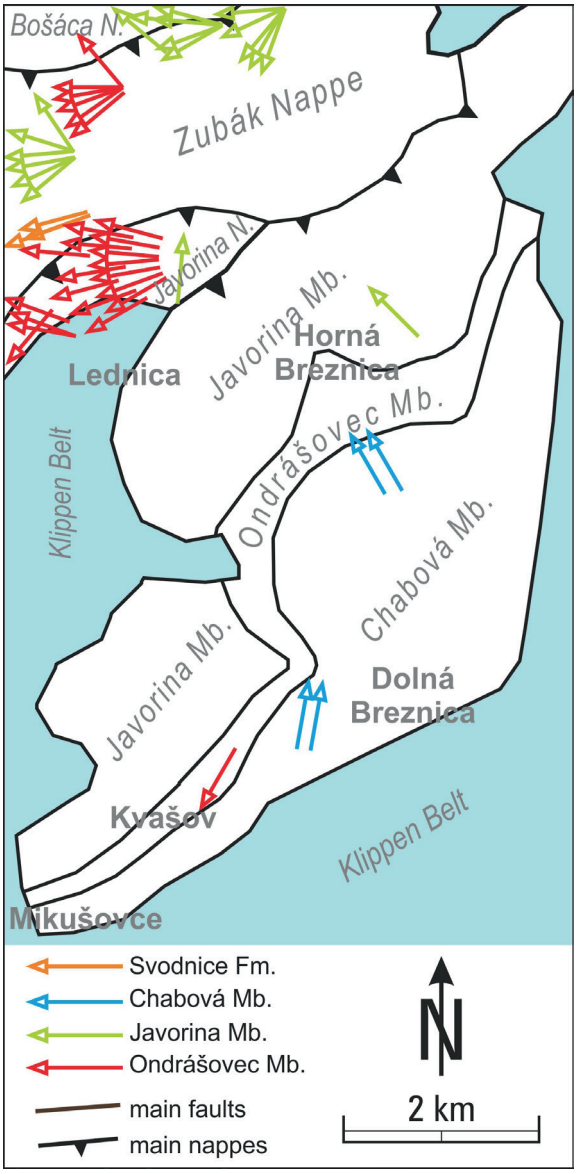


Fig. 5. Schematized map of the studied area shows the measured paleocurrent directions. Their lithostratigraphic and lithofacial classification is distinguished by colour. Unpublished paleocurrent measurements are supplemented in the neighbouring Javorina and Zubák nappes.

the paleotransport directions of Javorina Mb. of the Biele Karpaty Unit (Stráník et al., 1989; Marschalko, 1985 and unpublished data).

The Chabová Mb. deposits are the result of the sedimentation of a relatively smaller submarine fan. The paleotransport measurements direct to the north (2 x 330° and 2 x 10°). Together with the facial development, the paleotransport directions of Chabová Mb. in the studied area can be interpreted as the place of lateral supply of clastic material into the Magura Basin.

In this interpretation it is necessary to take into account the statistically insufficient number of measurements and possible tectonic rotation of the measured rock blocks, as the investigated area is significantly tectonically deformed.

Tectonics

The more detailed knowledge of the geological structure of the Biele Karpaty Unit flysch sequence SE of Lednica as well as its relation to the Klippen Belt were brought by geological mapping. It has been found that it is not a single continuous sequence as suggested by earlier works of Salaj et al. (1983) and Began et al. (1992, 1993). The area is formed by several tectonic blocks or slices. The slices and blocks are formed by flysch sequences of the Javorina and Chabová mbs. They are surrounded by tectonically strongly deformed Ondrášovec Mb. This had the function of a plastic tectonic gliding horizon at the base of displaced nappes and slices. During the movement of the nappes, blocks of the underlying formations were incorporated into the Ondrášovec Mb. Also, the nappe duplexes were observed (Fig. 6). The base of the Javorina Nappe in the Nová Bošáca and Horná Súča areas represents an example of duplexes (Pešková et al., 2021a). The structure of the narrow zone formed by Ondrášovec Mb. is so complicated that it is still not obvious whether the slice with Chabová Mb. was moved first as a nappe to the NW over the Javorina Mb. before thrusting/tilting over on the Klippen Belt, or it was the opposite process – back thrusting after tilting over the Klippen Belt. Based on the occurrence of the Chabová sandstones blocks in zone/belt with the Ondrášovec Mb., as well as the analogy

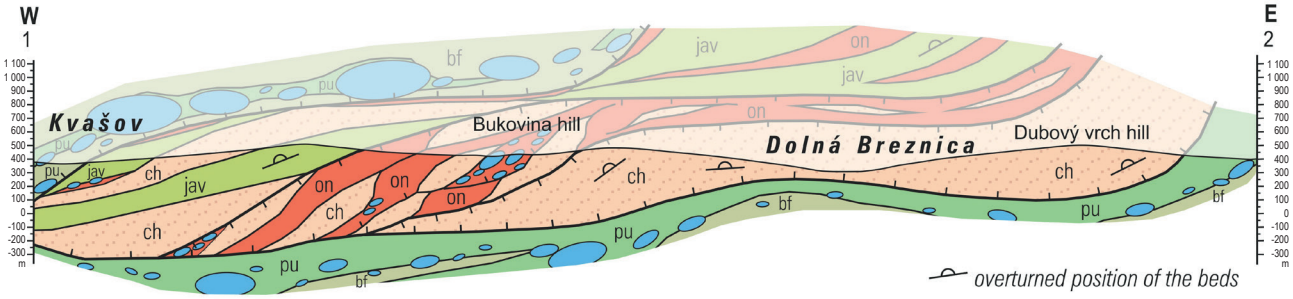


Fig. 6. Schematic section with the interpretation of the geological structure. Section line courses between Kvašov and Dolná Breznica villages.

with the Javorina Nappe and knowledge of the deposition conditions, the following development is more probable:

(1) In the first folding phase after the middle Eocene, the slice formed by Chabová Mb. shift to the NW over the slice formed by Javorina Mb. Small slices formed by the Chabová and Javorina mbs. were incorporated into the Ondrášovec Mb. at the contact of both slices.
(2) The slices were together turned back to the Klippen Belt to the SE. At the same time, a Vršatec slice was back-thrust over them to the SE.

By this mechanism, part of the Biele Karpaty Unit could be involved in the structure of Klippen Belt. The external position of the klippen integrated into the Magura Nappe can be explained in a similar way. A similar position of the klippen and overturned Krynica Unit is in the Oravská Magura Mts. (Potfaj et al., 1991).

Discussion

Flysch sequence SE of Lednica village, so-called the Kvašov development of the Klape Unit (Salaj et al., 1983) was interpreted as a set of various lithostratigraphic units of several tectonic units of the Inner and Outer Western Carpathians. This interpretation could be explained by a lack of outcrops and information and by the unique tectonic position of these deposits, which has no equivalent in the Western Carpathians. More detailed information on the position of the beds and the succession of the flysch sequence has not yet been published. For this reason, the previous authors determined that the sedimentation continuously passed from the Púchov marls, surrounding the klippen of the Klippen Belt, to the top into the Jarmuta Mb., upwards into variegated clays, and finally into the fine-grained flysch deposits (Salaj et al., 1983; Began et al., 1992, 1993). This interpretation of the sequence was also supported by the findings of microfauna, though probably redeposited. The authors did not find significant group of klippen at Bukovina hill NW from Dolná Breznica village. This group of klippen is situated directly in the zone with the variegated claystones. This fact may disprove the opinion of a contiguous sequence.

The fact that rock samples were not petrographically and paleontologically analysed in this work is a disadvantage of the processing of this article. However, the conditions and a number of outcrops in the field, suitable for sampling, is very limited and the field research do not provide enough suitable outcrops and samples for the analyses even at maximum effort, especially for the paleontological determination of rock age. It is therefore necessary to rely on field observations of debris lithology, which is fortunately clearly assignable to the lithostratigraphic units known from the Biele Karpaty Unit.

The Jarmuta and Proč mbs. are the alternative classification of the studied sequence instead of the Javorina and Chabová mbs. on the basis of similar lithology, age and tectonic position. The occurrence of Jarmuta and Proč mbs. in the western part of the Klippen Belt is many times rather fragmentary and uncertain (Mello et al., 2005, 2011; Potfaj and Teťák et al., 2014; Teťák and Potfaj et al., 2015). The above mentioned alternatives are based rather on their occurrence in Eastern Slovakia (Žec et al., 2006, 2011). It is possible to assume that the mentioned alternative lithostratigraphic units of the Jarmuta and Proč mbs. are close to the Biele Karpaty Unit in paleogeographic interpretations, but to speak about the complete conformity would not be correct. It is more appropriate to classify the studied sequence within the Biele Karpaty Unit.

Conclusions

During the rich history of the Klippen Belt research in the Považie region, the flysch sequence in the area SE of Lednica village has been assigned to different lithostratigraphic units of Inner and Outer Western Carpathians (Maheľ et al., 1962; Salaj et al., 1983; Began et al., 1992, 1993; Mello et al., 2005, 2011). The Kvašov development of the Klape Unit was defined in this area by Salaj et al. (1983). The authors presumed that it was a continuous sequence in the top of the Púchov marls of the Klippen Belt.

Geological research and mapping in the area SE of Lednica village brought several new findings important not only for the studied area, but also for understanding the relationship between the Klippen Belt and the Flysch Belt at all:

(1) Lithostratigraphically the flysch sequences belong alternatively to Ondrášovec, Javorina, Chabová and Bzová mbs. of the Biele Karpaty Unit of Magura Nappe, having an age range from the Campanian to the early Eocene.
(2) The sequence of the Biele Karpaty Unit is situated in an overturned position with the prevailing strike of the beds 250–360° and dip of the beds 20–50°.
(3) Six paleocurrent measurements were measured from Ondrášovec Mb. – 210°, Javorina Mb. – 315° and Chabová Mb. – 2 x 330° a 2 x 10°.
(4) The structure is significantly sliced, especially in the zone with the Ondrášovec Mb.
(5) So far undescribed group of the Bukovina hill klippen NW from the Dolná Breznica village and a group of klippen NW from Kvašov village have been identified. It was precised the contact of the Biele Karpaty Unit with the Klippen Belt accompanied by the Púchov marls, flysch sequences of the "klippen cover" and the Jurassic-Lower Cretaceous klippen.

Acknowledgement

This research was supported by the Ministry of Environment of the Slovak Republic within the project 11 15 *Geological map of the Biele Karpaty Mts. (northern part)* and within the State Geological Institute of Dionýz Štúr project *Identification, inventory and engineering geological mapping of slope deformations* supported from the Operational Programme Quality of Environment, ITMS code 310031N708. The authors wish to express their gratitude to the reviewers Michal Potfaj and Jozef Hók for useful comments, consultation and advice.

References

Began, A., Horniš, J., Maglay, J. & Salaj, J., 1992: Geologická mapa Bielych Karpát, časť Bradlové pásmo, M = 1 : 50 000. *Manuscript. Bratislava, archive St. Geol. Inst. D. Štúr (AP 9203).*

Began, A., Salaj, J., Horniš, J., Čechová, A. & Szalaiová, V., 1993: Vysvetlivky ku geologickej mape Bielych Karpát 1 : 50 000, časť Bradlové pásmo. *Manuscript. Bratislava, archive St. Geol. Inst. D. Štúr, 108 p.*

Maheľ, M. (ed.), Andrusov, D., Čechovič, V., Kamenický, L., Kuthan, M. & Matějka, A., 1962: Geologická mapa ČSSR 1 : 200 000, M-34-XXV, list Žilina. *Praha, ÚÚG.*

Marschalko, R., 1985: Sedimentologické a stratigrafické rezy bielokarpatskou jednotkou. *Manuscript. Bratislava, archive St. Geol. Inst. D. Štúr, 27 p.*

Mello, J., Potfaj, M., Teťák, F., Havrila, M., Rakús, M., Buček, S., Filo, I., Nagy, A., Salaj, J., Maglay, J., Pristaš, J. & Fordinál, K., 2005: Geologická mapa Stredného Považia 1 : 50 000. *Bratislava, St. Geol. Inst. D. Štúr.*

Mello, J., Potfaj, M., Teťák, F., Havrila, M., Rakús, M., Buček, S., Filo, I., Nagy, A., Salaj, J., Maglay, J., Pristaš, J. & Fordinál, K., 2011: Vysvetlivky ku geologickej mape Stredného Považia 1 : 50 000. *Bratislava, St. Geol. Inst. D. Štúr, 378 p.*

Pešková, I., Teťák, F. (eds.), Pelech, O., Sentpetery, M., Olšavský, M., Kováčik, M., Maglay, J. & Vlačiky, M., 2021a: Geologická mapa Bielych Karpát (severná časť) v mierke 1 : 50 000. *Bratislava, MŽP SR / St. Geol. Inst. D. Štúr.*

Pešková, I., Teťák, F. (eds.), Pelech, O., Sentpetery, M., Olšavský, M., Kováčik, M., Boorová, D., Laurinc, D., Demko, R., Maglay, J., Vlačiky, M., Žecová, K., Zeman, I., Gluch, A., Dananaj, I., Marcin, D. & Kúšik, D., 2021b: Vysvetlivky ku geologickej mape Bielych Karpát (severná časť) v mierke 1 : 50 000. *Bratislava, St. Geol. Inst. D. Štúr (in press).*

Potfaj, M., 1993: Postavenie bielokarpatskej jednotky v rámci flyšového pásma. *Geol. Práce, Spr., 98, 55 – 78.*

Potfaj, M., Samuel, M., Raková, J. & Samuel, O., 1991: Geologická stavba Kubínskej hole (Orava) (Geologic structure of Kubínska hoľa range). *Západ. Karpaty, Sér. Geol., 15, 25 – 66 (in Slovak, English summary).*

Potfaj, M., Teťák, F. (eds.), Havrila, M., Filo, I., Pešková, I., Olšavský, M. & Vlačiky, M., 2014: Geologická mapa Bielych Karpát (južná časť) a Myjavskej pahorkatiny v mierke 1 : 50 000. *Bratislava, MŽP SR / St. Geol. Inst. D. Štúr.*

Salaj, J., Began, A., Gašpariková, V., Hanáček, J., Kullman, E., Pristaš, J. & Šucha, P., 1983: Vysvetlivky k listu 25-434 Pruské. Čiastk. záver. správa. *Manuscript. Bratislava, archive St. Geol. Inst. D. Štúr, 98 p.*

Stráník, Z., Adamová, M., Bubík, M., Eliáš, M., Krejčí, O., Marschalko, R., Peslová, H., Švábenická, L. & Vůjta, M., 1989: Geologie hluckého vývoje bělokarpatské jednotky. *Manuscript. Bratislava, archive St. Geol. Inst. D. Štúr, 132 p.*

Teťák, F., Potfaj, M. (eds.), Havrila, M., Filo, I., Pešková, I., Boorová, D., Žecová, K., Laurinc, D., Olšavský, M., Siráňová, Z., Buček, S., Kucharič, Ľ., Gluch, A., Šoltés, S., Pažická, A., Iglárová, Ľ., Liščák, P., Malík, P., Fordinál, K., Vlačiky, M. & Köhler, E., 2015: Vysvetlivky ku geologickej mape Bielych Karpát (južná časť) a Myjavskej pahorkatiny v mierke 1 : 50 000. *Bratislava, St. Geol. Inst. D. Štúr, 306 p.*

Teťák, F., Pivko, D. & Kováčik, M., 2019: Depositional systems and paleogeography of Upper Cretaceous-Paleogene deep-sea flysch deposits of the Magura Basin (Western Carpathians). *Palaeogeogr. Palaeoclimatol. Palaeoecol., 533, 1 – 21.*

Žec, B. (ed.), Gazdačko, Ľ., Kováčik, M., Kobulský, J., Bóna, J., Pristaš, J. & Potfaj, M., 2006: Geologická mapa Nízkych Beskýd – stredná časť 1 : 50 000. *Bratislava, MŽP SR – St. Geol. Inst. D. Štúr.*

Žec, B. (ed.), Gazdačko, Ľ., Kobulský, J., Bóna, J., Potfaj, M., Pristaš, J., Žecová, K., Derco, J., Kucharič, Ľ., Marcin, D., Petro, Ľ., Zlinská, A., Siráňová, Z., Vaněková, H., Buček, S. & Konečný, P., 2011: Vysvetlivky ku geologickej mape Nízke Beskydy – stredná časť 1 : 50 000. *Bratislava, St. Geol. Inst. D. Štúr, 188 p.*

Litológia a pozícia bielokarpatskej jednotky juhovýchodne od Lednice (Biele Karpaty, Západné Karpaty)

V priebehu bohatej histórie výskumu bradlového pásma na Považí bola flyšová sekvencia v oblasti juhovýchodne od Lednice priraďovaná k rôznym litostratigrafickým jednotkám viacerých tektonických jednotiek Vnútorných Západných Karpát i Vonkajších Západných Karpát (obr. 1) (Maheľ et al., 1962; Salaj et al., 1983; Began et al., 1992, 1993; Mello et al., 2005, 2011). Salaj et al. (1983) tu vyčlenili tzv. kvašovský vývoj klapskej jednotky. Autori sa však zameriavali viac na štúdium jursko-spodnokriedových bradiel než na ich flyšový obal. Napriek neznalosti úložných pomerov sekvencie sa autori domnievali, že ide o súvislý sled v nadloží púchovských slieňovcov bradlového pásma. Doteraz neboli publikované informácie o pozícii vrstiev a tým ani dôkaz o postupe sekvencie. Preto sa autori domnievali, že sedimentácia plynulo prechádza z púchovských slieňov obklopujúcich bradlá bradlového pásma do nadložia do jarmutských vrstiev, ďalej do pestrých ílov a na záver do jemnozrnného flyšu (Salaj et al., 1983; Began et al., 1992, 1993).

Nedávny geologický výskum a mapovanie v tejto oblasti priniesli viacero nových poznatkov, významných nielen pre skúmanú oblasť, ale aj z hľadiska pochopenia vzťahu bradlového a flyšového pásma vôbec (obr. 2 a 3):

1. Flyšová sekvencia litostratigraficky patrí k ondrášoveckým, javorinským, chabovským a bzovským vrstvám bielokarpatskej jednotky magurského príkrovu (kampán – starší eocén).
2. Sekvencia bielokarpatskej jednotky je v prevrátenom slede, so sklonom 20 – 50° prevažne na SZ (250 – 360°).
3. Stavba je výrazne tektonicky porušená a zošupinatená, najmä v pruhu s ondrášoveckými vrstvami.
4. Podarilo sa zistiť zatiaľ neznámu skupinu bradiel Bukovina sz. od Dolnej Breznice a bradlá sz. od Kvašova. Spresnilo sa poznanie kontaktu bielokarpatskej jednotky s bradlovým pásmom s výskytom púchovských slieňovcov, flyšových sekvencií obalu bradlového pásma a jursko-spodnokriedových bradiel.
5. Meraním bolo získaných šesť výsledkov paleoprúdových meraní – ondrášovecké vrstvy 210°, javorinské vrstvy 315° a chabovské vrstvy 2x 330° a 2x 10° (obr. 5).

Doručené / Received: 13. 5. 2021
Prijaté na publikovanie / Accepted: 30. 6. 2021

Mineralia Slovaca, Web ISSN 1338-3523, ISSN 0369-2086
53 (2021), 57 – 68, © Authors 2021. CC BY 4.0

New formula for evaluation of strength pillar in the underground mine of Chaabet El-Hamra (Setif, Algeria)

Y. CHEIKHAOUI[1], S. BENSEHAMDI[1], H. CHENITI[1], A. I. KANLI[2] and A. BENSELHOUB[3]

[1]National School of Mining and Metallurgy, L3M Laboratory, Annaba, Algeria
[2]Department of Geophysical Engineering, 34320 Avcilar Campus, Istanbul University-Cerrahpaşa, Istanbul, Turkey
[3]Environmental Research Center (C.R.E), Annaba, Algeria
Corresponding author's e-mails: benselhoub@yahoo.fr, youcef.cheikhaoui@ensmm-annaba.dz

Abstract: This study aims to evaluate the characteristic strength of pillars in mining contexts, taking into account the effects of size and shape. The characteristic strength is estimated in terms of the probability of exceeding a specific value of pressure; when once exceeding, the failure appears. Also, the higher number of defects leads to a high probability of failure.

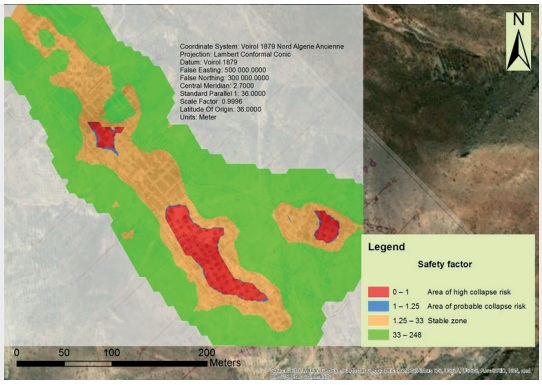
In this study, a new analytical formula is applied, which considers the effect of scale (size and shape) with the notion of probability in evaluating the risk of failure to assess the condition of the mine pillars without resorting to pillar level experiments, which would reduce costs and efforts.

It is used a data set from an underground mine (rock samples of zinc) in Setif-Algeria. The results shows the strength's decrease with an increase in volume. Furthermore, the pillars with a higher width to height ratio (w/h) have more strength than a slender one.

One of the advantages of the probabilistic strength measurement is its functional relation with the deformation at the pillars' level and the progress of the mining sites' works. It is necessary to choose an optimal critical size for the pillars to ensure good operation and safety.

Key words: Weibull criteria, back analysis method, scale effect, pillar stability, probability of survival

Graphical abstract



Highlights

- A new analytical formula was developed and applied to estimate large-scale strength from intact rock, which leads to more realistic values than the usual techniques used in geomechanics and field control.
- New formula takes into account the scale effect in the strength for a pillar as well as the estimate of its failure probability.

1 Introduction

The evaluation of the mechanical properties of a massif is influenced by the effect of scale for mining structures (Zengchao et al., 2009; Zhang et al., 2011), as well as the analysis of the risks associated with the exploitation of resources, particularly in mines, quarries, shafts, tunnels, etc.

In this study, we focused mainly on the pillars of underground mines where compressive strength is an essential parameter in stability studies, taking into account that the pillars are established in fractured rocks, where the stability must be inspected by testing (York & Canbulat, 1998; Medhurst & Brown, 1995).

The influence of the scale effect observed experimentally in solid mechanics can be attributed to the presence of defects in the material with increasing volume; and many scholars (Martin & Maybee, 2000; Cuisiat & Haimson, 1992; Heuze, 1980; Salamon & Munro, 1967) confirm that when the probability of defect increases, the mechanical properties (strength and hardness) decrease proportionally with size.

These probability random effects that govern the scale effect were for the first time studied by Weibull (1939).

This research scientist used the concept of probability of survival to assess the risk of failure. Weibull introduced the probabilistic criterion of failure that enables one to deduce a pillar's strength only as a function of its size, without considering the shape effect.

Experimental observations led Weibull to choose a power law to represent λ the parameter of Poisson distribution characterizing the population of defects in the material by:

$$\lambda = \frac{1}{V_0} \cdot \left(\frac{\sigma}{\sigma_0}\right)^m \quad (1)$$

Where:

σ – applied stress,
V_0 – the reference volume,
σ_0 – the solicitation stress associated with a survival probability of 37 %,
m – the Weibull module.

The Weibull module m is a material parameter that characterizes the dispersion of the defects within the material: a small value of this parameter indicates a higher value of dispersion of the material's defects.

By recovering the Poisson distribution writing that $P_F = 1 - P_S$ (P_F: probability of failure and P_S: probability of survival) with a volume V, we can estimate the probability of failure P_F.

$$P_F = 1 - \exp\left(-\frac{V}{V_0} \cdot \left(\frac{\sigma}{\sigma_0}\right)^m\right) \quad (2)$$

Many researchers have studied the assessment of the strength of pillars in-situ from laboratory tests (Hudson et al., 1972; Salamon & Munro, 1967; Zengchao et al., 2009; Zhang et al., 2011). When estimating a given material's mechanical properties (coal for example), each prediction's accuracy will depend on how accurate the sample characteristics reflect the massif to characterize. Thus, Hudson et al. (1972) reported that the difference in the length/diameter ratio of a sample has a significant effect on the compressive strength of rocks and the shape of the stress-strain curve post-peak segment. This is also evident, where he developed an analytical equation that considers the effect of the geometry of a pillar (by the w/h ratio) and the volume (Galvin et al., 1996).

The tests carried out on different rocks demonstrate that the strength is inversely proportional to the size of the samples analysed (York & Canbulat, 1998). This implies that a sample with a much more size will have a reduced strength. However, the laboratory results show the strength's stabilization as the size increases for coal, iron ore and altered quartzitic diorite. There is at least a specific limit size beyond which no further decrease in the strength is apparent (the absence of the scale effect from a critical volume for each type of rock). However, it should be noted that the largest volumes studied have a length of about 1 to 2 m and remain lower than those of a real pillar.

If the in situ pillar does not include a geological lamination joint, macro fracture, the rock can be described as an intact rock (York & Canbula, 1998). In this case, the rock mass's critical strength (for a size beyond which no additional decrease in the strength appears) can be taken as the strength of the in situ rock mass (the result found in the laboratory is considered the same as in the large scale). On the other hand, the latter cannot be used as the rock mass's critical strength if the pillar has natural or anthropogenic discontinuities (induced by blasting operation for example). In this case, the rock mass's critical strength can be evaluated through different methods that incorporate several factors. Either the rock mass can be approximated as a continuum (homogenizing approach a continuous model represents the rock mass behavior), the rock mass cannot be estimated as a continuum (presence of discontinuities).

Another school of thought suggests using a parameter as a representative of the strength value of a cube of one meter **(**retrospective method or back analysis method**)**.

Salamon & Munro (1967): $\sigma_P = kh^a w^b$ (3)

With:

h – the height of the pillar (m),
σ_P – the pillar strength (MPa),
w – the width of the pillar (m),
k (MPa) – the coefficient characterizing the value of the strength representative of a cube of one-meter side, a and b two numerical constants to be defined for each geomechanical context.

Bieniawski (1968): $\sigma_P = C + M\,(w/h)$ (4)

With:

h – the height of the pillar (m),
M – a constant linked to the nature of the studied rock,
w – the width of the pillar (m),
C (MPa) – the rock mass's critical strength (for a size beyond which no further decrease in the strength can appear).

Bieniawski's (Eq 4) linear formula cannot consider the volume and saves the geometric effect of the increase in the w/h ratio. On the contrary, Salamon & Munro's (Eq 3) formula distinguishes the shape effect of the scale effect. Subject expressing the pillar volume as a function of w and h ($V = w^2h$ for a square section pillar), equation 3 can be rewritten in the form of equation 5 (Galvin et al., 1996).

$$\sigma_P = kV^{\alpha} (w/h)^{\beta} \quad (5)$$

With

h – the pillar height,
σ_P – (MPa) The pillar's strength,
w – the width of the pillar,
V – it's the pillar volume,
k (MPa) – a coefficient characterizing the value of the strength representative of a cube of one-meter side. α and β represent two constants being defined for each mechanical geo context.

Our work aims to estimate the strength of pillars via grouped two approaches, the first which allows considering the shape properties and the size of the rock mass, and the second that makes it possible to integrate the concept of probability of failure in the assessment of the risk of failure.

The basic methodology of this hybrid approach was identified and validated by estimating the pillars' compressive strength in the case of coal (Cheikhaoui et al., 2020, 2021). We used the Australian coal case study data of Galvin's study to compare results, which gave us very similar results found in previous works.

2 The study area

As far as the location of the Chaabet El-Hamra deposit is concerned, it is situated as the crow flies about 250 kilometers South-East of Algiers and 50 km south of Setif, namely in the area of Chouf-Bouarket, 4.5 km from Ain-Azeland and 12 km SE of the Kherzet Youssef mining complex as shown in Fig 1.

According to the WGS 1984 coordinates scheme, it is located between 35° 45' N and 35° 48' N latitude and 5° 31' E and 5° 32' E Longitude.

2.1 Geological setting of the region

The Chaabet El-Hamra is located within the geological context of the Hodna district in the joint of three geological zones known as Tellian Atlas, the Sahara Atlas and the high plains, as demonstrated in Fig. 2.

During the Mesozoic time, the high plains overlaid a carbonate platform that remained shallow. From the Upper Triassic to Albian, the carbonate platform was fragile and subsiding (Lower Cretaceous). It is made up of over 2300 meters of sediments, terrigenous and carbonates (dolomitic series included). Many dolomitic sequences are mainly on the platform's northern and southern margins, distinguished by their significant mineralization. A tectonics of the horst and graben-type has resulted in asymmetrical folding, with diapir forming in the cores on occasion.

It is characterized mainly by Cretaceous deposits, of which the Hauterivian is of the most significant interest, as it contains the mineralization (Fig. 3):

a) Valanginian (n_2): The Valanginian (sterile) deposits outcrop east of the eastern fault and west of the deposit and are represented by alternating grey aleurolite with light grey quartz sandstones, sandstone and clay dolomites, limestones and grey-green marls.

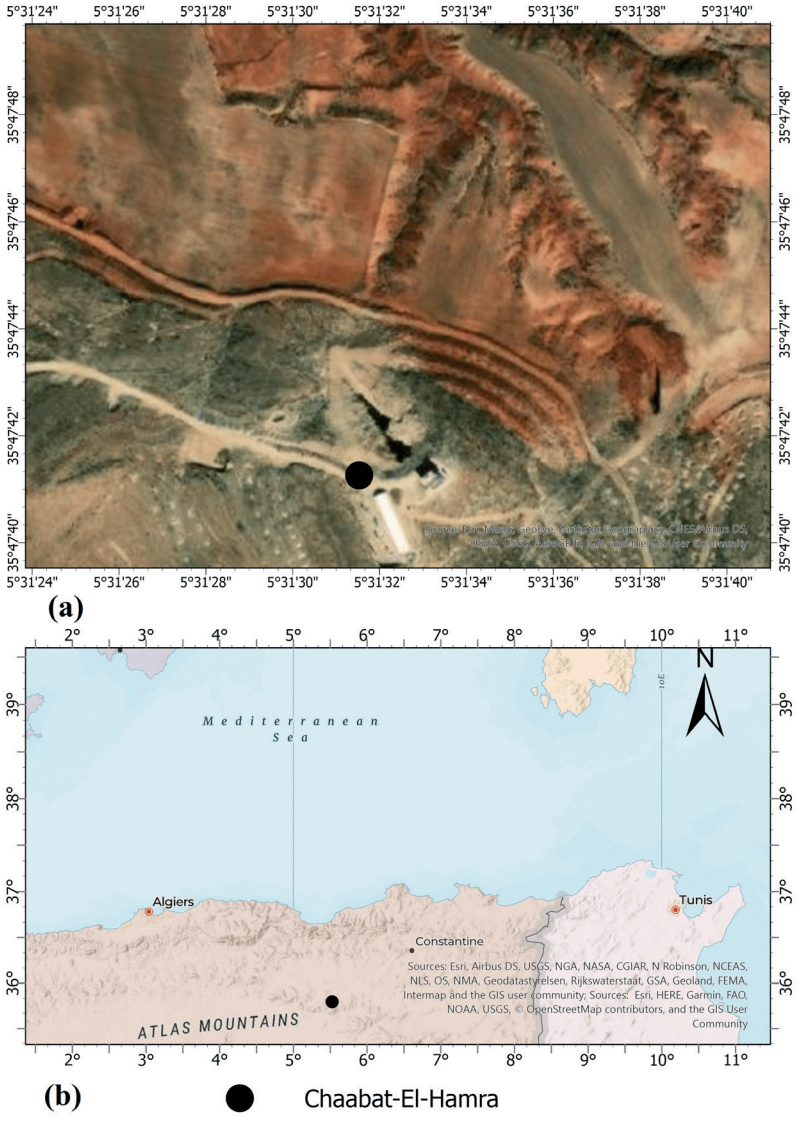


Fig. 1. The position of study area in the map of northern Algeria (b) and its satellite photo (a).

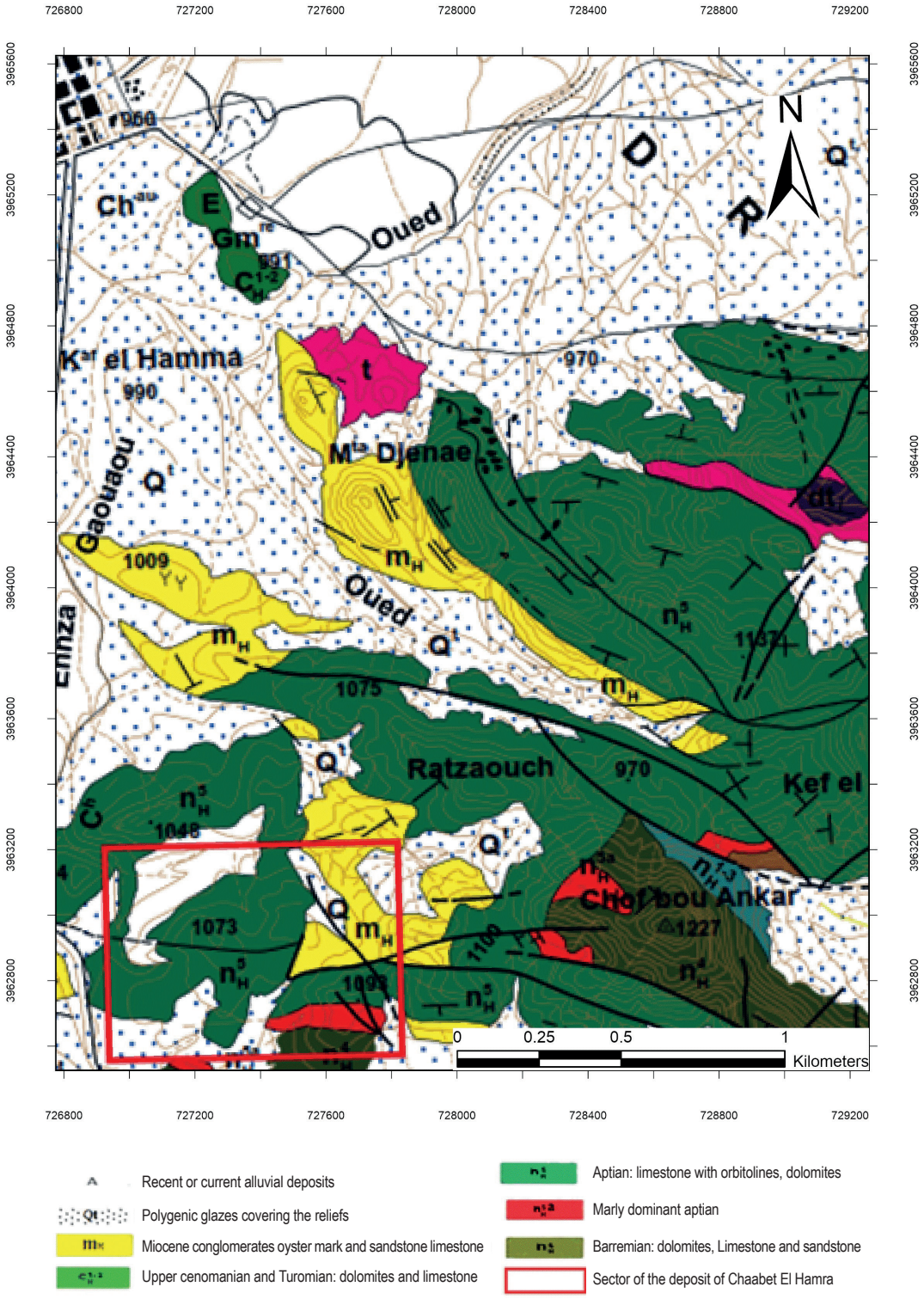


Fig. 2. Geological map of the studied area (taken from Vila, 1977).

b) Hauterivian (n_3): The zinc mineralization of industrial interest is located in the lower part of the Hauterivian, which varies from 100 to 150 m.
c) Barremian (n_4): It is developed to the northwest and south of the deposit.

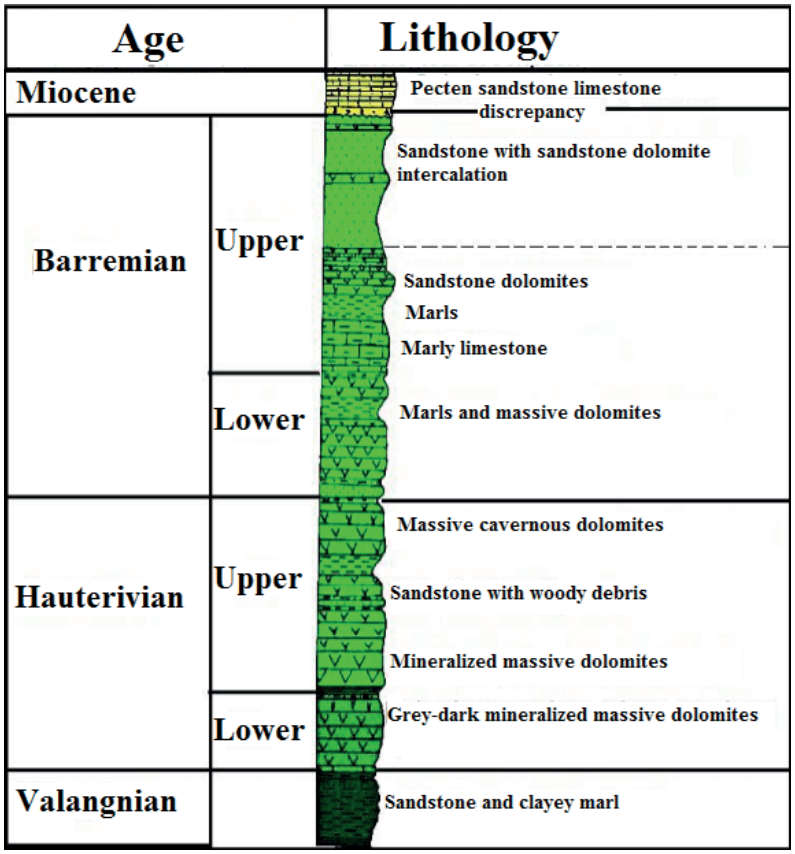


Fig. 3. Lithostratigraphic column of Chaabet El-Hamra ore deposit (Boutaleb, 2001).

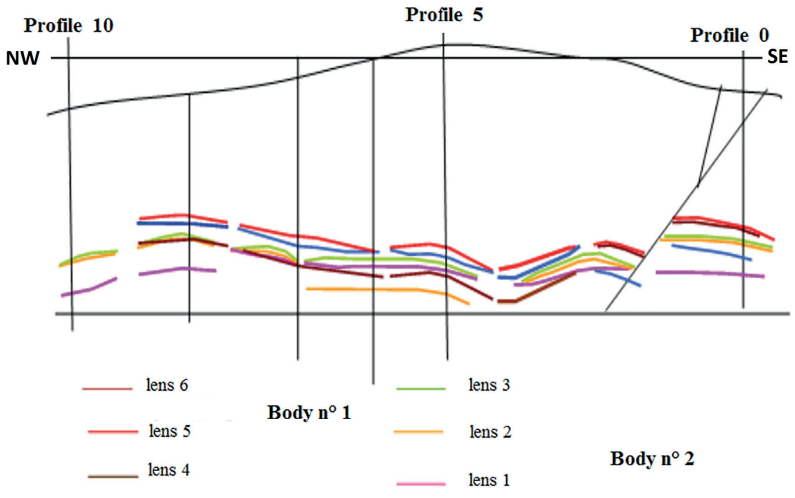


Fig. 4. Longitudinal section of the lenticular mineralization of Chaabet El-Hamra.

2.2 *Ore exploitation in mine*

The mineralization is flat dipping and sits in an anticline, extending over 500 meters along strike, 150 meters across strike, and ranging from 100 to 160 meters underneath the surface. As far as the thickness of mineralization is concerned, it ranges from 1 to 20 meters. Ore was trucked from the Chaabet El-Hamra mine to Kherzet Youcef to be processed into zinc concentrate.

In order to access the mineralized zone, there is an inclined shaft (decline) situated in the lowest point of the area, at Hill 1020, over a length of 830 meters in the waste rock. It is utilized for personnel circulation, equipment and ore transport. Also, it is considered as a fresh air intake to underground mining spaces.

2.3 *Deposit description and its vicinity*

The zinciferous ore of Chaabet El-Hamra deposit is composed of two main bodies called body No. 1 for the upper body and body No. 2 for the lower body as shown in Fig. 4 and as it is mentioned in the report of the Entreprise Nationale Des Produits Miniers Non Ferreux, ENOF (2013). These bodies are elongated in a band over 2700 m in direction and 100 to 400 m in dip. The ore bodies dip at an angle of 10° to the northwest.

The ore is hosted in porous or brecciated dolomite located in the lower part of the Hauterivian stage (Lower Cretaceous). The roof of the upper body (body No. 1) is dolomite with marly beds, while the wall of the lower body (body No. 2) is massive dolomite with concretions (spotted dolomite). The two ore bodies are stratiform, subparallel, and separated by an intercalary level consisting of poorly mineralized and sometimes sterile dolomite of variable strength. This level may be absent so that the two bodies merge into one continuous ore body. The average thickness of body No. 1 (upper body) is 5 meters, and that of body No. 2 (lower body) is 4 meters.

The Canadian mining group SIDAM Inc. (1992) has evaluated the geological reserves by the influence polygon method with an average cut-off grade of 3 %, a minimum exploitable thickness of 2 m, and a density 2.87.

3 Methodology

The main proposition supposes that the strength R_p of a pillar is explained by the strength K (of the intact rock), by corrective functions of shape F(f) volume G(v) and function of the probability effect H(ps) (Eq. 6).

Suggestion:

$$R_p = K \,.\, \mathrm{H(ps)} \,.\, \mathrm{F(f)} \,.\, \mathrm{G(v)}$$

Where:

F (shape): It depends on the geometry of the pillar.
G (volume): It depends on the pillar volume.
H (probability of survival): It is the probability of survival associated with an applied constraint, such as the probability of survival (P_S) = 1 – (P_F) probability of failure.
K is the strength of the specimen (MPa).

Tab. 1
Uni-axial compression strength (MPa) of zinc rock samples from Setif-Algeria.

Sample number	Uni-axial compression strength (MPa)	Sample number	Uni-axial compression strength (MPa)
1	47.4	8	43
2	82.6	9	90.5
3	159.9	10	102.3
4	92.5	11	61.1
5	40.4	12	112
6	108	13	155.5
7	80.9	14	93.2

Tab. 2
Weibull parameters of zinc rock sample.

Weibull parameters	Value	Geometric parameters	Value
m	2.36	W_{EP}/H_{EP} (l/d ratio)	0.5
σ_0(MPa)	103.61	V_0(m^3)	2.159×10^{-4}

The equalization of Eq. 7 developed in our previous works (Cheikhaoui et al., 2020) and (Cheikhaoui et al., 2020, 2021), taking into account scale and shape effects, is given as follows:

$$Rp(PS) = \sigma_0 \,.\, ln(1/P_s)^{1/m} \,.\, (w/h)^{\frac{ln\,(V_0\,\frac{1}{m})}{ln(Wep/Hep)}} \,.\, V^{-1/m} \text{ (MPa)} \quad (7)$$

Furthermore, if there is a set of N values of compressive strength measured experimentally on test specimens of the same material, volume V_0, and slenderness W_{ep}/H_{ep}, it is then possible to obtain the parameters of the Weibull's law m and σ_0.

That is to say, in general form:

$$R_{p,Ps}(MPa) = \sigma_0 \,.\, H(Ps) \,.\, G(volume) \,.\, F(shape) \quad (8)$$

We consider a set of 14 uni-axial compression tests to samples of zinc rock (see Table 1) with $V_0 = 2.159 \times 10^{-4}$ (m^3) and the length to diameter ratio l/d = 0.5 allowing the different parameters of Weibull's law to be calculated. The results are summarized in Table 2. The tests of compression are executed by the national company of non-ferrous mining products.

3.1. Pillar strength in chaabet El-Hamra mine

The strength formula of a *zinc* pillar found using Weibull parameters is written as follows:

$$R_{p(PS)} = 103.61\; ln(1/P_s)^{0.42}(w/h)^{5.15} V^{-0.42} \text{ (MPa)} \quad (9)$$

The strength formula of a zinc pillar according to the probability of survival Ps = 93 % meaning 7 % of the risk, is written as follows:

$$R_{p(0.93)} = 23.60(^{w}/_{h})^{5.15}\; V^{-0.42} \text{ (MPa)} \quad (10)$$

The curve in (Fig. 5) shows a decrease in strength with an increase in volume. This phenomenon represents the scale or size effect.

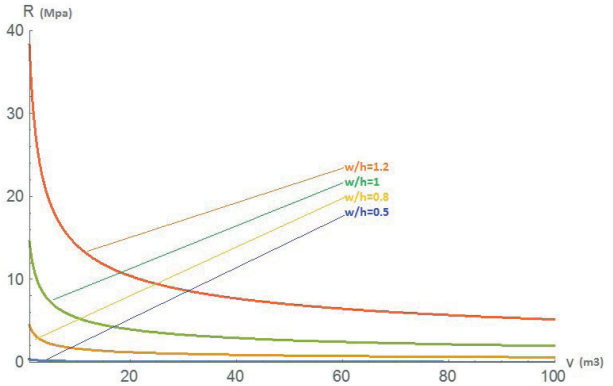


Fig. 5. Size effect on the strength of zinc pillars for different shapes (w/h = 0.5, 0.8, 1, and 1.2) according to the risk of 7 %. The formula developed using Weibull parameters m and σ0.

The strength variation follows a power law such that there is a decrease with increasing volume, which is consistent with previous research. We notice the shape effect in Fig. 5 such that the strength values increase with the increase of the shape ratio w/h.

The scale effect on pillar's strength is due to the various (micro) fractures (weaknesses) such as cracks in it.

The probability of survival is a statistical value depending on the number and types of fractures present in the rocks. In smaller volumes, the likelihood of finding of defects is more negligible, so the strength is higher.

It is noticed that the strength begins to stabilize after a specific volume that is called critical volume, or there is no variation of strength with the increase of the volume. This critical volume depends on the form w/h ratio for the same type of rock.

It is suggested that the reduction in strength is due to the greater opportunity for inevitable failure, the building blocks of the intact rock, as more and more of the weaknesses are included in the test sample. Eventually, when a sufficiently large number of weaknesses are included in the sample, the strength reaches a constant value.

Figure 6 shows the shape effect where the strength increases with the increase in the w/h ratio of the pillar.

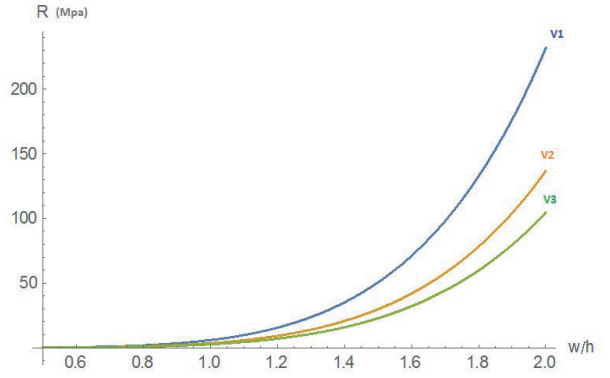


Fig. 6. Shape effect on the strength of a zinc pillars of different sizes (V1 = 18 m^3, V2 = 27 m^3 and V3 = 50 m^3) according to the risk of 7 %. The formula developed using Weibull parameters m and σ0.

In our case, m = 2.36, we notice an exponential evolution of strength with the increase of the w/h ratio. The size effect is always present such that the small volume has the highest strength values and a critical value of w/h ratio such that the strength tends rapidly to a large value.

A rock mass's strength is usually described as a constant cohesive component and normal stress or confinement-dependent component. Hence for pillars with w = h or ratios greater than 1, the strength should increase as the confining stress increases.

3.2 Probability of survival for pillars

Formula 7 allows us to introduce the probabilistic distribution of defects and the probability of activation of these defects, that is to say, the probability of failure. If there is a series of defects, when one of these defects (the discontinuities) is activated, the failure occurs. The relation proposed as an analytical approach for estimating the strength of a pillar such that $R_p = \sigma_f$ The stress to be applied for at least one of the defects is activated (the failure), so:

$$P_s = EXP\left[\left({}^{w}/_{h}\right)^{a} . v^{-m}\right)/(-m\sigma_p)] \text{ with } a = \frac{\ln\left(v_0{}^{-m}\right)}{\ln\left({}^{w_{ep}}/_{h_{ep}}\right)} \quad (11)$$

Such as:

v_0 – specimen volume (m^3).

v – pillar volume (m^3).

${}^{w_{ep}}/_{h_{ep}}$ – ratio of the shape of the specimen.

${}^{w}/_{h}$ – pillar shape ratio.

m – the parameters of the Weibull's.

σ_p – the stress applied (MPa).

$$P_s = EXP\left[\left({}^{w}/_{h}\right)^{5.15} . v^{-0.42}\right)/(-0.42\sigma_p)] \quad (12)$$

Tab. 3

Summary of the calculations of the ratio and the average slenderness for all the blocks.

Block	Number of pillars of the block	Average width of the pillars [m]	Average height of the pillars [m]	w/h (average)	Average extraction ratio τ [%]
4/1	32	2.4	5	0.5	82.8
4-5/2	10	3.7	2	1.84	81
5-6/4	22	3.9	2.7	1.5	72.3
5-6/3	20	2.5	2.4	1	82.4
6/3	12	2.4	2.5	1	84.3
4-5-6/13	23	2.3	6.5	0.4	83
5-6/12	9	3	2.5	1.2	77.8
4-5-6/5	17	3.4	4.5	0.8	76.4
5/1	29	3.1	2	1.6	77.1

As the exploitation in the mine do by chambers and pillars, the stress σ_p (MPa) applied to the center of the pillar is related to the extraction ratio τ and σ_v (MPa) the vertical stress linked to the higher ground load. The formula can be written as follows (in Brady & Brown, 1985):

$$\sigma_p = \sigma_v \frac{1}{1-\tau} \quad (13)$$

Such as

$$\sigma_v = \gamma_{av}.h_{av} \quad (14)$$

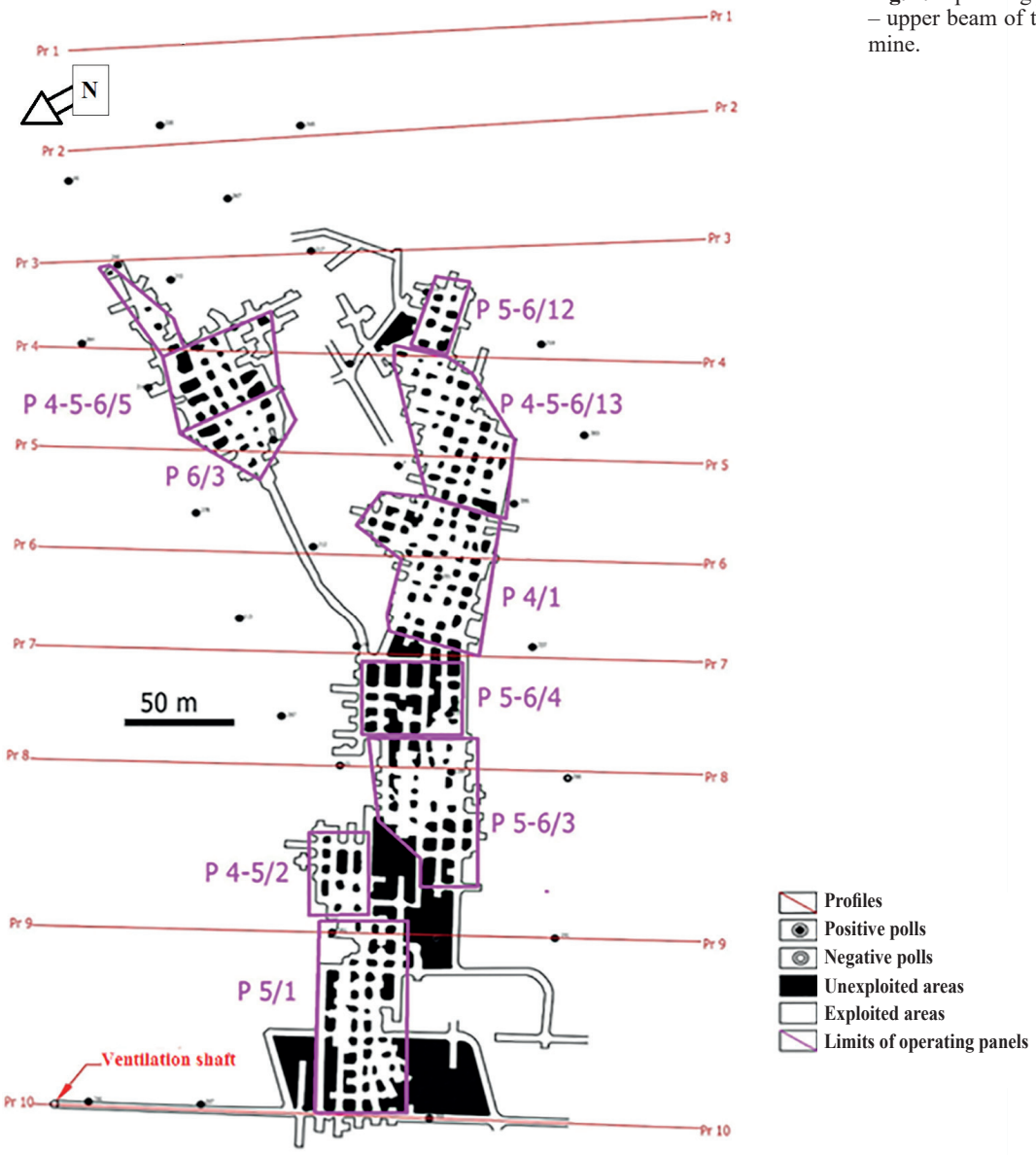


Fig. 7. Operating plan for the upper part – upper beam of the Chaabet El-Hamra mine.

γ_{av} – The average specific gravity (N/m^3),

h_{av} – The thickness average of the cover land (m).

In our case:

$\sigma_v = \gamma_{av}.h_{av} = 106.5 \times 27.4 \times 10^3 = 2918.1$ kN/m^2 = 2.9 MPa.

Table 3 summarizes the geometric parameters and the calculation of the ratios for all the blocks (see Fig. 7).

It appears from this table that the extraction ratio varies from 0.72 (lowest rate for the 5-6/4 panel) to 0.85 (largest for the 6/3 panel). The lowest rate corresponds to the largest average pillar width, and conversely, the largest corresponds to the smallest pillar width.

4 Results and discussion

4.1 Probability of survival in chaabet El-Hamra mine

The blocks (5-6/4), (4-5/2) and (5/1) in the mine are the most insusceptible to failure with an estimated probability of failure less than 16 % (see the Tab. 4); this is because w/h ratio of this pillar is greater than 1.5 (the shape effect). For the other blocks, the risk of failure is more than 49 % (essentially, when the w/h ratio of the pillar is less than 1, the risk of failure is significant).

$P_{Soverall} = [Ps_{(4/1)} + Ps_{(4-5/2)} + Ps_{(5-6/4)} + Ps_{(5-6/3)} + Ps_{(6/3)} + Ps_{(4-5-6/13)} + Ps_{(5-6/12)} + Ps_{(4-5-6/5)} + Ps_{(5/1)}]/9$ so : $Ps_{overall} = 37.52$ %.

$P_{Foverall} = [Pf_{(4/1)} + Pf_{(4-5/2)} + Pf_{(5-6/4)} + Pf_{(5-6/3)} + Pf_{(6/3)} + Pf_{(4-5-6/13)} + Pf_{(5-6/12)} + Pf_{(4-5-6/5)} + Pf_{(5/1)}]/9$ so : $Pf_{overall} = 62.48$ %.

And this is confirmed by the following relation $P_F + P_S = 1$.

Tab. 4

Stress σ_p applied, σ_v the vertical stress, probability of survival (Ps), and probability of failure (Pf) of each panel of the mine.

Block of pillars	w/h (average)	Depth [m]	σ_v in [MPa]	σ_p in [MPa]	Probability of survival Ps	Probability of failure Pf = 1 – Ps
(4/1)	0.5	106.5	2.91	23.5	1.39913E-34	1
(4-5/2)	1.84	106.5	2.91	20.3	0.922	0.0771
(5-6/4)	1.5	106.5	2.91	13.1	0.8385	0.1614
(5-6/3)	1	106.5	2.91	30.7	0.1129	0.8870
(6/3)	1	106.5	2.91	32.9	0.2509	0.8994
(4-5-6/13)	0.4	106.5	2.91	27.3	2 E-134	1
(5-6/12)	1.2	112.3	3.07	20.4	0.5107	0.4892
(4-5-6/5)	0.8	106.5	2.91	19.8	0.00056	0.9994
(5/1)	1.6	100	2.74	16.5	0.8908	0.1091

We can estimate the probability of survival (overall mine stability) by:

4.2 Stability of Chaabet El-Hamra mine

In our case study of Chaabet El-Hamra, the mine depth varies between 106.5 and 112 m. In the mining method room and pillar; the pillars are generally square in shape and variable dimensions according to the adopted extraction ratio. This extraction rate varies between 72 % and 84 %. Former mechanical tests were performed to determine the uniaxial compression strength of the zinc rock. The range of variation is between 40.4 and 159.9 MPa. Also, nine blocs (contain 174 pillars) were analysed to distinguish between stable and unstable pillars in the mine.

We performed an estimation of the safety factor based on estimation of strength with a probability of failure $P_F = 7$ % and the direct data collected from the mine's pillars (in particular width and height).

The pillar stress was calculated using an analytical method (tributary area) to estimate the average vertical stress on the pillars. Figure 8 shows the distribution of the safety factor for underground zinc mines using interpolation with a gaussian kernel, the yellow and the green zones correspond to stable zones; the red zone is the most sensitive to collapse and the blue for probable collapse zones. We note the average safety factor for stable mines is equals to 1.2.

The safety factor values indicate that there are blocs in the mine at risk of failure, so there are pillars to intervene in first to be stable. Further detailed analysis is recommended for the pillars with an average safety factor is less than one and still stable.

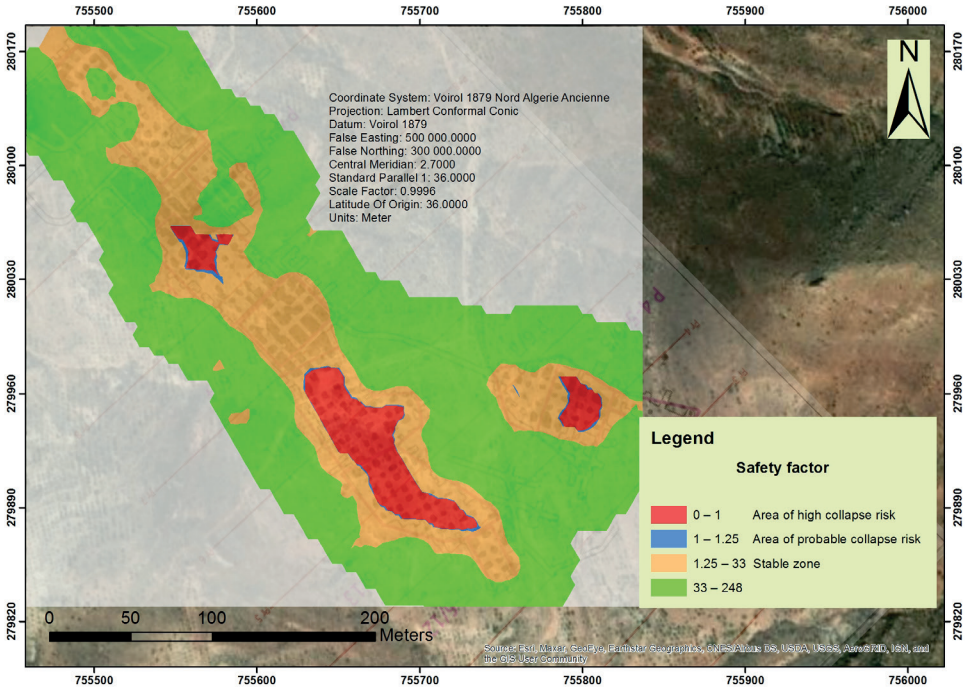


Fig. 8. Safety factor map.

5 Conclusion

New formula developed by combining two formulas, based on a relationship between the back-analysis aspect of Galvin et al. (1996) and the probabilistic aspect of Weibull (1939), explicitly reproduces the effect of volume and shape. It allows us to interpret the influence of both factors on the strength of

a pillar. We have used the Weibull's parameters derived after an approximation with Galvin's formula. The results described in this research show that the strength decreases when volume increase but increases when width increases (a substantial pillar is more resistant than a slender pillar).

The analysis of the stability of the pillars of the Chaabet El-Hamra mine (those pillars which exist in the Hauterivian lithology containing mineralization) indicates that the pillars in blocks (5-6/4), (4-5/2), and (5/1) in the mine are insusceptible to failure with an estimated probability of failure of 11 % and 16 % but in other blocs the risk of failure is very high. The probability of survival (overall mine stability) is $Ps_{overall} = 37.52$ %.

One of the advantages of the probabilistic strength measurement is its functional relation with the deformation at the pillars' level and the progress of the works of the mining sites. They possibly have the most significant impact on the overall strength of the mine. Therefore, it is necessary to choose an optimal critical size for the pillars to ensure good operation and safety.

In conclusion, the new formula (Strength – Probability of Survival) of the pillar considers the pillar stress ratio and pillar of strength. The stress can be determined using the tributary area and the pillar strength through Weibull's parameters. Sophisticated tools are helpful to understand the rock mass and mines (pillars) behavior. However, the influence of the geostatic distribution of discontinuity is to be considered in our next contributions.

6 References

Bazant, Z. P. & Yu, Q., 2004: Size effect in fracture of concrete specimens and structures: New Problems and Progress. *Proceedigns of 5th International Conference on Fracture Mechanics of Concrete and Concrete Structures, 44, 5, 7–15.*

Bieniawski, Z. T., 1968: The effect of specimen size on compressive strength of coal. *Int. J. Rock Mechanics Mining Sci., 5, 325–335.*

Brady, B. H. G. & Brown, E. T., 1985: Rock Mechanics for Underground Mining, 1st ed. *Allen & Unwin, London.*

Boutaleb, A., 2001. Les minéralisations à Pb-Zn du domaine Sétifen-Hodna: gîtologie, pétrographie des dolomies, micro-thermométrie et implications métallogéniques. *Thèse de Doctorat, USTHB, 350 p.*

Cheikhaoui, Y., Deck, O., Omraci, K. & Cheniti, H., 2021: The scale and shape effects on the characteristic strength of a rock mass: Application to mining pillars. In: Abdel Wahab, M. (ed.): Proceedings of 1st International Conference on Structural Damage Modelling and Assessment. *Lecture Notes Civil Eng., 110. Springer, Singapore.*

Cheikhaoui, Y., Deck, O., Omraci, K. & Cheniti, H., 2020: Characteristic strength of mining pillars in the presence of size and shape effects. Ukrainian Mining Forum, 2020. *Materials of the International Conf., Oct. 4–5. 2020, Dnipro, Zhurfond, 2020, 134–139.*

Cuisiat, F. D. & Haimson, B. C., 1992: Scale effects in rock mass stress measurements. *Int. J. Rock Mechanics Mining Sci. & Geomech. Abstracts, 29, 2, 99–117.* https://doi.org/10.1016/0148-9062(92)92121-R.

ENOF, 2013: Exploitation plan of the Chaabet El Hamra mine, Algiers.

Galvln, J. M., Hebblewhite, B. K. & Salamon, M. D. G., 1996: Australian coal pillar performance. *Int. Soc. Rock Mechanics News J., 4, 1.*

Heuze, F. E., 1980: Scale effects in the determination of rock mass strength and deformability. *Rock Mech. Felsmech. Mecanique Roches, 12, 167–192.*

Hudson, J. A., Crouch, S. L. & Fairhurst, C., 1972: Soft, stiff and servo-controlled testing machines: A review with reference to rock failure. *Eng. Geol., 6, 155–189.*

Lim, W., McDowell, G. & Collop, A., 2004: The application of Weibull statistics to the strength of railway ballast. Granular Matter, 6, Springer-Verlag, 229–237. https://doi.org/10.1007/s10035-004-0180-z.

Martin, C. D., Lu, Y. & Lan, H., 2012: Scale effects in a Synthetic Rock Mass. *Harmon. Rock Eng. Environ., CD, 1–6.*

Martin, C. D. & Maybee, W. G., 2000: The strength of hard-rock pillars. *Int. J. Rock Mechanics Mining Sci., 37, 8, 1239–1246.* https://doi.org/10.1016/S1365-1609(00)00032-0.

Medhurst, T. P. & Brown, E. T., 1998: A study of the mechanical behaviour of coal for pillar design. *Int. J. Rock Mechanics Mining Sci., 35, 8, 1087–1105.* https://doi.org/10.1016/S0148-9062(98)00168-5.

Salamon, M. D. G. & Munro, A. H., 1967: A study of the strength of coal pillars. *J. South African Inst. Min. Metall, 68.*

Scholtès, L., Donzé, F. & Khanal, M., 2011: Scale effects on strength of geomaterials, case study. *Coal. J. Mechanics Physics Solids, 59, 5, 1131–1146.* https://doi.org/10.1016/j.jmps.2011.01.009.

Sidam, 1994 : Projet Non Ferreux RAPPORT FINAL. *Le groupe minier SIDAM, Québec.*

Simon, R. & Deng, D., 2009: Estimation of scale effects of intact rock using dilatometer tests results. *ldots of 62nd Canadian Geotechnical Conference, Halifax, 481–488.*

Vila, J. M., 1977: Notices explicatives des cartes au 1/200 000 de Constantine et de Sétif et descartes au 1/50 000 de la même région.

Weibull, W., 1939. A statistical theory of the strength of material. Ingeniorsvetenskaps akademiens, Handlingar, NR 151. *General-stabens Litografisca Anstalts Forlag, Stockholm.*

York, G. & Canbulat, I., 1998. The scale effect, critical rock mass strength and pillar system design. *J. South African Inst. Mining Metallurgy, 23–36.*

Zengchao, F., Yangsheng, Z. & Dong, Z., 2009: Investigating the scale effects in strength of fractured rock mass. *Chaos, Solitons Fractals, 41, 2377–2386.*

Zhang, Q., Zhu, H., Zhang, L. & Ding, X., 2011: Study of scale effect on intact rock strength using particle flow modeling. *Int. J. Rock Mech. Min. Sci., 48, 1320–1328.*

Nový matematický postup hodnotenia pevnosti pilierov na príklade banskej prevádzky Chaabet El-Hamra (Setif, Alžírsko)

Článok prezentuje zdokonalenú metodiku určovania charakteristickej pevnosti ochranných pilierov so zohľadnením ich veľkosti a tvaru. Táto metodika bola aplikovaná v podzemnom dobývacom priestore na Zn rudy Chaabet El-Hamra (Setiv, Alžírsko).

Lokalita Chaabet El-Hamra (obr. 1 a 2) je situovaná na rozhraní troch geologických jednotiek: Tell Atlas (Malý Atlas), Saharský Atlas a Východná Meseta (Východomarocké náhorné stepi). Karbonátová platforma v období mezozoika postupne poklesávala. Je pokrytá terigénnymi sedimentmi a ďalšími karbonátmi v celkovej hrúbke vyše 2 300 m. Na severnom a južnom okraji platformy sa vyskytujú sekvencie dolomitov kriedového veku, ktoré sú nositeľmi bilančnej Zn mineralizácie (obr. 3). Ťažená časť stratiformného ložiska Chaabet El--Hamra (s rozmermi 500 x 150 m a hrúbkou 1 – 20 m; obr. 7) má sklon 10° na SZ. HĺbkA dobývacích priestorov je v rozmedzí 106,5 – 112 m. Použitá dobývacia metóda je typu komora – pilier. Piliere majú štvorcový prierez rôznych rozmerov v závislosti od lokálnej miery výťažnosti (obr. 7; znázornené čierne objekty v dobývacom priestore). Výťažnosť sa pohybuje v rozmedzí 72 – 84 %. Na začiatku ťažby boli mechanickými skúškami určené hodnoty jednoosovej kompresie ťaženého materiálu s obsahom zinkovej rudy, ktoré sa pohybovali v rozsahu 40,4 – 159,9 MPa. V súčasnosti sa v dobývacom priestore nachádza 174 pilierov. Odhad bezpečnostného faktora založeného na zistení pevnosti ťaženého materiálu, pravdepodobnosti zlyhania a rozmerov pilierov (šírka a výška) preukázal hodnotu 7 %.

Celé ložisko budujú dve hlavné mineralizované polohy (č. 1 – horná poloha s priemernou hrúbkou 5 m, č. 2 – dolná poloha s hrúbkou 4 m; obr. 4). Tieto pretiahnuté polohy dosahujú smernú dĺžku vyše 2 700 m a po sklone majú 100 až 400 m. Zn ruda sa nachádza v poréznych alebo zbrekciovatených dolomitoch spodnohoterivského veku. Rudné polohy sú paralelné a spravidla oddelené slabo mineralizovaným alebo nemineralizovaným dolomitom.

Ložisko je z povrchu sprístupnené úpadnicou dlhou 830 m. Vyťažená ruda z Chaabet El-Hamra sa dopravuje po cestnej komunikácii na susediacu banskú lokalitu Kherzet Youcef, kde sa z nej získava zinkový koncentrát.

Veľkosť podzemných dobývacích priestorov má vplyv na mechanické vlastnosti masívu (Zengchao et al., 2009; Zhang et al., 2011). Podstatným parametrom pri štúdiu stability je pevnosť v tlaku, pričom je dôležité zohľadniť aj primárnu frakturáciu v ochranných pilieroch (York a Canbulat, 1998; Medhurst a Brown, 1995). Pri charakteristickej pevnosti pilierov sa posudzuje hľadisko pravdepodobnosti prekročenia konkrétnej hodnoty tlaku, čo by spôsobilo vznik porúch v horninovom masíve. Výhodou novej metodiky je aplikácia nového analytického vzorca, ktorý zohľadňuje vplyv veľkostných proporcií (veľkosti a tvaru) a aspekt pravdepodobnosti pri hodnotení rizika vzniku porúch v banských pilieroch bez potreby experimentálnych meraní na úrovni pilierov. Týmto spôsobom nová metodika prináša úsporu finančných nákladov a času. Výhodou pravdepodobnostného určovania pevnosti je zohľadnenie vzťahu deformácie pilierov a postupu prác na banských lokalitách.

Aspekt veľkostných proporcií (mierky) v mechanike pevných látok zistený experimentálne súvisí s reálnou prítomnosťou väčšieho počtu diskontinuít v materiáli pri jeho väčšom objeme. Ak sa zväčšením objemu horninového prostredia zvyšuje pravdepodobnosť výskytov diskontinuít, mechanické vlastnosti tohto prostredia (pevnosť a tvrdosť) sa v ochranných pilieroch úmerne znižujú (Martin a Maybee, 2000; Cuisiat a Haimson, 1992; Heuze, 1980; Salamon a Munro, 1967).

Pravdepodobnostné kritérium, ktoré umožňuje odvodiť pevnosť piliera ako funkciu jeho veľkosti, tzv. efekt mierky, zaviedol Weibull (1939; matematické vyjadrenia 1 a 2). Pri štúdiu pevnosti pilierov v laboratórnych podmienkach (Hudson et al., 1972; Salamon a Munro, 1967; Zengchao et al., 2009; Zhang et al., 2011) sa zvýraznila dôležitosť reprezentatívnosti parametrov vzorky z daného horninového masívu. Ak pilier in situ neobsahuje geologické diskontinuity (napr. vrstvovitosť či tektonické porušenie) alebo antropogénne porušenie (napr. strelnými prácami), možno ho považovať za neporušené horninové prostredie (York a Canbula, 1998). V takom prípade kritickú pevnosť horninového masívu (pri danej veľkosti, nad ktorou sa už nevyskytne ďalšie zníženie pevnosti) možno považovať za reálnu pevnosť horninového masívu in situ (t. j. výsledky zistené v laboratórnych podmienkach sa považujú za korešpondujúce s reálnymi výsledkami v horninovom masíve).

Inú, retrospektívnu metodiku (tzv. metódu spätnej analýzy) zaviedli Salamon a Munro (1967) a Bieniawski (1968; matematické vyjadrenia 3 a 4).

V tomto článku prezentujeme metodiku určovania pevnosti pilierov spojením oboch metodík. Nový vzorec (6), ktorý bol vyvinutý kombináciou dvoch matematických vyjadrení z uvedených metodík na základe vzťahu medzi aspektom spätnej analýzy (Galvin at al., 1996) a pravdepodobnostným aspektom (Weibull, 1939), umožňuje

interpretovať vplyv oboch faktorov na pevnosť pilierov (matematické vyjadrenia 7 – 14). Distribúciu bezpečnostného faktora znázorňuje obr. 8. Žltou a zelenou farbou sú v ňom vyjadrené stabilné oblasti, červená farba znázorňuje oblasti s rizikom zavalenia a modrá farba znázorňuje oblasti s vysokou pravdepodobnosťou zavalenia. Priemerný bezpečnostný faktor stabilných častí bane je 1,2.

Výsledky prezentované v tomto článku preukazujú, že keď sa zväčšuje objem piliera, jeho pevnosť klesá, ale so zväčšovaním šírky piliera sa jeho pevnosť zvyšuje (masívny pilier je odolnejší ako štíhly pilier).

Doručené / Received: 19. 4. 2021
Prijaté na publikovanie / Accepted: 30. 6. 2021

Mineralia Slovaca, Web ISSN 1338-3523, ISSN 0369-2086
53 (2021), 69 – 80, *© Authors 2021. CC BY 4.0*

Influence of bacteria on toxic elements leaching from the contaminated soil

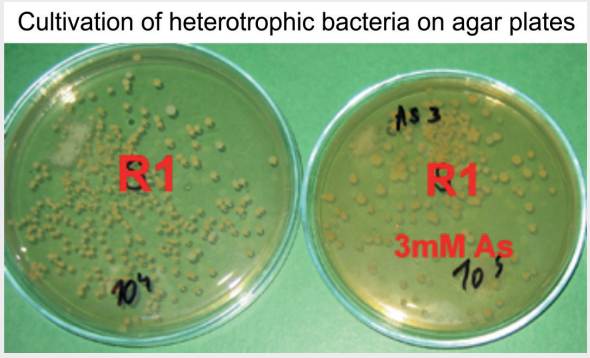
ZUZANA DANKOVÁ[1,*], IVETA ŠTYRIAKOVÁ[1, 2], KATARÍNA ČECHOVSKÁ[1], JAROSLAV ŠUBA[1, 2], JARMILA NOVÁKOVÁ[3], VIERA KOLLÁROVÁ[4], ALEXANDRA BEKÉNYIOVÁ[1], EVA LENHARDTOVÁ[1], ERIKA FEDOROVÁ[1] and JAROSLAV BRIANČIN[5]

[1]State Geological Institute of Dionýz Štúr, Regional Centre Košice,
Department of Applied Technology of Raw Materials, Jesenského 8, SK-040 01 Košice, Slovak Republic;
[2]ecolive, s. r. o., Košice, Slovak Republic
[3]State Geological Institute of Dionýz Štúr, Regional Centre Spišská Nová Ves,
Division of Geoanalytical Laboratories, Markušovská cesta 1, SK-052 01 Spišská Nová Ves, Slovak Republic
[4]State Geological Institute of Dionýz Štúr, Department of Special Laboratories, Mlynská dolina 1,
SK-817 04 Bratislava 11, Slovak Republic
[5]Slovak Academy of Sciences, Institute of Geotechnics, Watsonova 45, SK-040 01 Košice, Slovak Republic

Abstract: The study is focused on better understanding of bacterial activity in biological-chemical leaching in soil remediation process. The heterotrophic bacteria isolated from the contaminated soil from the locality Richnava (Eastern Slovakia) showed good resistance towards As, in both experiments with bacterial growth on solid nutrient media (agar plates), as well as in liquid nutrient media (glass tubes), especially to molarity of 0.3 mM As. Even though the toxic character of elements presented in studied soil was not proven by the method of Toxic Characteristic of Leaching Process (TCLP), the microbiological study pointed at the bacterial activity in disruption of bounds between the mineral grains and toxic elements, especially of As bounded on Fe coatings of mineral grains. That was confirmed by changes of mineral grains surface observed by optical and scanning electron microscopy. The Simple Bioavailability Extraction Test (SBET) pointed at the bacteria influence in biological-chemical leaching of the soil, where bioassessment of studied toxic elements decreased after the soil treatment, except of Fe and As. The results from the sequential extraction analyses showed the decrease of As content in the residual fraction as well, contrary to the other toxic elements, after the biological-chemical leaching and its increase in the bioavailable fractions.

Key words: contaminated soil, sequence extraction analysis, bacteria resistance

Graphical abstract



Highlights

- Heterotrophic indigenous bacteria showed good resistance towards As.
- Biological-chemical leaching decreased the content of As in the residual, non-biodegradable, fraction of the contaminated soil.
- Repeating of cycles of chemical and biological-chemical leaching is promising way for the soil remediation.

1. Introduction

Soil contamination by toxic elements is one of the main environmental problem in the world. An international trend of enforcing more stringent legislation on landfill disposal, e.g. European Union Landfill Directive (Council of the European Union 1999), has prompted a strong drive on the land remediation industries to develop remedial technologies for sustainable resource recycling/conservation (Tsang & Yip, 2014).

Heavy metals are natural elements, in their basic level being just atoms. That is why their degradation and metabolism is not possible. Instead, microorganisms have evolved coping strategies to either transform the element to a less-harmful form or bind the metal intra- or extracellularly, thereby preventing any harmful interactions in the bacterial cell. Plus, they are able to actively transport the metal out of the cell cytosol (Nwagwu et al., 2017).

The bioleaching process can be a promising alternative technology for heavy metal polluted soils remediation due to the simplicity of the operation, low costs and eco-friendliness. Certain types of bacteria have been used in remediation processes of contaminated soil for decades due to their capacity to detoxify certain heavy metals,

their high surface area to volume ratio, and their capacity to promote plant growth and metal accumulation on plant tissues (Pires et al., 2017). Soil bacteria communities play an important role in nutrient cycling, plant symbioses, decomposition, and other ecosystem processes. Selection of the proper microbial agent is one of the most critical steps in order to remove heavy metal from the soil (Xu et al., 2020).

Microbes deal with poisonous chemicals by applying enzymes to convert one chemical into another form and taking energy or utilizable matter from this process. Despite its toxicity, the ancient and constant exposure of bacteria to arsenic has led to the microbe colonization of arsenic-rich environments throughout the development of metabolism coupled biotransformation processes, i.e. reduction, oxidation, that affects geochemistry, speciation and toxicity of this element. Due to the ability of bacteria to metabolize highly toxic arsenic compounds into a less toxic form, the isolation and study of arsenic resistant bacteria is attractive for the establishment of processes to ameliorate the bioavailability of arsenic in contaminated soil and water (Alaniz-Andrade et al., 2017).

Bioaccumulation mainly involves the biosorption or physiological uptake of arsenic by microbial metabolically active and passive processes. Microbial-mediated arsenic reactions may occur thereafter, which is part of the most important phenomena involved in arsenic metabolism. Because of its high efficiency, low cost, and most importantly its eco-friendly nature, bioaccumulation presents an interesting option for the removal and recovery of arsenic from the contaminated environments (Pandey & Bhatt, 2015).

This research study deals with the explaining of the bacterial contribution in the soil leaching and continues on the results from the research of contaminated soil bioleaching published by Štyriaková et al. (2019). The resistance of heterotrophic autochthonous bacteria isolated from the contaminated soil towards the As was studied. The toxic characteristic of leaching process, bioassessment of studied toxic elements as well as sequential extraction analyses were provided to evaluate the influence of bacteria onto toxic elements leaching. The experimental results were completed by the electron microanalyses.

2. Materials and Methods

2.1. Soil sample

The soil sample was taken from the Richnava locality (denoted as R1). The sampling site was a garden often flooded by the Hornád river. The river was polluted because flowing through the localities, heavy loaded with products of anthropogenic activities – especially mining and metallurgical industry. The soil was sieved to grain size below 4 mm. The oversized product consisted of anthropogenic sludge and larger rock grains. The grains below 4 mm were used for experimental purposes. According to the XRD analysis the main mineral phase of studied soil was quartz, creating more than 70 %, than siderite and Mg-siderite (12 %). Other minor phases were plagioclase (4.3 %), muscovite (2.4 %), K-feldspar and chlorite (both approximately 1 %), calcite (1.8 %), dolomite (1.4 %) and barite, hematite and illite (below 1.0 %) (Štyriaková et al., 2019).

2.3. Microbiological analysis of soil

Microbiological analyses were performed with the aim to determine the count of heterotrophic bacteria in contaminated soil that are tolerant towards high concentration of toxic As. The resistance of heterotrophic bacteria isolated from the contaminated soil towards As was tested by bacterial cultivation on the solid nutrient media – agar plates (Trypton soya agar – TSA) and in the liquid nutrient media TSB (Trypton-soya broth) with the addition of 0.3 mM and 3 mM As respectively. The bacterial turbidity was determined using the McFarland standard (2002).

McFarland standard is a chemical solution of barium chloride and sulphuric acid. The result of the chemical reaction is a fine precipitate of barium sulphide. After the suspension shaking its turbidity is visually comparable with the bacterial suspension of known concentration. The degree of turbidity is in the range of 0.5–10 and represents the different bacterial density, count of bacterial cells (Tab. 1). The measured value of absorbance corresponds with the particular value of McFarland standard. On this basis it is possible to determine the approximated count of bacterial cells for each sample.

Tab. 1
McFarland standard for determination of count of bacterial cell in media in dependence on measured value of absorbance.

McFarland standard	Absorbance	Grown bacterial cells [ml]
0.5	0.125	1.5 x 108
1	0.25	3.0 x 108
2	0.5	6.0 x 108
3	0.75	9.0 x 108
4	1	1.2 x 109
5	1.25	1.5 x 109
6	1.5	1.8 x 109
7	1.75	2.1 x 109
8	2	2.4 x 109
9	2.25	2.7 x 109
10	2.5	3 x 109

The value of absorbance of media was measured in selected time intervals by UV VIS spectrometer Spectroquant Pharo 300 (Merck, Germany) at wavelength of 540 nm. As the blank control the uninoculated TSB medium was used.

2.3. Chemical and biological chemical leaching of soil

According to the method of soil remediation published by Štyriaková et al. (2019), the studied sample was leached in three steps. Through the glass column of 80 mm in diameter and 340 mm high containing 1 kg of the contaminated soil percolated with 2 l of media containing 10 mM Ethylenediaminetetraacetic acid disodium salt dihydrate (Na_2EDTA, denotes as chelant ch1). Subsequently, 1.5 l of medium with Ethylenediamine-*N*,*N*′-disuccinic acid trisodium salt (Na_3EDDS, denoted as chelant ch2) percolated through the glass bottle containing 800 g of chemically leached soil. After that 700 g of as-treated soil was bioleached using 3 l of media with 2 mM chelant ch1 and nutrients.

For the bioleaching experiments the heterotrophic bacteria *Bacillus* spp. isolated from the sediment of water dam Ružín were used. The samples were heated at 80 °C for 15 min to kill vegetative cells. The sediment contained the spore-forming bacteria at a concentration of 10^5 CFU/g active in Fe dissolution (Štyriaková et al., 2016). The isolates were grown in Trypton soya broth at 28 °C for 18 h. Following the cells were centrifuged at 4 000 rpm for 15 min and washed twice with the saline solution (0.9 wt % NaCl). These bacteria were inoculated into the parallel columns before the medium percolation (to ensure the activity of autochthonous bacteria). The stimulation of indigenous heterotrophic bacteria using nutrients in the form of fertilizers verified the mobilization of toxic elements from the soil samples.

2.4. Toxicity and bioassessment of soil

Soil toxicity was determined using Toxic Characteristic of Leaching Process (TCLP) according to the US EPA 1311 method (Khorasanipour & Eslami, 2014). The soil sample of 50 grams was treated by solution of 1 N NaOH and vinegar acid of pH 4.2 for 18 hours under the vigorous stirring. The permissible concentration of elements extracted from the soil or waste are listed in Tab. 2. The limits are supplemented by values according to the solid-waste extraction procedure for leaching toxicity HJ/T 300-2007 (IEPT) (Xu et al., 2019).

Tab. 2

TCLP and IEPT limits.

	Cu	Pb	Zn	As	Ba	Cd	Cr
TCLP limit [mg/l]	–	5	–	5	100	1	5
IEPT [mg/l]	50	3	50	1.5	–	0.3	10

The bioassessment of the toxic elements present in the contaminated soil was tested by Simple Bioavailability Extraction Test (SBET). The soil sample of 5 grams was treated by solution of 0.4 M glycine of pH 1.5 (adjusted by HCl) under the vigorous stirring for 1 hour at 37 °C (Report No.: 1542820-003-R-Rev0, 2016; Kim et al., 2009).

2.5. Sequential extraction analysis of soil

The as-received soil sample, chemically leached samples by chelants ch1, ch2 and biological-chemical leached sample were subjected to sequential extraction analysis with the aim to determine the content of toxic elements in biologically available and unavailable fractions. The sequential extraction analysis was provided according to the method described by Mackových et al. (2000).

2.6. Optical and electron microscopy, electron microanalysis

The changes of separated grains after the biological-chemical leaching were observed by binocular optic microscope with camera Nicon P-FMD (Japan).

The particular soil grains were observed by electron micro analyzer CAMECA SX-100, providing the point chemical analyses, line profiles, RTG quantitative and qualitative maps, backscattered electron (BEI) and secondary electron (SEI) images.

More detailed study of morphology and grain surface were studied by scanning electron microscopy FE MIRA 3 (Tescan, Czech Republic) equipped by XRD energy-dispersive (EDX) analyser of chemical composition (Oxford Instruments).

3. Results

3.1. Microbiological analysis of soil

The detailed chemical and mineralogical analysis of the soil sample R1 was described by Štyriaková et al. (2019). The contamination by studied toxic elements decreased, according to the contamination criteria, in order Ba > As > Sb > Cu (Tab. 3). Also, the plants growing in this locality showed the presence of higher As concentrations (Štyriaková et al., 2019).

Tab. 3

Concentration of studied elements present in the contaminated soil.

R1 [mg/g]	As	Sb	Ba	Cu	Zn	Pb	Ni	Cd	Hg
	364	61	3 303	692	541	143	86	1	31
IT [mg/g]	65	25	900	500	1 500	250	180	10	2.5
ID [mg/g]	70	40	1 000	600	2 500	300	250	20	10

ID – Permissible limit of contaminant concentration in soils
IT – Critical limit of contaminant concentration in soils

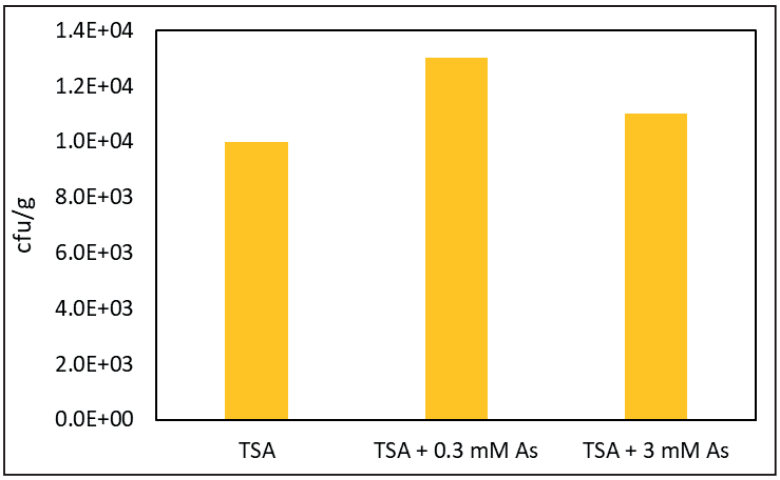


Fig. 1. Comparison of heterotrophic bacteria cultivation on agar plates (TSA), and on plates with addition of As.

High concentration of As should be released from the soil matrix by the biological-chemical processes and lead to gradual contamination of plants and. From this reason the microbiological analyses were performed with the aim to determine the count of the heterotrophic bacteria in contaminated soil that are tolerant towards high concentration of toxic As.

The highest resistance towards As was observed for the TSA medium with 0.3 mM As, 1.3 x 10^4 colony forming unit (cfu/g). For the TSA with 3mM As the bacteria growth reached 1.1 x 10^4 cfu/g (Fig. 1). The resistance of bacteria does not correspond with the As concentration in the soil sample. It is influenced by the soil utilization for agriculture, behind with the continuous supply of organic matter and biogenic elements in the form of fertilizer relates.

The experiments in TSB were performed in the glass tubes containing nutrient medium and in the glass reagent flasks containing nutrient medium with 5 g of contaminated soil.

During the whole experiment more prominent bacterial growth was observed in the flasks. The values of absorbance reached higher values (higher medium turbidity). The available nutrients for bacteria growth in flasks were provided not only from the TSB media but also from the present soil. The process was finished after 90 hours with higher bacteria growth. In the glass tubes, the experiment was finished earlier, after 70 hours.

During the first 40 hours the more expressive bacterial growth was observed in the glass tubes with the As addition. After 43 hours the stagnation of growth can be observed for all tubes and after 48 hours the slight decrease was detected. While the measured values of absorbance were similar for TSB and TSB with 0.3 mM As, the highest values were obtained for TSB with 3 mM As (Fig. 2).

The bacterial growth in flasks was of jump character. After 27 hours the slight increase was observed for all samples. More expressive increase was detected after 50 hours and after 69 hours the slowing down of the growth occurred (Fig. 3). In the first

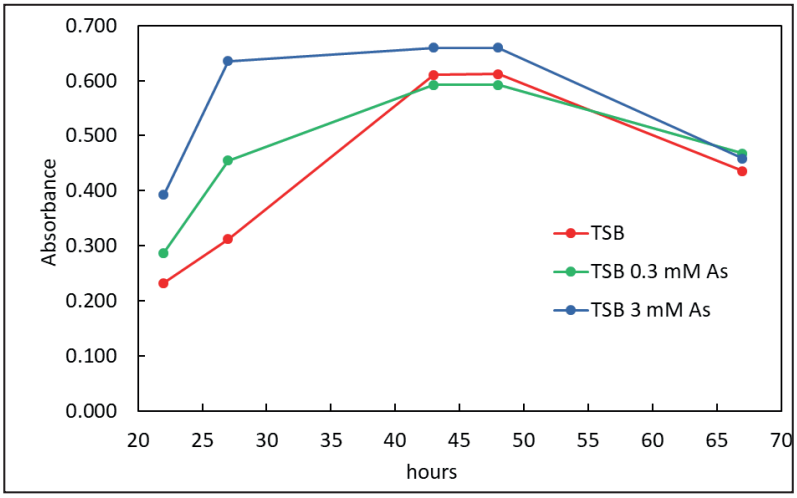


Fig. 2. Comparison of growth of bacteria isolated from the contaminated soil in glass tubes containing TSB and TSB with addition of 0.3 and 3 mM As by absorbance measuring using UV VIS spectrometer.

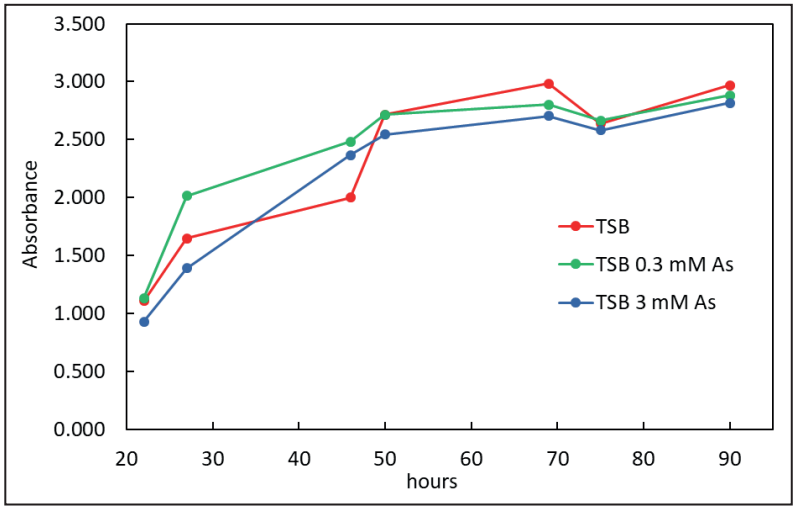


Fig. 3. Comparison of growth of bacteria isolated from the contaminated soil in glass flasks containing soil and TSB and TSB with addition of 0.3 and 3 mM As by absorbance measuring using UV VIS spectrometer.

hours of experiment the more expressive increase was observed for flask contained TSB with 0.3 mM As what also corresponds with the results obtained from the experiments of isolated bacteria growth provided on agar plates. For all studied media the maximum bacteria growth was reached after 43 hours and was in the range 6 x 10^8 – 9 x 10^8 cfu/ml.

In flasks the highest value of absorbance was measured after 69 hours and it was higher than 2.7, what represents more than 3 x 10^9 cfu/ml. The mineral particles present in the soil are a source of biogenic elements that stimulate bacterial metabolism, reproduction and growth. Thus the growth of the resistant bacterial cells was higher in the flask than in the tubes containing only the TSB medium. In this case it is not possible to determine the count of bacterial cell by the McFarland standard. More appropriate method is direct counting under the microscope in Burker chamber. From the reason of unavailable device equipment this method was not applied to evaluate the measurements of absorbance.

3.2. *Toxic characteristics and bioassessment of soil*

The TCLP test was applied on leaching of the as-received soil (R1) and soil after the biological-chemical leaching (R1 L). Except the Ba, higher concentrations of studied elements were released from the R1 L sample, but they were under the limited values according to the TCLP and IEPT limits (Fig. 4).

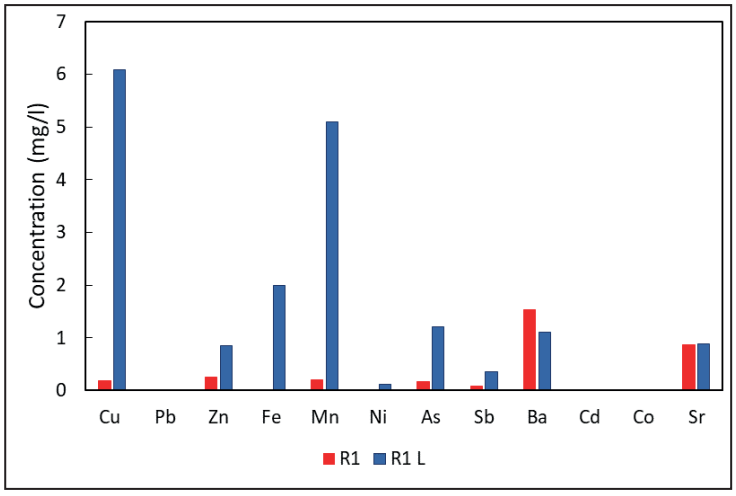


Fig. 4. Concentrations of studied toxic elements in leachates after the TCLP test applied on as-received and biological-chemical leached soil sample.

According to the results of the SBET test, the biological-chemical leaching of the sample led to the decrease of bioassessment of Cu, Pb, Zn, Mn, Ba and Sr (Fig. 5). On the other hand, the bioassessment of Fe and As increased, probably due to the disruption of their bounds in the structure of leached mineral grains. This result pointed at the further possibility of As extraction by the process of acid leaching (pH lower than 2), that should be effective in As concentration, lowering in the soil up to limited values.

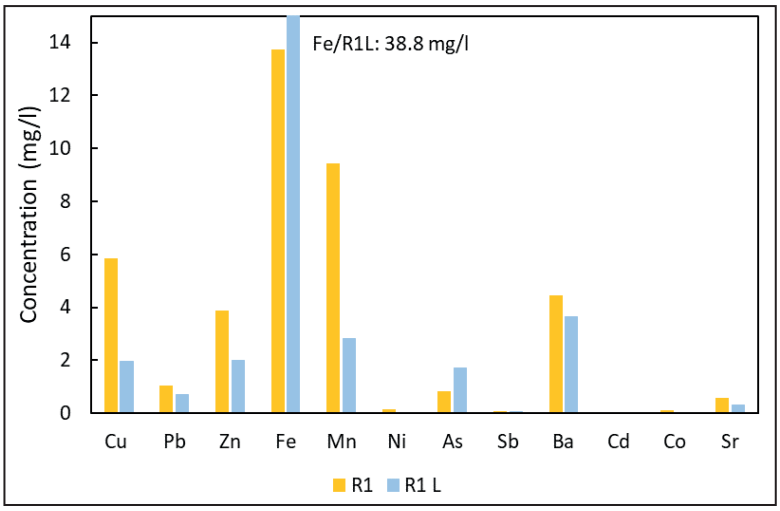


Fig. 5. Concentrations of studied toxic elements in leachates after the SBET test applied on as-received and biological-chemical leached soil sample.

3.3. *Sequential extraction analysis*

To explain the effect of combined three step chemical and biological-chemical leaching on soil decontamination, the sequential extraction analysis was provided.

The fractions (1) to (4) represent the forms of risk chemical elements that are available for organisms in their living environment and they are the most hazardous for their contamination. The used reagents imitate the nature processes of liberation of elements from the primary bounds into the solutions and their recombination into secondary minerals. The fraction (1) is soluble in water, (2) exchangeable and/or carbonate, (3) reducible, and (4) oxidizable/organo-sulfide. The fraction (5) representing residual, encompasses the elements in form of no real risk for organisms present in given environment.

In the R1 sample the content of Cu (49.2 %), Pb (85.1 %), Zn (40.3 %) and Co (33.0 %) was the highest in the reducible fraction, content of Ni (51.1 %), As (52.0 %), Sb (92.0 %), Ba (65.5 %) and Cr (77.6 %) in the residual fraction and Hg (93.8 %) in the organo-sulfide fraction (Fig. 6). After the chemical leaching by chelant ch1, the highest ratio of Pb (78.6 %), Zn (40.2 %) and Co (26.1 %) was still in the reducible fraction (the same ratio of Co

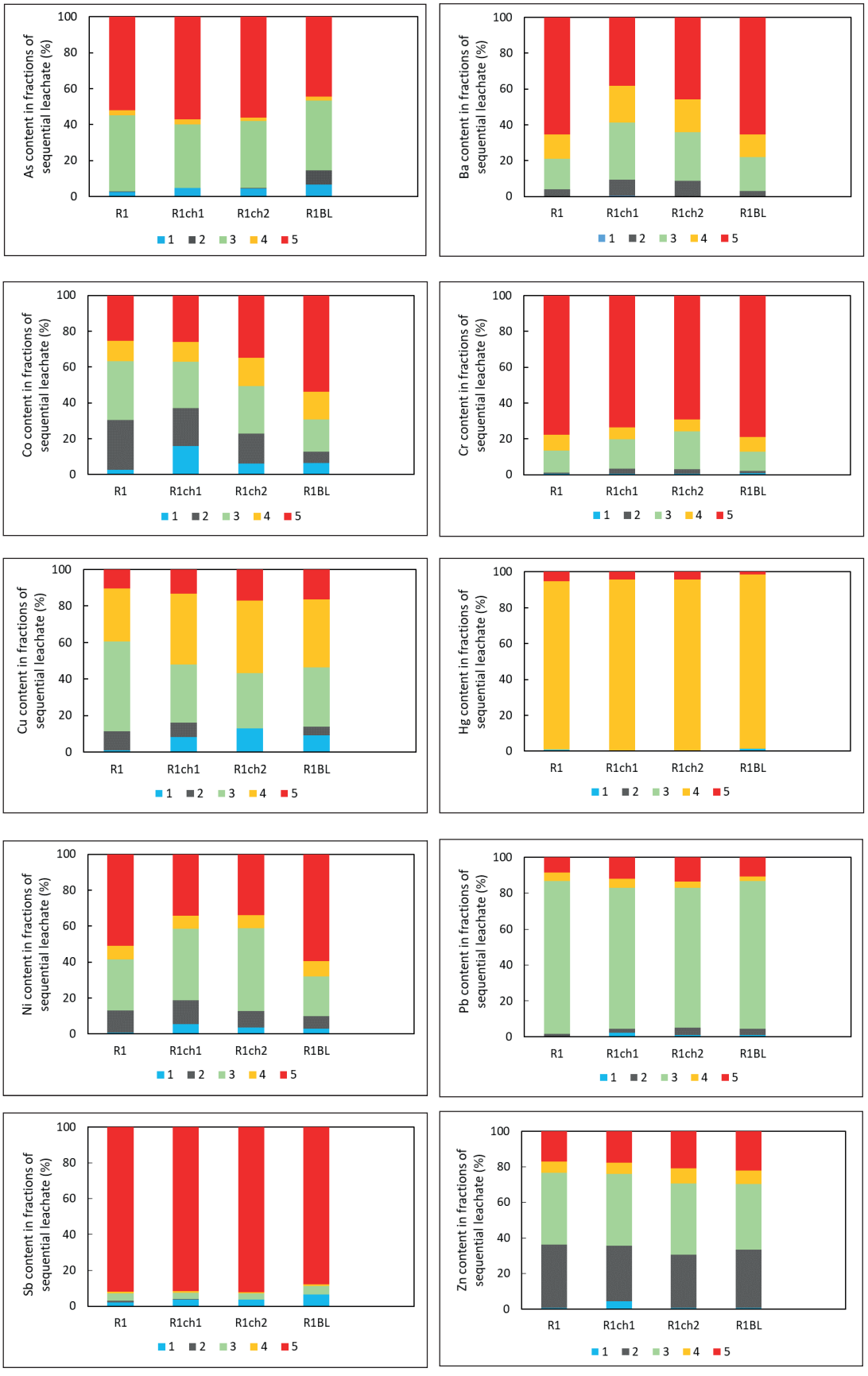


Fig. 6. Content of studied toxic elements in the fractions of sequential leachate as received in soil, soil after chemical (R1ch1, R1ch2) and and biological-chemical leaching (RIBL).

also in residual), but their content decreased after chemical leaching in behalf of water soluble fraction (Pb, Zn, Co), ion exchangeable and carbonate fraction (Pb) and organo-sulfide (Pb, Zn) fraction. For Cu the increase of its content in the fractions (1), (4) and (5) was observed. The highest ratio of Cu was in the organo-sulfide fraction. The chemical leaching by chelant ch1 also led to increase of content of Ni, Ba and Cr in the fractions (1), (2) and (3), of As in (1) and (2), of Sb, Co in the fraction (1). Also, the ratio of As and Co was increased in the reducible fraction, As for more than 5 % and Co 0.5 % (Fig. 6).

After the chemical leaching by chelant ch2 the highest content of Cu (39.5 %) and Hg (95.3 %) stayed in the organo-sulfide fraction, Pb (78.6 %), Zn (40.1 %) and Ni (45.9 %) in the reducible fraction and As, Sb, Ba, Co and Cr in the residual fraction. For all studied toxic elements, except of Ni and As, the increase of their concentrations in the residual fraction was observed (for Ba of 7.39 %). The content of Cu increased in the fractions (1) and (4), Pb in (2), Zn in (4), Ni, Co in the fractions (3) and (4), As and Cr in the fraction (3) (Fig. 6).

After the biological-chemical leaching the highest ratio of Cu (37.3 %) and Hg (97.0 %) was again in the organo-sulfide fraction, content of Pb (82.4 %) and Zn (36.7 %) in the reducible fraction and other studied elements in the residual fraction. In comparing with R1ch2, the concentration of Cu, Pb, As, Sb and Hg decreased in the biologically unavailable fraction. The most significant decrease was observed for As (of 11.5 %) in behalf of fractions (1), (2) and (3) (Fig. 6).

From these results it can be concluded that the repeated chemical and biological-chemical leaching of contaminated soil should lead to more expressive decrease of As, but also of Cu, Pb and Sb concentrations in the studied soil.

3.4. Optical and electron microscopy, electron microanalysis

Grain body was composed mostly of aluminosilicates with different content of Fe with admixture of quartz, feldspars, chlorite, siderite, and also with minor ratio of apatite and rutile (Štyriaková et al., 2019).

Disrupted structure of Fe coatings was observed on the marginal sites of grains after the biological-chemical leaching. The heterotrophic bacteria used in the leaching process are able to disrupt a less resistant structure of Fe oxides and hydroxides. The point analysis in the sites with higher content of Fe did not show and presence of significant content of As and other studied toxic elements (Fig. 7, Tab. 4). This pointed at their effective removal from the grain surface by biological-chemical leaching.

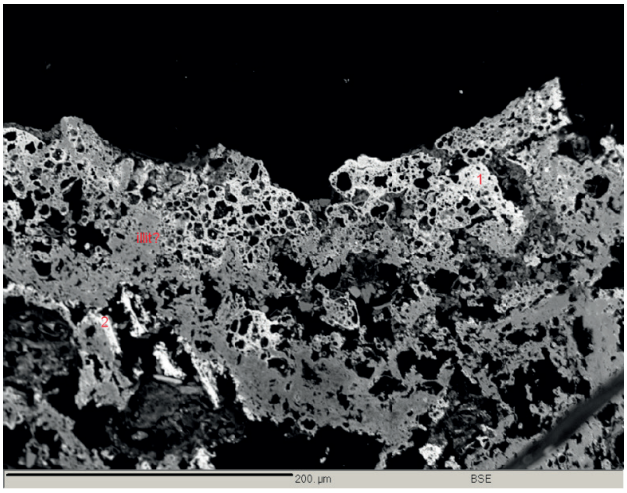


Fig. 7. BSE image of separated grain (11R) with the marked place of point EDX analysis.

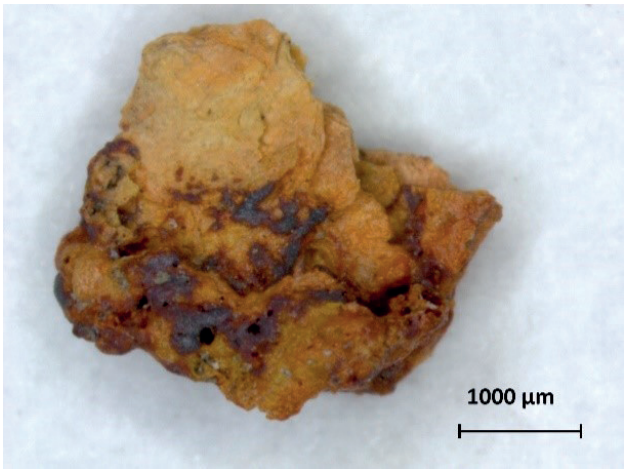




Fig. 8. Separated grain 7R (left) and grain after the biological-chemical leaching (right) observed by optical microscope.

The disruption of less resistant forms of Fe oxides and hydroxides were also observed by optic microscope. The surface of separated grain 7R after the biological-chemical

leaching changed visibly (Fig. 8). The application of heterotrophic bacteria caused the Fe dissolution from the structure, with which the As removal (and other toxic elements bounded in Fe coatings) is expected as well.

Tab. 4

Point analysis of separated grain from the Figure 7.

11R wt. %	Fe	Mn	Si	Al	Mg	Na, Ca, K	Cu, Ni, Zn, Pb, Co, Cr, Sb, As	O, ost.
an1	25.18	0.01	10.75	5.39	0.97	1.14	0.08	56.48
an2	27.95	0.08	2.94	9.42	5.03	0.40	0.38	53.80

Detailed morphology of surface of separated grain 7R after the leaching was observed by scanning electron microscope. The mentioned surface structure disruption was observed as a presence of expressive pores on the grain surface (Fig. 9). More resistant forms of Fe oxides were observed in the form of spherical particles created agglomerates on the grain surface (Fig. 10).

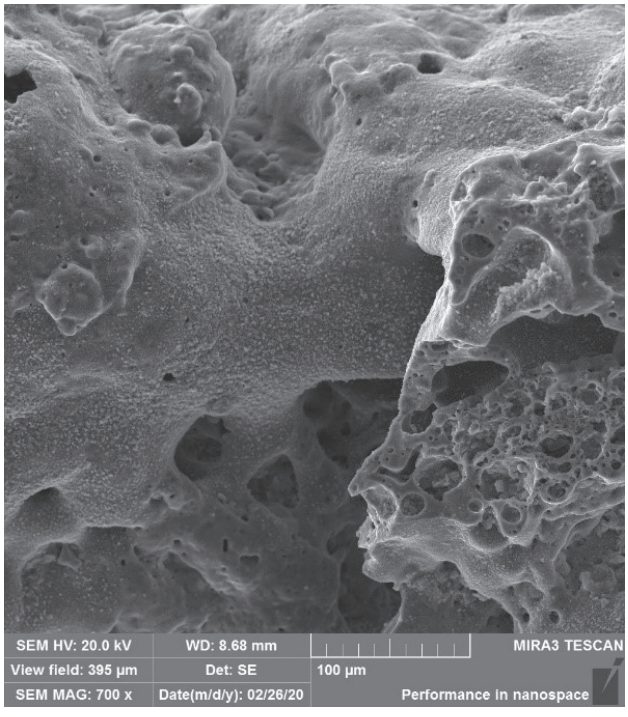


Fig. 9. Morphology of the surface of separated grain 7R after the biological-chemical leaching at magnification 700x.

Chemical analysis of separated grain 7R by EDX confirmed the presence of basic structural elements of matrix, as well as Fe particles on its surface (Fig. 11). The presence of As or other toxic elements was not detected, what corresponds with the results from the electron microanalysis (Fig. 12).

The using of three different microscopic methods to analyse the separated grains allows to confirm the effect of biological-chemical leaching on toxic elements removal from the contaminated soil, especially As.

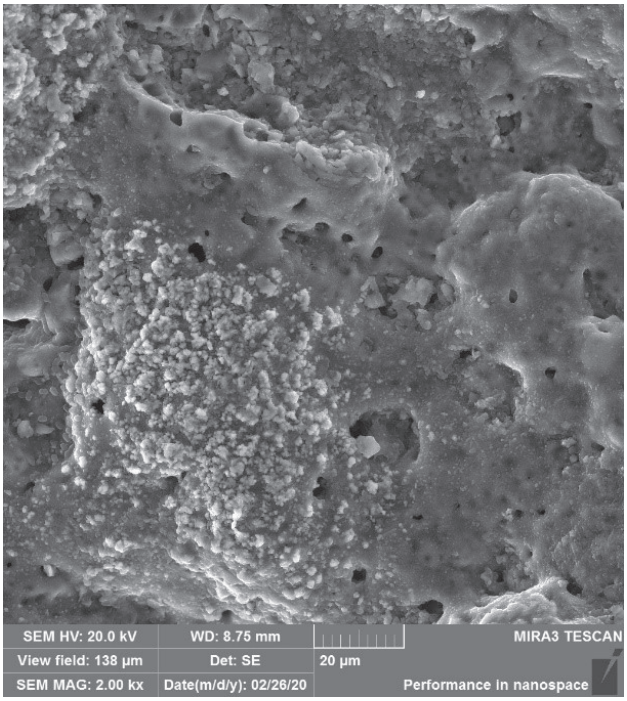


Fig. 10. Morphology of the surface of separated grain 7R after the biological-chemical leaching at magnification 2 000x.

4. Conclusion

The study was focused on more detailed characterization of the bacterial influence on the toxic elements leaching from the contaminated soil. The analysed toxic elements did not show expressive toxic character. On the other hand, the studied soil was often fertilized, what represents good conditions for bacteria activities in disruption of bonds between the minerals and toxic elements in the soil after the nutrient supply. Also, they showed good resistance onto As in their environment. The series of experiments were carried out in order to study the bioavailability of toxic elements in contaminated and treated soil. The bioavailability of Cu, Pb, Zn, Mn, Ba, Co and Sr decreased after the soil treatment, but the bioavailability of Fe and As increased. Also, the sequential extraction analyses pointed at the decrease of As content in the residual fraction after the biological-chemical leaching. The results presented in the study confirmed the possibility of soil decontamination by repeated cycles of chemical and biological-chemical leaching, what is promising way for the soil remediation with regard to the natural environment.

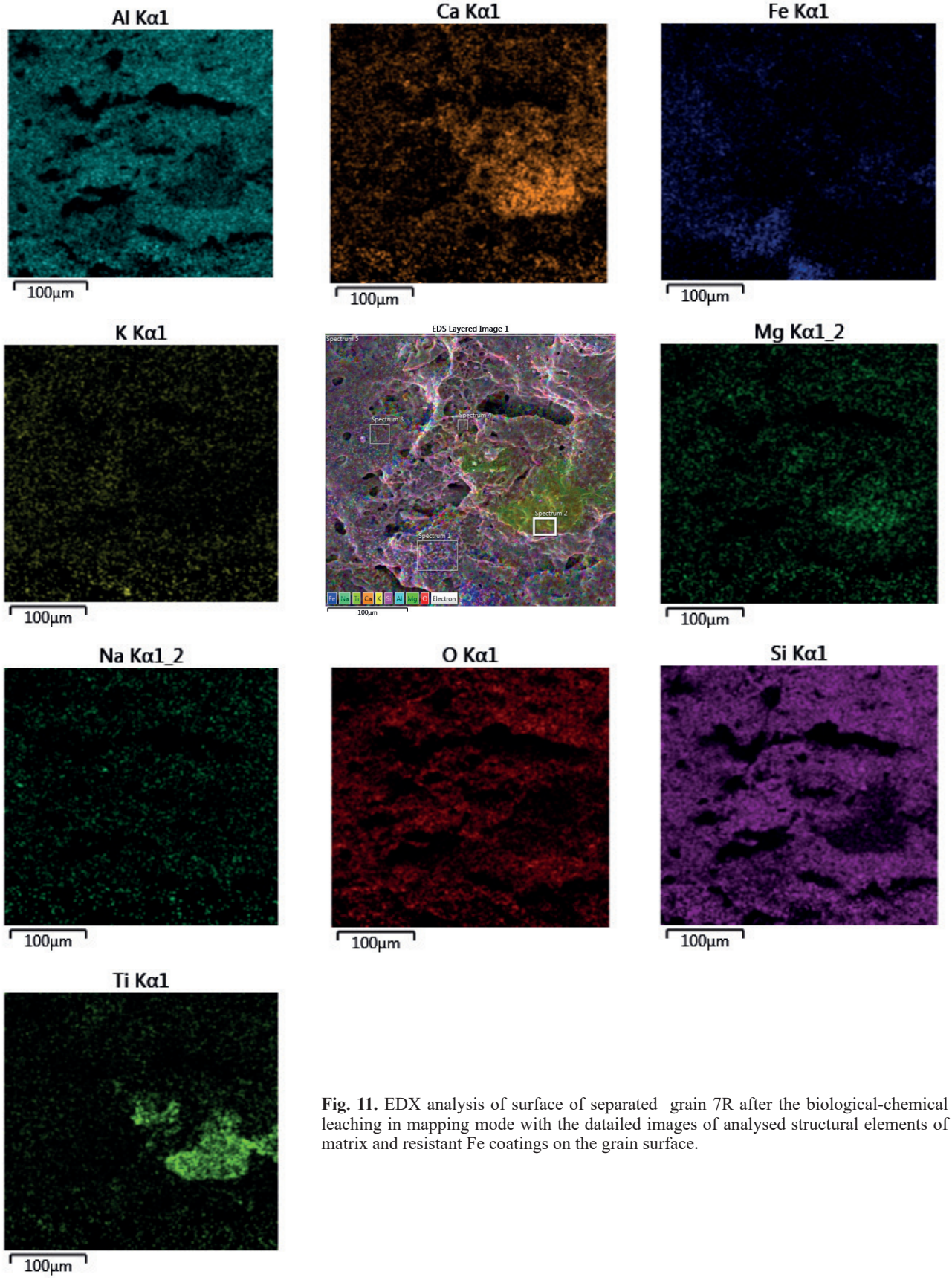


Fig. 11. EDX analysis of surface of separated grain 7R after the biological-chemical leaching in mapping mode with the datailed images of analysed structural elements of matrix and resistant Fe coatings on the grain surface.

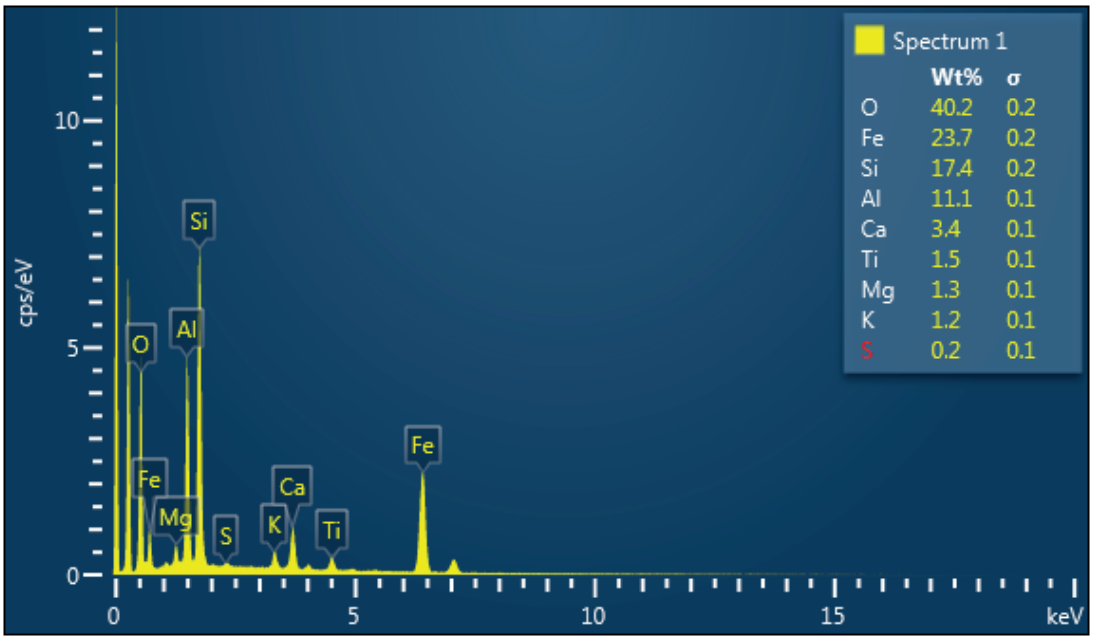


Fig. 12. EDX spectrum of separated grain 7R after the biological-chemical leaching – analysis in the point 1 on Fig. 11.

Acknowledgement

The authors are thankful for financial support by the Ministry of Environment of the Slovak Republic – geological task GT 02 18 *Development of technologies during the remediation process of the contaminated environment*. Thanks are expressed also to reviewers Zuzana Bártová (Slovak Academy of Sciences) and Michal Hegedus (Synthon, s.r.o., Czech Republic), improving quality of primary manuscript.

5. References

Alaniz-Andrade, A. L., Letechipía de León, C., Ramírez--Santoyo, R. M., Guzmán-Moreno, J. & Vidales-Rodríguez, L. E., 2017: Arsenic tolerance in bacterial cultures isolated from metal contaminated soil. *Acta Univ. Multidisc. Sci. J., 27, 9–18.*

Khorasanipour, M. & Eslami, A., 2014: Determination of elements leachability from Sarcheshmeh Porphyry Copper Mine tailings: Application of toxicity characteristic leaching procedure. *Environ. Processes, 1, 387–403.*

Kim, K. R., Owens, G. & Naidu, R., 2009: Heavy metal distribution, bioaccessibility and phytoavailability in long-term contaminated soils from Lake Macquarie, Australia. *Aust. J. Soil Res., 47, 166–176.*

Mackových, D., Nováková, N., Šoltýsová, H. & Lučivjanský, P., 2000: Determination of some toxic elements specific forms in soils and sediments after sequential extraction. 4th European Furnace Symposium and 15th Slovak Spectroscopic Conference, Podbanské, 125.

McFarland Standard, 2002: Dalynn Biologicals, Catalogue No. TM50-TM60.

Nwagwu, E. CH., Moltong Yilwa, V., Egbe, N. E. & Onwumere, G. B., 2017: Isolation and characterization of heavy metal tolerant bacteria from Panteka stream, Kaduna, Nigeria and their potential for bioremediation. *African J. Biotechnol., 16, 32–40.*

Pandey, N. & Bhatt, R., 2015: Arsenic resistance and accumulation by two bacteria isolated from a natural arsenic contaminated site. *J. Basic Microbiol., 55, 1275–1286.*

Pires, C., Franco, A. R., Pereira, S. I. I., Henriques, I., Correia, A., Magan, N. & Castro, P. M. L., 2017: Metal(loid)-contaminated soils as a source of culturable heterotrophic aerobic bacteria for remediation applications. *Geomicrobiol. J., 34, 760–768.*

Report Number: 1542820-003-R-Rev0, 2016: Accounting for bioavailability in contaminated land site – specific health risk assessment. *Golder Associates, Wellington, New Zealand.*

Štyriaková, I., Štyriak, I., Balestrazzi, A., Calvio, C., Faè, M. & Štyriaková, D., 2016: Metal leaching and reductive dissolution of iron from contaminated soil and sediment samples by indigenous bacteria and *Bacillus* Isolates. *Soil Sed. Contamin., 25, 519–535.*

Štyriaková, I., Danková, Z., Košuth, M., Šuba, J., Nováková, J. & Kollárová, V., 2019: Removal of toxic elements from the minerals particles of contaminated soil by chemical and biological leaching. *Miner. Slov., 51, 206–215.*

Tsang, D. C. W. & Yip, A. C. K., 2014: Comparing chemical-enhanced washing and waste-based stabilisation approach for soil remediation. *J. Soils Sed., 14, 936–947.*

Xu, M., Liu, Y., Deng, Y., Zhang, S., Hao, X., Zhu, P., Zhou, J., Yin, H., Liang, Y. , Liu, H., Liu, X., Bai, L., Jiang, L. & Jiang, H., 2020: Bioremediation of cadmium-contaminated paddy soil using an autotrophic and heterotrophic mixture. *RSC Advances, 10, 26090–26101.*

Xu, P., Zhao, Q., Qiu, W. & Xue, Y. 2019: The evaluation of the heavy metal leaching behavior of MSWI-FA added alkali-activated materials bricks by using different leaching test methods. *Int. J. Environ. Res. Public Health, 16, 1151–1167.*

Vplyv baktérií na lúhovanie toxických prvkov z kontaminovanej pôdy

Cieľom štúdie bolo bližšie charakterizovať vplyv baktérií na uvoľňovanie toxických prvkov z kontaminovanej pôdy v procese biologicko-chemického lúhovania. Experimenty sa realizovali na vzorke pôdy z lokality Richnava. Vzorka pôdy R1 pochádzala z oblasti kontaminovanej nánosmi rieky Hornád, ktorá preteká lokalitami zaťaženými metalurgickým priemyslom, ako aj niekdajšou banskou činnosťou. Chemická analýza poukázala na jej znečistenie toxickými prvkami v poradí Ba > As > Hg > Sb > Cu. Na experimentálne účely sa použila kontaminovaná pôda a pôda po procese trojstupňového biologicko-chemického lúhovania, opísaného bližšie v príspevku Štyriakovej et al. (2019).

Vzorka kontaminovanej pôdy s hmotnosťou 1 kg bola umiestnená v sklenenom valci s priemerom 80 mm a výškou 340 mm, ktorým perkoloval roztok 10 mM etyléndiamíntetraoctanu sodného (Na_2EDTA, ďalej označený ako ch1) s objemom 2 l. Potom chemicky lúhovanou vzorkou s hmotnosťou 800 g perkolovalo 1,5 l roztoku 10 mM etyléndiamínsukcínu sodného (Na_3EDDS, ďalej označený ako ch2) a následne sa vzorka (700 g) biologicko-chemicky lúhovala 3 l média s obsahom 2 mM chelátu ch1 a živín. Pôda po jednotlivých stupňoch lúhovania bola neskôr analyzovaná pomocou sekvenčnej extrakčnej metódy.

Mikrobiologickými analýzami sa zisťovali počty heterotrofných baktérií nachádzajúcich sa v kontaminovanej pôde, ktoré tolerujú prítomnosť vysoko toxického prvku arzénu. Arzén sa môže uvoľňovať z pôdneho matrixu biochemickými procesmi a spôsobovať postupnú kontamináciu rastlín alebo podzemnej vody, a tak spolu s inými prvkami ohroziť životné prostredie.

Rezistencia heterotrofných baktérií izolovaných z pôdy proti As sa overovala kultiváciou baktérií na tuhom živnom médiu – agarových platniach (tryptónovo-sójový agar – TSA) s prídavkom 0,3 mM a 3 mM As a v tekutom živnom médiu TSB (tryptónovo-sójový bujón) s prídavkom 0,3 mM a 3 mM As. Experimenty sa realizovali v skúmavkách obsahujúcich živné médium a vo fľašiach obsahujúcich živné médium a 5 g skúmanej pôdy. Absorbancia médií sa merala vo vybraných časových intervaloch na UV VIS spektrometri Spectroquant Pharo 300 pri vlnovej dĺžke 540 nm.

Heterotrofné baktérie izolované z kontaminovanej pôdy preukázali dobrú odolnosť [počet baktérií vyše $1,2 \cdot 10^5$ kolóniu tvoriacich jednotiek (KTJ)/g) proti koncentrácii As (0,3 mM)] v tuhom médiu – na agarových platniach (obr. 1). V tekutom živnom médiu sa získali len veľmi malé rozdiely v raste počtu baktérií v závislosti od koncentrácie As v médiu, pričom v prvých hodinách priebehu experimentu bol najvýraznejší rast baktérií v médiu s 0,3 mM As. Zodpovedá to aj výsledkom získaným na agarových platniach (obr. 2). Rast baktérií bol výraznejší vo fľašiach, ktoré okrem živného média obsahovali aj prídavok kontaminovanej pôdy. To umožnilo zvýšenie prísunu živín na rast počtu heterotrofných baktérií (obr. 3). Výsledky poukázali na fakt, že rezistencia baktérií proti As v pôde nesúvisí s jeho koncentráciou, ale je ovplyvnená využívaním pôdy na pestovanie plodín, ktorým je zabezpečený pravidelný prísun organických látok a biogénnych prvkov pre prítomné mikroorganizmy vo forme hnojív.

Test toxicity metódou US EPA (1311) aplikovaného procesu lúhovania pri vzorkách vstupnej pôdy a pôdy po biologicko-chemickom lúhovaní neviedol k prekročeniu limitných hodnôt koncentrácie vybraných toxických prvkov v zmysle kritérií TCLP a IEPT (obr. 4, tab. 2).

Test bioprístupnosti s využitím kyseliny chlorovodíkovej preukázal zníženie bioprístupnosti sledovaných toxických prvkov vo vzorke pôdy po biologicko-chemickom lúhovaní, s výnimkou Fe a As (obr. 5). Ich bioprístupnosť v upravenej vzorke pôdy sa zvýšila. Naznačuje to ďalšiu možnosť odstránenia As a Fe procesom kyslého chemického lúhovania, ak by sa zmenili podmienky pH na menej ako 2, pričom by bolo možné znížiť hlavne nadlimitnú koncentráciu As.

Vstupná vzorka a vzorky z jednotlivých stupňov chemického a biologicko-chemického lúhovania (podľa postupu uvádzaného Štyriakovou et al.) bola následne podrobená päťstupňovej sekvenčnej extrakčnej analýze na zistenie mobility sledovaných toxických prvkov a ich bioprístupnosti (Mackových et al., 2000).

Vo vstupnej vzorke pôdy sa nachádzali Cu (49,2 %), Pb (85,1 %), Zn (40,3 %) a Co (33,0 %) v najväčších podieloch v redukovateľnej frakcii, Ni (51,1 %), As (52,0 %), Sb (92,0 %), Ba (65,5 %) a Cr (77,6 %) v reziduálnej frakcii a Hg (93,8 %) v organicko-sulfidickej frakcii (obr. 6). Po chemickom lúhovaní pôdy chelátom ch1 ostáva najväčší podiel Pb (78,6 %), Zn (40,2 %) a Co (26,1 %) v redukovateľnej frakcii (Co rovnako 26,1 % aj v reziduálnej frakcii), no pri všetkých troch prvkoch sa ich podiel oproti vstupnej vzorke pôdy vo frakcii (3) znížil v prospech frakcie rozpustnej vo vode (Pb, Zn, Co), ionovymeniteľnej a karbonátovej (Pb) a organicko-sulfidickej (Pb a Zn) frakcie. Pri Cu je možné pozorovať nárast koncentrácie vo frakciách (1), (4) a (5), pričom najväčší podiel Cu sa nachádzal v organicko-sulfidickej frakcii. Chemické lúhovanie chelátom ch1 viedlo ďalej k zvýšeniu podielu Ni, Ba a Cr vo frakciách (1), (2) a (3), As

v (1) a (2), Sb a Co vo frakcii (1). V redukovateľnej frakcii sa okrem spomínaného obsahu Cu, Pb a Zn zvýšil aj obsah As (o vyše 5 %) a Co (0,5 %) (obr. 6). Po chemickom lúhovaní pôdy chelátom ch2 ostávajú v najväčšom podiele Cu (39,5 %) a Hg (95,3 %) v organicko-sulfidickej frakcii, Pb (78,6 %), Zn (40,1 %) a Ni (45,9 %) v redukovateľnej frakcii a As, Sb, Ba, Co a Cr v reziduálnej frakcii. Pri všetkých sledovaných prvkoch okrem Ni a As pozorujeme nárast ich koncentrácie v reziduálnej frakcii (Ba o 7,39 %), v prípade Cu nárast koncentrácie vo frakciách (1) a (4), Pb vo frakcii (2), Zn v (4), Ni a Co v (3) a (4) a pri As a Cr vo frakcii (3) (obr. 6). Po biologicko-chemickom lúhovaní pôdy (BL) ostáva najvyšší podiel Cu (37,3 %) a Hg (97,0 %) v organicko-sulfidickej frakcii, Pb (82,4 %) a Zn (36,7 %) v redukovateľnej frakcii a ostatných sledovaných prvkov v reziduálnej frakcii (obr. 6). V prípade Cu, Pb, As, Sb a Hg však v porovnaní s pôdou po lúhovaní s ch2 sa znížila ich koncentrácia v biologicky neprístupnej frakcii, pričom významným znížením je koncentrácia As (o 11,5 %) v prospech frakcií (1), (2) a (3) (obr. 6).

Po chemickom lúhovaní vstupnej pôdy chelátmi ch1 a ch2 ostali vo vzorke pôdy vo zvýšenej koncentrácii As, Sb, Ba a Hg. Sú to prvky, ktorých najvyšší podiel podľa výsledkov sekvenčnej extrakčnej analýzy je viazaný v reziduálnej frakcii, teda biologicky neprístupnej. Vo vzorkách po trojstupňovom lúhovacom cykle však táto analýza preukázala preskupenie ich obsahu, najmä As, do biologicky prístupných frakcií. Zvýšila sa ich mobilita, a teda aj možnosť ďalšej extrakcie použitím chemických a biologicko-chemických postupov. Opakovanou aplikáciou navrhnutého procesu by teda bolo možné znížiť najmä koncentráciu As a Sb na požadované hodnoty v zmysle indikačných kritérií.

Pozorovaním jednotlivých separovaných zŕn z pôdy pred biologicko-chemickým lúhovaním a po ňom sa binokulárnym optickým mikroskopom potvrdilo odstránenie menej odolných Fe povlakov na povrchu zŕn po biologicko-chemickom lúhovaní, v ktorých je prioritne viazaný arzén (obr. 8). Elektrónovým mikroanalyzátorom bolo možné po okrajoch biologicko-chemicky lúhovaných zŕn pozorovať narušené štruktúry Fe povlakov, keďže heterotrofné baktérie využité v procese biochemického lúhovania sú schopné rozrušiť menej odolné štruktúry oxidov a hydroxidov železa (obr. 7). Bodová analýza v miestach s vyšším podielom Fe nepreukázala prítomnosť vysokého obsahu As ani ostatných sledovaných toxických prvkov. Poukazuje to na fakt, že tieto prvky boli procesom biologicko-chemického lúhovania odstránené z povrchu separovaného zrna (tab. 4). Detailnejšia morfológia povrchu vybraného separovaného zrna po biologicko-chemickom lúhovaní bola pozorovaná skenovacím elektrónovým mikroskopom. Už spomínané narušenie štruktúry menej odolných Fe povlakov na povrchu zrna vplyvom heterotrofných baktérií sa prejavilo prítomnosťou výrazných pórov (obr. 9, 10).

Štúdia bola zameraná na detailnejšiu charakterizáciu vplyvu baktérií na lúhovanie toxických prvkov z kontaminovanej pôdy, pričom sa preukázala relatívne vysoká rezistencia heterotrofných autochtónnych baktérií proti As v ich prirodzenom prostredí. Výsledky prezentované v tejto štúdii zároveň poukazujú na možnosť efektívnej dekontaminácie pôdy prostredníctvom opakovaných cyklov chemického a biologicko-chemického lúhovania s využitím heterotrofných baktérií. Predstavuje to perspektívnu metódu remediácie pôdy znečistenej anorganickými kontaminantmi s ohľadom na životné prostredie.

Doručené / Received: 26. 4. 2021
Prijaté na publikovanie / Accepted: 30. 6. 2021

Inštrukcie autorom

Etika publikovania, záväzná pri publikovaní v časopise Mineralia Slovaca: *www.geology.sk/mineralia položka* ***Publikačná etika***

1. Geovedný časopis Mineralia Slovaca publikuje scientometricky hodnotné recenzované pôvodné vedecké články s vysokým citačným potenciálom. V úvode príspevku musí autor jasne deklarovať, čím konkrétnym je jeho príspevok prínosný pre rozvoj geovied. Rešeršné štúdie sa publikujú len ojedinele.

2. Články na publikovanie (manuskripty) sa do redakcie zasielajú poštou (dva vytlačené exempláre a CD so všetkými súbormi v editovateľnej podobe) alebo e-mailom (editovateľné súbory a kompletná verzia vo formáte PDF).

3. Súčasne s článkom je potrebné redakcii poslať autorské vyhlásenie o originalite textu a obrázkov. Kópie obrázkov z iných publikácií musia byť legalizované získaním práva na publikovanie. Vyhlásenie musí obsahovať meno autora (autorov), akademický titul a trvalé bydlisko.

4. Rozsah manuskriptu na publikovanie je najviac 25 rukopisných strán (MS Word, Times New Roman, veľkosť písmen 12 bodov, riadkovanie 1,5) vrátane literatúry, obrázkov a vysvetliviek. V prípade veľkého odborného prínosu sú v ojedinelých prípadoch povolené aj dlhšie články.

5. Články sú publikované v angličtine alebo v slovenčine. Články v slovenčine musia obsahovať anglický preklad názvu, abstraktu, kľúčových slov, resumé a popisov k obrázkom a tabuľkám. Články písané v angličtine musia obsahovať slovenské resumé.

Text

1. Abstrakt stručne sumarizuje článok. Môže mať najviac 200 slov a nemá obsahovať citácie. Počet kľúčových slov je maximálne 6. Text má mať úvod, charakteristiku (stav) skúmaného problému, použitú metodiku, nové zistenia, ich interpretáciu, diskusiu, záver a zoznam literatúry. Východiskové údaje musia byť zreteľne odlíšené od interpretácií. V texte musia byť odvolávky na všetky použité obrázky a tabuľky.

2. Hierarchiu nadpisov v texte je potrebné vyznačiť ceruzkou na ľavom okraji strany manuskriptu: 1 – najvyššia, 2 – nižšia, 3 – najnižšia.

3. V texte sa uprednostňuje citácia v zátvorke, napr. (Dubčák, 1987; Hrubý et al., 1988), pred formou ... podľa Dubčáka (1987).

4. Pozícia obrázkov a tabuliek v texte sa označí. Nie je vhodné, aby text v editore MS Word obsahoval vložené obrázky, ale náhľadová verzia v pdf ich má obsahovať.

5. Grécke písmená treba identifikovať na ľavom okraji slovom (napr. sigma). Potrebné je odlišovať pomlčku od spojovníka. Symboly, matematické značky, názvy skamenelín a pod., ktoré sa majú vysádzať kurzívou, autor v rukopise podčiarkne vlnovkou.

Obrázky a tabuľky

1. Ilustrácie a tabuľky vysokej kvality bývajú publikované buď **na šírku stĺpca (81 mm), alebo strany (170 mm).** Optimálna veľkosť písma a čísiel v publikovaných obrázkoch je 2 mm. Články v slovenčine musia mať popisy v obrázkoch a tabuľkách v slovenčine, záhlavie tabuliek a texty pod obrázkami a tabuľkami sú v slovenčine a angličtine. Články v angličtine majú všetky texty v angličtine. **Maximálny rozmer ilustrácie a tabuľky vytlačený v časopise je 170 x 230 mm.** Väčšie (skladané) ilustrácie sú publikované len v ojedinelých prípadoch.

2. Pri počítačovej tvorbe obrázkov odporúčame používať programy s vektorovým zobrazením (Corel Draw, Adobe Illustrator a pod.). Čiary tzv. vlasovej hrúbky, softvérová alebo rastrová výplň plôch (napr. v Corel Draw) nie sú prípustné. Výplne v obrázkoch musia pozostávať zo samostatne vysádzaných objektov.

3. Ilustrácie vrátane fotografií musia obsahovať **grafickú mierku** v centimetrovej či metrovej škále, prípadne sa rozmer zobrazených objektov vyjadrí v popise obrázka. Mapy a profily musia mať aj **azimutálnu orientáciu** a jednotné vysvetlivky, ktoré sa uvedú pri prvom obrázku. Zoskupené obrázky, napr. fotografie a diagramy, sa uvádzajú ako jeden obrázok s jednotlivými časťami označenými písmenami (a, b, c atď.).

4. Pri zasielaní fotografií vo forme počítačových súborov (formáty JPG alebo TIF) sa požaduje rozlíšenie minimálne 600 DPI. Publikovanie farebných ilustrácií môže byť spoplatnené.

Literatúra

1. Minimálne 50 % citácií musí reprezentovať publikácie od roku 2000. V zozname literatúry sa v abecednom poradí uvádza len literatúra citovaná v danom článku.

2. Spôsob uvádzania literatúry v zozname literatúry

Knižná publikácia: Gazda, L. & Čech, M., 1988: Paleozoikum medzevského príkrovu. *Bratislava, Alfa, 155 s.*

Časopis: Vrba, P., 1989: Strižné zóny v metapelitoch. *Miner. Slov., 21, 135 – 142.*

Zborník: Návesný, D., 1987: Vysokodraselné ryolity. *In: Romanov, V. (ed.): Stratiformné ložiská gemerika. Špec. publ. Košice, Slov. geol. spol., 203 – 215.*

Manuskript: Radvanský, F., Slivka, B., Viktor, J. & Srnka, T., 1985: Žilné ložiská jedľoveckého príkrovu gemerika. Záverečná správa z úlohy SGR--geofyzika. *Manuskript. Spišská Nová Ves, archív Št. Geol. Úst. D. Štúra, 28 s.*

3. Pri článku viac ako dvoch autorov sa v texte cituje iba prvý autor s dodatkom et al., ale v zozname literatúry sa uvádzajú všetci.

Instructions to authors

Publication ethics, being obligatory for publishing in the journal Mineralia Slovaca: *www.geology.sk/mineralia item* ***Publication ethics***

1. Geoscientific journal Mineralia Slovaca publishes scientometrically valuable original peer-reviewed scientific articles with a high citation potential. In the introduction of each article the author(s) must clearly declare, which innovative data the paper brings for the development of geosciences. The retrieval studies are published only exceptionally.

2. The articles for publishing (manuscripts) must be sent to Editorial Office by post (two printed copies and CD with editable files), or by e-mail (editable files plus complete preview version in PDF format).

3. Simultaneously with the article the Editorial Office must receive the author´s proclamation that no part of the manuscript was already published and figures and tables are original as well. Copied illustrations from other publications must contain a copyright.

4. The extent of the manuscript for publishing is limited to 25 manuscript pages (MS Word, 12 points Times New Roman, line spacing 1.5) including figures, tables, explanations and references. In the case of contribution with a high scientific value, the longer manuscripts for publishing are exceptionally permitted.

5. Articles can be published in Slovak or English languages. The title, abstract, key words, shortened text (resumé), as well as description to figures and tables in Slovak articles are published also in English. Articles published in English contain Slovak resumé.

Text

1. Abstract briefly summarizing the article is limited to 200 words, no references are allowed. The maximum number of key words is 6. Text of the article has to contain the introduction, characterization (state) of investigated problem, applied methodology, obtained new data, discussion, conclusion and references. The obtained data must be distinctly separated from interpretations. All applied figures and tables must be referred in the text.

2. The hierarchy of headings in the manuscript must be indicated by a pencil note: 1 – highest level, 2 – lower, 3 – lowermost level.

3. The references in the text prefer parentheses, e.g. (Dubčák, 1987; Hrubý et al., 1988). The form "according to Dubčák (1987)" should be used only exceptionally.

4. Position of figures and tables must be indicated in the manuscript. Editable text of manuscript sent to editorial office must be without figures and tables, though the preview PDF has to contain them in a correct position.

5. Greek letter in the text must be identified at the left margin of the text (e.g. sigma). The text should strictly distinguish the dash from hyphen. Symbols, mathematic signs, names of fossils, etc., which should be printed in italics, must be underlined by the wavy line in the manuscript.

Figures and tables

1. The high quality figures and tables can be published either in **maximum width of column (81 mm) or page (170 mm).** The optimum size of letters and numbers in the camera-ready figure is 2 mm. Articles published in Slovak contain the Slovak descriptions in figures and tables, the tables headings and descriptions beneath figures and tables are in Slovak and English. English articles contain all texts in English. **Maximum dimension of figures and tables in the journal is 170 x 230 mm. Larger (fanfolded)** illustrations are published only exceptionally.

2. For figures drawing the editorial office recommends the vector graphics editors (Corel Draw, Adobe Illustrator, etc.). The very thin lines (hair lines), the pre-defined software or raster fillings of polygons (e.g. in Corel Draw) are not allowed. The filling must consist from separately set objects.

3. Each illustration including photographs must contain graphic (metric) scale, eventually the dimensions of visualized objects have to be stated in the describing text to figure. Maps and profiles must contain also the azimuth orientation, their detail explanations are stated at the first figure. Grouped figures, e.g. photographs and diagrams, are compiled as one figure with separate parts designated by letters (a, b, c, etc.).

4. The photographs sent as JPG of TIF files are required for having minimum 600 DPI resolution. Publishing of colour illustrations can be charged by a fee.

References

1. Minimum 50 % of referred works must represent contemporary publications after 2000. The references in alphanumeric order encompass only literature cited in the article.

2. Examples of referring:

Book: Gazda, L. & Čech, M., 1988: Paleozoic of the Medzev nappe. *Bratislava, Alfa, 155 p.*

Journal: Vrba, P., 1989: Shear zones in the metapelite complexes. *Miner. Slov., 21, 135–142.*

Anniversary volume: Návesný, D., 1987: High-potassium rhyolites. *In: Romanov, V. (ed.): Stratiform deposits of Gemericum. Spec. publ. Košice, Slov. geol. soc., 203–215.*

Manuscript: Radvanský, F., Slivka, B., Viktor, J. & Srnka, T., 1985: Vein deposits of the Jedľovec nappe of Gemericum. Final report from the project SGR-geophysics. *Manuscript. Spišská Nová Ves, Archive Št. Geol. Úst. D. Štúra, 28 p.*

3. The article with more than two authors is referred by the name of the first author with the amendment et al., but the list of references contains names of all authors.

Ďalšie informácie/Further information: mineralia.slovaca@geology.sk; zoltan.nemeth@geology.sk

OBSAH – CONTENT

PÔVODNÉ ČLÁNKY – ORIGINAL PAPERS

Baláž, P.
Results of the first phase of the deep-sea polymetallic nodules geological survey in the Interoceanmetal Joint Organization licence area (2001–2016)
Výsledky prvej fázy geologického prieskumu hlbokomorských polymetalických konkrécií v prieskumnom území Spoločnej organizácie Interoceanmetal (2001 – 2016)

Pelech, O., Boorová, D., Hók, J. & Rakús, M.†
Upper Cretaceous limestone olistoliths in the Rázová Formation (Horné Belice Group), Považský Inovec Mts. (Western Carpathians)
Olistolity vápencov vrchnej kriedy v rázovskom súvrství hornobelickej skupiny Považského Inovca (Západné Karpaty)

Teťák, F.
Lithology and position of the Biele Karpaty Unit SE of Lednica (Biele Karpaty Mts., Western Carpathians)
Litológia a pozícia bielokarpatskej jednotky juhovýchodne od Lednice (Biele Karpaty, Západné Karpaty)

Cheikhaoui, Y., Bensehamdi, C., Cheniti, H., Kanli, A. I. & Benselhoub, A.
New formula for evaluation of strength pillar in the underground mine of Chaabet El-Hamra (Setif, Algeria)
Nový matematický postup hodnotenia pevnosti pilierov na príklade banskej prevádzky Chaabet El-Hamra (Setif, Alžírsko)

Danková, Z., Štyriaková, I., Čechovská, K., Šuba, J., Nováková, J., Kollárová, V., Bekényiová, A., Lenhardtová, E., Fedorová, E. & Briančin, J.
Influence of bacteria on toxic elements leaching from the contaminated soil
Vplyv baktérií na lúhovanie toxických prvkov z kontaminovanej pôdy

Indexed / Abstracted / Accessed by SCOPUS and EBSCO
Indexované / abstraktované / sprístupňované databázami SCOPUS a EBSCO

www.geology.sk/mineralia